

AD-A104 185

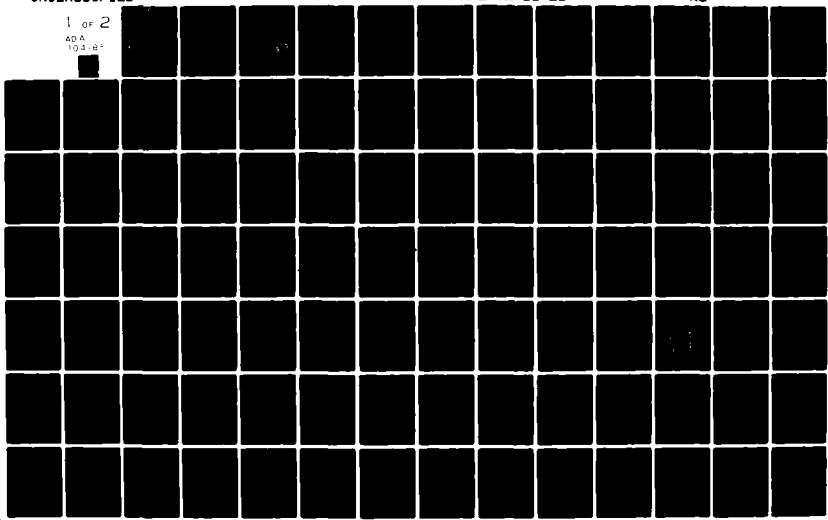
CALIFORNIA INST OF TECH PASADENA GUGGENHEIM JET PROP--ETC F/G 21/2
MEASUREMENTS OF ENERGY LOSSES ASSOCIATED WITH INTERACTIONS BETW--ETC(U)
JUL 81 F E CULICK, K MAGIAWALA, J WAT, E AWAD F04611-80-X-0013

UNCLASSIFIED

AFRPL-TR-81-22

NL

1 of 2
404
194-87



LEVEL

(P)

AFRPL-TR-81-22

MEASUREMENTS OF ENERGY LOSSES ASSOCIATED WITH INTERACTIONS
BETWEEN ACOUSTIC WAVES AND NON-UNIFORM STEADY FLOW

Daniel and Florence Guggenheim Jet Propulsion Center
California Institute of Technology
Pasadena, California 91125

AD-A104/185
Authors: F. E. C. Culick, Professor of Engineering
K. Magiawala, Research Fellow
J. Wat, Graduate Student
E. Awad, Graduate Student
T. Kubota, Professor of Aeronautics

July 1981

DTIC FILE COPY

Final Report for Period 15 February 1979 - 30 November 1980

DTIC
SEP 16 1981
H
APPROVED FOR PUBLIC RELEASE;
DISTRIBUTION UNLIMITED

AIR FORCE ROCKET PROPULSION LABORATORY
DIRECTOR OF SCIENCE AND TECHNOLOGY
AIR FORCE SYSTEMS COMMAND
EDWARDS AFB, CALIFORNIA 93523

NOTICES

When U.S. Government drawings, specifications, or other data are used for any purpose other than a definitely related Government procurement operation, the Government thereby incurs no responsibility nor any obligation whatsoever, and the fact that the Government may have formulated, furnished, or in any way supplied the said drawings, specifications, or other data, is not to be regarded by implication or otherwise, or in any manner licensing the holder or any other person or corporation, or conveying any rights or permission to manufacture, use, or sell any patented invention that may in any way be related thereto.

FOREWORD

The program described in this report was carried out at the Jet Propulsion Laboratory, California Institute of Technology, under Air Force Rocket Propulsion Laboratory MIPR No. F04611-80-X-0013 through an agreement with the National Aeronautics and Space Administration, NAS7-100, Task Order RD-182, Amendment No. 36. This investigation is entitled, "Combustion Stability Measurements - Tasks II and III," and was technically monitored by Mr. Jay Levine.

The program was carried out under Caltech/JPL Work Orders 61513 and 61514 with the general supervision of Mr. Leon D. Strand, Energy and Materials Research Section, Jet Propulsion Laboratory.

This technical report is approved for release and distribution in accordance with the distribution statement on the cover and on the DD Form 1473.


JAY N. LEVINE
Project Manager

JAY N. LEVINE
Project Manager

W.C. AndrePont
Chief, Combustion Technology Office

FOR THE COMMANDER

Eugene G. Haberman
EUGENE G. HABERMAN
Chief, Propulsion Analysis Division

Unclassified

SECURITY CLASSIFICATION OF THIS PAGE (When Data Entered)

REPORT DOCUMENTATION PAGE		READ INSTRUCTIONS BEFORE COMPLETING FORM
1. REPORT NUMBER <i>(18) AFPL-TR-81-22</i>	2. GOVT ACCESSION NO. <i>AD-A104 185</i>	3. PECIPIENT'S CATALOG NUMBER
4. TITLE (and subtitle) <i>(6) Measurements of Energy Losses Associated with Interactions Between Acoustic Waves and Non-Uniform Steady Flow</i>	5. TYPE OF REPORT & PERIOD COVERED <i>(9) Final report, 1 Feb 79-30 Nov 80</i>	
7. AUTHOR(s) <i>(10) F.E.C. Culick E. Awad K. Magiawala T. Kubota</i>	6. PERFORMING ORG. REPOR <i>(15) FO4611-80-X-0013</i>	
9. PERFORMING ORGANIZATION NAME AND ADDRESS <i>Daniel and Florence Guggenheim Jet Propulsion Center, California Institute of Technology, Pasadena, CA 91125</i>	10. PROGRAM ELEMENT, PROJECT, TASK AREA & WORK UNIT NUMBERS <i>(16) 573010BP (17) 70</i>	
11. CONTROLLING OFFICE NAME AND ADDRESS <i>Air Force Rocket Propulsion Laboratory/PAC Edwards AFB, California 93523</i>	12. REPORT DATE <i>April 1981</i>	
14. MONITORING AGENCY NAME & ADDRESS (if different from Controlling Office) <i>(11)</i>	13. NUMBER OF PAGES <i>(13) 43.9</i>	
15. SECURITY CLASS. (of this report) <i>Unclassified</i>		
15a. DECLASSIFICATION/DOWNGRADING SCHEDULE		
16. DISTRIBUTION STATEMENT (of this Report) <i>Approved for Public Release: Distribution Unlimited</i>		
17. DISTRIBUTION STATEMENT (of the abstract entered in Block 20, if different from Report)		
18. SUPPLEMENTARY NOTES <i>(S H)</i>		
19. KEY WORDS (Continue on reverse side if necessary and identify by block number) <i>Acoustics with Mean Flow Acoustic Waves Nozzle Damping Resonance Tubes Solid Rocket Instability Nozzle Admittance Combustion Instability Impedance Tube</i>		
20. ABSTRACT (Continue on reverse side if necessary and identify by block number) <i>An experimental program has been conducted to study interactions between acoustics waves and two types of non-uniform average flow occurring in solid propellant rockets. Measurements in a resonance tube confirmed the existence of an energy loss associated with interactions between a longitudinal acoustic field and an average flow entering through a lateral boundary. The measured loss was approximately five times as large as that predicted by a simple one-dimensional analysis.</i>		
(over) →		

~~SECURITY CLASSIFICATION OF THIS PAGE(When Data Entered)~~

However, due to the large experimental uncertainty associated with these results, the confidence level of their quantitative validity is low. In the second part of the program, a small supersonic wind tunnel has been operated open cycle with the test section, upstream of a choked nozzle, used as an impedance tube to measure the admittance function for the nozzle. Limited results for simulated submerged nozzles suggest that secondary flow has little influence on the admittance function for the aft end of the chamber.

7

Accession For	
NTIS GRA&I	<input checked="" type="checkbox"/>
DTIC TAB	<input type="checkbox"/>
Unannounced	<input type="checkbox"/>
Justification	
By	
Distribution	
Avail	Series
Dist	

P

~~SECURITY CLASSIFICATION OF THIS PAGE(When Data Entered)~~

TABLE OF CONTENTS

	<u>Page</u>
I. INTRODUCTION	9
II. MEASUREMENTS OF FLOW TURNING LOSSES	18
2.1 Analysis of the Flow Turning Loss	18
2.2 Analysis of the Apparatus	26
2.3 Description of the Apparatus and Instrumentation	31
2.3.1 Cold Flow Resonance Tube	31
2.3.2 Impedance Tube	33
2.4 Calibration Procedures and Estimates of Errors	33
2.5 Measurement of the Admittance Functions for Cylindrical Porous Tubes	36
2.6 Measurements of the Flow Turning Loss	51
III. MEASUREMENTS OF THE ADMITTANCE FUNCTION FOR A CHOKED NOZZLE	61
3.1 Analysis of the Impedance Tube	64
3.2 Description of the GALCIT Supersonic Wind Tunnel and Experimental Apparatus	68
3.3 Preliminary Tests	75
3.4 Procedures for Data Reduction	77
3.4.1 Application of Analysis of the Impedance Tube	79
3.4.2 Numerical Reduction of Data for the Amplitude and Phase Distributions	90
3.4.3 Some Test Cases	93
(a) Sensitivity of the Numerical Technique	93
(b) Results for a Rigid Flat Plate	95
(c) Examples Showing Importance of Obtaining Data Near Pressure Minima	96

TABLE OF CONTENTS (Continued)

	<u>Page</u>
3.5 Summary of Tests Conducted	98
3.6 Calibration Procedures and Estimates of Errors	98
3.6.1 Calibration of the Secondary Air Supply	98
3.6.2 Calibration of Microphones and Other Instruments	100
3.6.3 Sources and Estimates of Errors	101
3.7 Results for Measurements of the Admittance Function	102
3.7.1 Conical Nozzles, No Secondary Flow	102
3.7.2 Submerged Nozzles with Secondary Flow	109
IV. SUMMARY AND CONCLUSIONS	118
4.1 Flow Turning Losses	118
4.2 Measurements of the Admittance Function for a Choked Nozzle	119
V. REFERENCES	122

LIST OF FIGURES

<u>Figure Number</u>	<u>Page No.</u>
1. Resonance Tube with Piston Drivers and Lateral Flow Elements	
2. Sketch Showing Definitions for the Resonance Tube	
3. Schematic Diagram of the Resonance Tube and Associated Apparatus	
4. End Fixture for the Impedance Tube	
5. Schematic Diagram of the Impedance Tube and Associated Apparatus	
6. Flow Characteristics of Porous Flat Plates and Cylindrical Samples	
7. Real Part of the Admittance Function, Plate F	
8. Real Part of the Admittance Function, Plate G	
9. Real Part of the Admittance Function, Plate H	
10. Real Parts of the Admittance Functions versus Pressure Drop	
11. Admittance Function Measured for Lateral Flow Element 1	
12. Admittance Function Measured for Lateral Flow Element 2	
13. Net Attenuation Coefficient Measured with Lateral Flow	
14. Measured Attenuation Coefficient for Flow Turning Losses	
15. Schematic of the GALCIT Supersonic Wind Tunnel	
16. Sketch of the Test Section in the Supersonic Wind Tunnel	
17. Sketch of an Impedance Tube with Flow	
18. Drawings of the Nozzle Tested	
19. Instrumentation for Measurements of the Nozzle Admittance Function	
20. Calculated Amplitude Distribution, Showing the Influence of a_0	
21. Calculated Phase Distribution, Showing the Influence of a_0	

LIST OF FIGURES (Continued)

<u>Figure Number</u>	<u>Page No.</u>
22. Calculated Amplitude Distribution, Showing the Influence of the Sign of a_0	
23. Calculated Phase Distribution, Showing the Influence of the Sign of a_0	
24. Calculated Amplitude Distribution, Showing the Influence of κ	
25. Calculated Phase Distribution, Showing the Influence of κ	
26. Admittance Function Measured for a Conical Nozzle, $M = 0.04$	
27. Admittance Function Measured for a Conical Nozzle, $M = 0.1$	
28. Admittance Function Measured for a Nozzle with Secondary Flow, No Submergence, $M = 0.04$	
29. Admittance Function Measured for a Nozzle with Secondary Flow, Maximum Submergence, $M = 0.04$	

LIST OF TABLES

<u>Table Number</u>	<u>Page No.</u>
1. Data for the Admittance Functions of the Porous Plates	
2. Summary of Results for the Porous Flat Plates	
3. Final Results for the Admittance Function for the Lateral Flow Elements	
4. Data for the Attenuation Coefficient with Lateral Flow ($1/2"$ Vent, $f = 445$ Hz.)	
5. Values of the Admittance Function for the Faces of the Driver Pistons, $f = 442$ Hz. (Ref. 4)	
6. Values of the Attenuation Coefficient for the $1/2"$ Circular Vent, $f = 442$ Hz. (Ref. 4)	
7. Values of the Admittance Function for the Lateral Flow Elements, $f = 445$ Hz. (Average of values in Table 3)	
8. Values of the Attenuation Coefficient for Flow Turning Losses, $f = 445$ Hz.	
9. Summary of the Characteristics of the Nozzles Used for Admittance Measurements	
10. Results of Calculations for the Sensitivity to Random Errors	
11. Results for Measurement with a Rigid Flat Plate	
12. Summary of the Tests Conducted for Measurements of the Nozzle Admittance	

LIST OF SYMBOLS

A few symbols defined in the text and used but briefly are not included in this list.

\bar{a}	speed of sound
A_b	admittance function for a porous plate
A_p	admittance function for a piston
A_t	admittance function for a transverse cylindrical element
C_p	specific heat for the gas
C_v	specific heat for the gas
D	diameter of the chamber
D_c	port diameter for a cylindrical grain
e_0	stagnation internal energy for the gas
E_ℓ^2	integral defined by eq. (2.23) for the ℓ^{th} longitudinal mode
δ	acoustic energy density, eq. (2.19)
G	defined by eq. (3.26) and (3.28)
h_{0s}	stagnation enthalpy for gases entering at lateral boundary
k	complex wavenumber, $k = (\omega - ia)/\bar{a}$
k_ℓ	wavenumber for the ℓ^{th} longitudinal mode, $k_\ell = \omega_\ell/\bar{a}$
K	wavenumber defined by eq. (3.9)
L	length of the chamber
L_0	displacement of a cylindrical grain
L_b	length of grain along the lateral boundary
m	mass flux (mass/area-sec.)
m_b	mass flux of gas at and normal to a surface
M	Mach number
M_b	Mach number for the gas leaving a burning surface, $M_b = u_b/\bar{a}$

M_p	Mach number of axial flow at a piston
M_t	Mach number of flow normal to a transverse element
\hat{n}	unit vector outward at a boundary
p	pressure
\hat{p}_ℓ	spatial mode shape of pressure for the ℓ^{th} longitudinal mode
p_0	stagnation pressure
q	perimeter of a surface
R	gas constant, for the gas only
R_b	response function, defined by eq. (E.35)
S_b	area of burning surface in one-half of a T-burner
S_{be}	area of burning surface on one end of a T-burner
S_{bs}	area of burning surface on the lateral boundary in one-half of a T-burner
S_c	port area for a cylindrical grain,
S_{c0}	cross-sectional area of the burner
t	time
T	temperature
ΔT	temperature difference between the gas in the chamber and the gas leaving the burning surface, $\Delta T = T_s - G$
u	speed of gas in axial direction
u_b	speed of gas leaving a lateral surface
u_s	axial speed of gases entering at lateral boundary
u_p	velocity of a piston
V	volume, $V = LS_{c0}$ for a uniform tube
w	mass flux at lateral boundary
z	coordinate parallel to the axis if a tube, eq. (2.5)
a	decay or growth constant, in $\exp(at)$
a_{ft}	decay constant associated with flow turning, eq. (2.28)

a_p	decay constant associated with piston drivers, eq. (2.33)
a_t	equation (2.34)
a_v	decay constant associated with the vent
β	$\beta = 2L_b/L$
β_0	$\beta_0 = 2L_0/L$
γ	ratio of specific heats for the gases, $\gamma = C_p/C_v$
δ	defined by eq. (3.11)
\wp	defined by eq. (3.11)
μ	viscosity
ν	kinematic viscosity, μ/ρ
ρ	gas density

Subscripts and Superscripts

(̄)	time-averaged value
()'	fluctuation value
(^)	amplitude for a harmonic motion, e.g. $p' = \hat{p} \exp(i\omega t)$
() _e	value for an end surface
() _l	value for the l^{th} longitudinal mode
() _s	value for a side (lateral) surface
() ⁽ⁱ⁾	imaginary part
() ^(r)	real part
() ₊	denotes wave travelling to right
() ₋	denotes wave travelling to left

I. INTRODUCTION

This report summarizes work carried out during the past two years on two problems arising from the interactions between acoustic fields and non-uniform flow fields. Both problems are associated with the more general subject of the stability of acoustic waves in solid propellant rocket motors. One purpose of the present work was to demonstrate what could be learned with experiments performed at room temperature. It is important to distinguish those problems which are purely fluid mechanical and therefore which can be studied without the serious complications accompanying combustion processes.

In Section II we describe the first measurements of the loss of acoustic energy accompanying the flow of gas inward through the lateral boundary of a chamber containing acoustic waves. The flow entering normal to the surface must turn to the axial direction parallel to the boundary; simultaneously each fluid element of the mean flow must acquire acoustic energy. It is this second process, involving action of the unsteady field in the chamber upon the entering flow, which appears as a loss of energy for the existing acoustic field.

Consider, for example, the case of a longitudinal acoustic field in a closed chamber. For our purposes we may assume that there are no viscous or other losses, so the field will exist forever if nothing else happens. But now imagine that some gas is leaked in at the lateral boundary. If there is no way for the gas to escape the chamber, the average pressure and density rise and the amplitude of the acoustic field must decrease in order to conserve acoustic energy. Let m_i , δ_i be the initial values of total mass and density of acoustic energy

in the chamber, and let m_i , δ_i be the final values. Classically one obviously has, for the conservative system,

$$m_i \delta_i = m_f \delta_f$$

and because $m_f > m_i$, therefore $\delta_f < \delta_i$. But δ_f is proportional to the square of the amplitude of the pressure oscillation, so the amplitude is reduced by the addition of mass.

The same argument works in reverse: if the bit of mass is removed, the amplitude will be increased to its initial value. Now in steady flow, each element of mass entering is matched by an equal amount departing. Thus the preceding argument suggests that a steady mean flow should not disturb the acoustic field. The conclusion is incorrect and the argument fails, because in the real case the influences of viscous forces cannot be ignored. For a non-uniform flow field, the forces required to accelerate the incoming fluid necessarily involve inelastic processes and energy is dissipated. In fact, half of the work done by the gas in the chamber on the incoming fluid is dissipated as heat and half provides the acoustic energy acquired by the entering mass (Ref. 1). As a result there is necessarily a loss of energy associated with the inward flow of gas which initially has no acoustic energy.

That energy loss - a loss for the acoustic field existing in the chamber - is often referred to as the 'flow turning loss' because turning of the average flow is necessarily involved. It is really a rate of loss, proportional to the velocity of the incoming flow perpendicular to the

1. Culick, F. E. C. "Remarks on Entropy Production in the One-Dimensional Approximation to Unsteady Flow in Combustion Chambers", Comb. Sci. and Tech., V. 15 (1977), pp. 93-97.

boundary. Its existence was first predicted theoretically (Ref. 2) in computations based on the one-dimensional approximation but has not previously been measured. The measurement technique used in the present work is an extension of that used in earlier work (Refs. 3, 4 and 5).

A resonance tube with provision for introducing and exhausting an average flow is the central apparatus (see Figure 1, p. 19). Flow enters through the porous faces of pistons fitted to the ends of the tube. The pistons are driven to excite standing acoustic waves. The flow exhausts through a vent in the center of the tube, enforcing symmetry of the average flow field. For measurements of the flow turning losses, cylindrical porous tubes are mounted at intermediate positions between the ends and the center. In principle, the procedure is straightforward. The forcing frequency is varied across the fundamental resonant frequency of the system, and the slope of the resonance curve is determined. The width of the curve is proportional to the net losses in the system.

In the previous work, the losses associated with the porous pistons and the gains associated with the exhaust vent were determined over a

-
2. Culick, F. E. C. "The Stability of One-Dimensional Motions in a Rocket Motor", Comb. and Sci. and Tech., V. 7 (1973), pp. 165-175.
 3. Magiawala, K. "Measurements of Energy Exchange Between Acoustic Fields and Non-Uniform Flow Fields", Ph.D. Thesis, California Institute of Technology (May 1978).
 4. Culick, F. E. C. and Magiawala, K., "Measurements of Energy Losses Associated with Interactions Between Acoustic Waves and a Steady Flow Field", Air Force Rocket Propulsion Laboratory, Report AFRPL-TR-78-6 (March 1978).
 5. Magiawala, K. and Culick, F. E. C. "Measurements of Energy Exchange Between Acoustic Fields and Non-Uniform Steady Flow Fields", J. Sound and Vib. (to be published).

range of average Mach number. Those results are used here, so the flow turning loss is then found by performing additional tests with the cylindrical elements in place.

Serious difficulties arise because the quantities to be measured are relatively small and are determined indirectly by forming the differences of relatively large numbers. Thus great care must be taken to achieve as high precision as possible. The procedures followed have been described fully in References 3 and 4. We encountered further obstacles here in determining the admittance functions for the cylindrical samples. There are two reasons. First, we have been unable to devise a means of measuring the admittance of a curved sample, so we have been forced to assume that the values are the same as those for a flat sample. Second, it is a consequence of the way in which the materials are manufactured that we have been unable to obtain flat samples having the same porosity as the cylindrical samples. We have therefore used values extrapolated from those actually measured. The technique is described in Section 2.5.

Those problems have contributed substantially to experimental uncertainties in the final results. Our measurements have shown that the flow turning loss does indeed increase with the average flow speed, but is approximately three times the value predicted by the approximate one-dimensional analysis. The experimental errors are quite large. We have reduced the measurement errors as far as possible, and it appears that the only way to reduce the uncertainties in the final results is to use larger apparatus with higher flow rates. The absolute numerical values to be measured would therefore be larger, thereby reducing the

relative sizes of the experimental errors. This conclusion applies to all experimental work with measurements for problems involving interactions between acoustic waves and non-uniform flow fields.

In Section III we describe measurements of the loss of acoustic energy due to the action of a choked exhaust nozzle. This influence, represented by an admittance function, is a substantial contribution to attenuation of longitudinal waves in a rocket motor. The influence of a de Laval nozzle was first examined theoretically long ago (Refs. 6 and 7). The first measurements, using apparatus with steady flow (Ref. 8) verified theoretical predictions but were limited to simple nozzles. The admittance function was determined by direct measurement of the velocity fluctuations with a hot wire anemometer, and the pressure oscillations with a static pressure probe. By far the most extensive measurements were those reported in References 9-12 using a blow-down facility. Some results were obtained (Ref. 11) for the admittance of a nozzle with secondary flow.

-
6. Tsien, H.S. "The Transfer Function of Rocket Nozzles", ARSJ, V. 22, No. 31 (May-June 1952), p. 139.
 7. Crocco, L. and Cheng, S.-T. Theory of Combustion Instability in Liquid Propellant Rocket Motors, AGARDograph No. 8, Butterworths Publications, Ltd., London (1958) Appendix C.
 8. Crocco, L., Monti, R. and Grey, J. "Verification of Nozzle Admittance Theory by Direct Measurement of the Admittance Parameter", ARSJ, V. 31, No. 6 (June 1961) pp. 771-775.
 9. Zinn, B.T. et al "Experimental Determination of Three-Dimensional Liquid Rocket Nozzle Admittances", AIAA J., V. 11, No. 31 (Mar. 1973), pp. 267-272.
 10. Bell, W.A., Daniel, B.R. and Zinn, B.T. "Experimental and Theoretical Determination of the Admittances of a Family of Nozzles Subjected to Axial Instabilities", J. Sound and Vib., V. 30, No. 2 (1973), pp. 179-190.

Although the method used in Ref. 8 seems to have given reasonable results, there are considerable difficulties associated in measuring the small acoustic velocities, including distortion and low signal/noise ratio. Moreover many measurements should be made over a plane near the entrance to the nozzle, and averaged, in order to give a proper representation of the influence of the entire nozzle. That procedure was not followed in Ref. 8. This technique would likely become particularly tedious and time consuming for a nozzle with secondary flow. In that case considerable effort would likely be required to determine the best reference plane for defining the admittance function.

The data reported in Refs. 8-12 seem to be quite reasonable, although there is no discussion of experimental errors or the cost of tests. It appears that the cost of using a blow-down facility for this purpose might be quite high. The section upstream of the nozzle is used as an impedance tube, so the acoustic pressure must be measured at many locations. For transient tests, many pressure transducers are required, and data processing becomes a major expense because of the equipment required.

A primary purpose of the present program has been to determine how well one might use a small continuously operating supersonic wind tunnel to measure the nozzle admittance. The main advantages are the cost (\$25 per hour for the tunnel) and the flexibility of continuous operation

-
11. Zinn, B. T. et al "Damping of Axial Instabilities by the Minuteman II, Stage III and Minuteman III, Stage III, Exhaust Nozzles", Georgia Institute of Technology, Report AFRPL-TR-72-71 (August 1972).
 12. "Nozzle Design Considerations for Attenuation of Axial Instabilities in the Minuteman II and III, Stage III Rocket Motors", Georgia Institute of Technology, Report AFRPL-TR-73-69 (September 1973).

which permits studying various aspects of the problem with relative ease.

For example, the spatial characteristics of the average and unsteady flow field are particularly important because to reduce the data, as in Refs. 9-12 and here, the assumption is used that the flow fields are uniform over a cross-section of the tube. The mean flow obviously cannot be, because of the growth of the boundary layers. How significantly this approximation affects the final results has yet to be established; time did not permit examining the problem in this work. However, we have obtained some results showing that the acoustic field is not one-dimensional under all conditions.

It is also possible with the techniques used here to obtain the necessary measurements with only two pressure transducers and therefore only two channels of data. Overall, then, the cost of the equipment is much below that of a blow-down facility. The quality of the data should be better - i.e. one should be able to reduce the experimental errors because the techniques are simpler with steady operation - but this has not been proved with the present work.

In principle, the use of the subsonic section of a wind tunnel as an impedance tube is really quite straightforward. We had assumed, on the basis of the work reported in Refs. 9-12, that the well-known technique based on measurements of the pressure amplitude would be directly applicable. After considerable effort and time, we concluded that the assumption is wrong. It happens that if the losses at the end of the impedance tube are relatively small, as the case is for choked nozzles, it is essential that both the amplitude and phase of the acoustic pressure be measured. Both pieces of information must be used to obtain accurate

results for the real and imaginary parts of the admittance function.

This problem is discussed in Sections 3.2 and 3.6.

Because we have examined the influences of secondary flow and submergence, the configurations tested have shapes for which the admittances cannot be calculated with any available analysis. The values inferred from our measurements seem to be reasonable, with the possible exception of an apparent energy gain at the highest frequency used (2000 Hz). That may be due to resonance within the plenum chamber surrounding the nozzle, a provision required for the introduction of secondary flow. In any case the experimental uncertainty is large.

The signal/noise ratio causes problems which increase with the Mach number of the average flow. Up to $\bar{M} = 0.04$ a tracking filter (bandwidth = 0.5 Hertz) is entirely adequate. The values for the admittance function can be determined with less than 5% error. For $\bar{M} \geq 0.1$ the problem is more serious in the vicinity of pressure minima. The signal/noise ratio is of course much reduced, but results could be extracted by numerical averaging (which we have not done in this program). A more serious difficulty we encountered was apparent fluctuation of the axial location of the pressure minimum. Time did not permit thorough examination of the problem, and we cannot state whether it is soluble simply by averaging the data. If it cannot be handled in that manner, then the use of the tunnel as an impedance tube may be blocked for higher Mach numbers.

Should that be the case, then one would be forced to return to direct measurements, as in Ref. 8. However, the best technique for measuring the velocity is now laser-Doppler anemometry. There are

certain practical problems when circular transparent test sections must be used, but it appears that this might be a fruitful course to follow in any case. The importance of nozzle losses in the problem of combustion instability demands that a method be developed which is relatively cheap; reliable; and can be used routinely to measure the acoustical properties of nozzles used in operational rocket motors.

II. MEASUREMENTS OF FLOW TURNING LOSSES

Since the existence of the flow turning loss was first predicted in Ref. 1, there has been a certain amount of controversy concerning both the qualitative and quantitative truth of the result; see Ref. 13, for example, for a brief discussion. The data reported here constitute the first evidence, obtained from purely acoustics experiments, showing that the loss does arise in real flows. It is therefore appropriate to begin here with a short résumé of the theoretical origins, after which we describe the experimental work carried out in the present program.

2.1 Analysis of the Flow Turning Loss

The flow turning loss first appeared in the analysis (Ref. 1) of longitudinal acoustic waves in a combustion, using the one-dimensional approximation. This is essentially an extension to unsteady flow with combustion of the problem of flow in a duct with mass addition (e.g. Ref. 14, Chapter 8). The pressure loss in flow with mass addition (see Table 8.1 of Ref. 14) corresponds to the loss of acoustic energy associated with mass addition in the present case.

We can demonstrate the result by considering the simplest problem of flow in a uniform channel with no combustion. Within the one-dimensional approximation, the general conservation equations and the equation of state can be written

-
13. Culick, F. E. C. (Ed.), "T-Burner Testing of Metallized Propellants", AFRPL Report TR-74-28 (Oct. 1974).
 14. Shapiro, A. H. The Dynamics and Thermodynamics of Compressible Fluid Flow. The Ronald Press Company, New York (1953).

$$\frac{\partial p}{\partial t} + \frac{\partial}{\partial z} (\rho u) = w \quad (2.1)$$

$$\frac{\partial}{\partial t} (\rho u) + \frac{\partial}{\partial z} (\rho u^2) + \frac{\partial p}{\partial z} = u_s w \quad (2.2)$$

$$\frac{\partial}{\partial t} (\rho e_0) + \frac{\partial}{\partial z} (\rho u e_0) + \frac{\partial}{\partial z} (\rho u) = h_{0s} w \quad (2.3)$$

$$p = \rho RT \quad (2.4)$$

where

$$w = \frac{1}{S_c} \int m_b dq \quad (2.5)$$

The source term on the right hand side of (2.2) represents the initial axial momentum of the gas flowing in at the boundary, and the right hand side of (2.3) represents the enthalpy (internal energy plus p-v work) carried in. The mass addition at the boundary is m (mass/area-second); the perimeter is q ; and S_c is the cross-sectional area. Subscript zero, $()_0$, denotes the stagnation value: $e_0 = e + u^2/2 = C_v T + u^2/2$ and $h_0 = e + p/\rho + u^2/2$.

Equation (2.2) can be re-written, with use of (2.1):

$$\rho \frac{\partial u}{\partial t} + \rho u \frac{\partial u}{\partial z} + \frac{\partial p}{\partial z} = (u_s - u)w \quad (2.6)$$

The right hand side of this equation represents the force required to accelerate the added mass to the local axial speed u . That this is an inelastic and therefore dissipative process may be understood in an elementary way from the equations of mechanics. A clear and extended discussion of the point may be found in Ref. 15.

15. Rauscher, M. Introduction to Aeronautical Dynamics, John Wiley and Sons, Inc., New York (1953) p. 50.

Similarly, (2.3) can be re-formed and the kinetic energy removed by subtracting u times the last equation to give

$$\rho C_v \frac{\partial T}{\partial t} + \rho u C_v \frac{\partial T}{\partial z} + p \frac{\partial u}{\partial z} = (h_{0s} - e_0)w - u(u_s - u)w \quad (2.7)$$

We have chosen, as in earlier works, to treat the mass addition and its influences as sources averaged over the cross-section of the channel. One could also begin with the equations for two- or three-dimensional flow and average over the cross-section. The influences of the sources at the boundary then arise through the boundary conditions. With some assumptions concerning definitions of averaged quantities ("closure conditions") the same equations (2.1)-(2.3) can be recovered; some details of this procedure may be found in Ref. 16.

It is convenient to use the equation for the pressure, constructed by adding C_v times the continuity equation (2.1), to (2.7) and using the equation of state (2.4); the final result is:

$$\frac{\partial p}{\partial t} + \gamma p \frac{\partial u}{\partial z} + u \frac{\partial p}{\partial z} = [a^2 + \gamma R \Delta T + \frac{1}{2}(u^2 - u_s^2)]w + \frac{R}{C_v} u(u - u_s)w \quad (2.8)$$

where $\Delta T = T_s - T$ is the local temperature difference between the bulk flow in the channel and the entering flow.

We now assume that the flow enters with no axial motion, $u_s = 0$, and with temperature equal to the local temperature in the duct, so $T_s = T$; these assumptions apply to the experiments described below.

Equations (2.6) and (2.8) become

-
16. Van Moorhem, W.K. "An Investigation of the Origin of the Flow-Turning Effect in Combustion Instability", 17th JANNAF Combustion Meeting (September 1980).

$$\rho \frac{\partial u}{\partial t} + \rho u \frac{\partial u}{\partial z} + \frac{\partial p}{\partial z} = -uw \quad (2.9)$$

$$\frac{\partial p}{\partial t} + \gamma p \frac{\partial u}{\partial z} + u \frac{\partial p}{\partial z} = a^2 w + (\frac{R}{C_v} - \frac{1}{2}) u^2 w \quad (2.10)$$

Analysis of the stability of small disturbances is based on the linearized forms of these two equations; set $u = \bar{u} + u'$ etc., and ignore terms of order u'^2 and \bar{u}^2 to find

$$\rho \frac{\partial u'}{\partial t} + \frac{\partial p'}{\partial z} = -(uw)' - \rho \frac{\partial}{\partial z} (\bar{u} u') \quad (2.11)$$

$$\frac{\partial p'}{\partial t} + \gamma \bar{p} \frac{\partial u'}{\partial z} = (a^2 w)' - \bar{u} \frac{\partial p'}{\partial z} - \gamma p' \frac{du}{dz} \quad (2.12)$$

We assume that while the average speed \bar{u} varies with position, the average density, temperature and therefore pressure are constant.

Now form the wave equation for the pressure fluctuation by differentiating (2.12) with respect to time and substituting (2.11); with some rearrangement we find

$$\begin{aligned} \frac{\partial^2 p'}{\partial z^2} - \frac{1}{a^2} \frac{\partial^2 p'}{\partial t^2} &= - \frac{\partial}{\partial z} (uw)' - \frac{\partial}{\partial t} (\frac{a^2}{a^2} w)' - \rho \frac{\partial^2}{\partial z^2} (\bar{u} u') + \frac{\gamma}{a^2} \frac{\partial p'}{\partial t} \frac{d\bar{u}}{dz} \\ &\quad + \frac{\bar{u}}{a^2} \frac{\partial^2 p'}{\partial t \partial z} \end{aligned} \quad (2.13)$$

For our purposes, to demonstrate the appearance of the flow turning loss, only the first terms on the right hand sides of (2.11) and (2.13) are required. The wave equation (2.13) with the boundary condition to be applied at the ends of the channel, given by (2.11) are

$$\frac{\partial^2 p'}{\partial z^2} - \frac{1}{a^2} \frac{\partial^2 p'}{\partial t^2} = - \frac{\partial}{\partial z} (uw)' \quad (2.14)$$

$$\frac{\partial p'}{\partial z} = - (uw)' \quad (z=0, L) \quad (2.15)$$

An arbitrary disturbance treated within linear analysis can be represented as a Fourier synthesis of sinusoidal waves. Stability is assured only if all contributions over the entire frequency range are stable. Hence we can treat stability by examining the typical wave having frequency ω , and write

$$p' = \hat{p} e^{i\omega t} \quad (2.16)$$

where $k = (\omega - i\alpha)/a$ is the complex wavenumber. Substitute (2.16) into (2.14) and (2.15) to find

$$\frac{d^2 \hat{p}}{dz^2} + k^2 = - \frac{d}{dz} (\hat{u}\hat{w}) \quad (2.17)$$

$$\frac{d\hat{p}}{dz} = - (\hat{u}\hat{w}) \quad (z=0, L) \quad (2.18)$$

We shall give $\hat{u}\hat{w}$ explicitly below.

For stability, the imaginary part, α , must be negative. This represents a loss of acoustic energy. It is a property of this linear system that if the time averaged total energy is $\langle \delta \rangle$, proportional to the square of the pressure fluctuation, then the constant α is related to the rate of change of energy by

$$2\alpha = \frac{1}{\langle \delta \rangle} \frac{d\langle \delta \rangle}{dt} \quad (2.19)$$

Hence the problem comes down to calculating the decay or growth constant, α , due to the perturbations represented by the right hand sides of (2.14) and (2.15). This is done most directly by comparing the problem containing perturbations with the unperturbed problem. For the latter case, the mode shape \hat{p}_ℓ and wavenumber k_ℓ are governed by the equations

$$\frac{d^2 \hat{p}_\ell}{dz^2} + k_\ell^2 \hat{p}_\ell = 0 \quad (2.20)$$

$$\frac{d\hat{p}_\ell}{dz} = 0 \quad (z=0, L) \quad (2.21)$$

Multiply (2.17) by \hat{p}_ℓ , (2.20) by \hat{p} , subtract the two equations, and integrate over the length of the chamber, $0 \leq z \leq L$ to find

$$\int_0^L [\hat{p}_\ell \frac{d^2 \hat{p}}{dz^2} - \hat{p} \frac{d^2 \hat{p}_\ell}{dz^2}] dz + (k^2 - k_\ell^2) \int_0^L \hat{p} \hat{p}_\ell dz = - \int_0^L \frac{d}{dz} (\hat{u} \hat{w}) \hat{p}_\ell dz$$

Now integrate the first term by parts and use the boundary conditions (2.18) and (2.21) to produce the formula for k^2 :

$$k^2 = k_\ell^2 + \frac{1}{E_\ell^2} \int_0^L (\hat{u} \hat{w}) \frac{d\hat{p}_\ell}{dz} dz \quad (2.22)$$

where

$$E_\ell^2 = \int_0^L \hat{p} \hat{p}_\ell dz \approx \int_0^L \hat{p}_\ell^2 dz \quad (2.23)$$

Finally, we expand the product uw to obtain the explicit form of the flow turning loss. Assume that the mass flux inward is constant over the perimeter, so $w = m_b q / S_c$, and linearization proceeds as follows:

$$\begin{aligned} (uw)' &= (\bar{u} + u')(\bar{w} + w') - \bar{u}\bar{w} \\ &\cong \bar{u}w' + u'\bar{w} = (\bar{u}m'_b + u'm_b)(q/S_c) = (\hat{u}\hat{w})e^{iakt} \end{aligned}$$

Note that m'_b is the fluctuation of the mass flux inward at the boundary, while u' is the acoustic velocity parallel to the surface. When this formula is substituted into the last term of (2.22), u' and therefore \hat{u} , is, to the order treated here, replaced by the unperturbed acoustic velocity,

$$(uw)' \approx (\bar{u}\hat{m} + \hat{u}_l\bar{m}_b) \frac{q}{S_c} e^{i\bar{k}t} = (\hat{u}w)e^{i\bar{k}t} \quad (2.24)$$

The formula (2.22) is therefore

$$k^2 = k_l^2 + \frac{q/S_c}{E_l^2} \left[\int_0^L \bar{u}\hat{m}_b \hat{p}_l dz + \int_0^L \bar{m}_b \hat{u}_l \frac{d\hat{p}_l}{dz} dz \right] \quad (2.25)$$

The first term in brackets represents the response of the incoming flow to disturbances and will later be written in terms of the admittance function for the surface. It is the second term which represents the flow turning loss. For the unperturbed acoustic field, classical acoustics gives the result $\hat{u}_l = (i/\bar{\rho}\bar{a}k_l) d\hat{p}_l / dz$ so the integral can be written

$$\int \bar{m}_b \hat{u}_l \frac{d\hat{p}_l}{dz} dz = \frac{i}{\bar{\rho}\bar{a}k_l} \int_0^L \bar{m}_b \left(\frac{d\hat{p}_l}{dz} \right)^2 dz \quad (2.26)$$

Now $k^2 = (\omega - ia)^2 / \bar{a}^2 \approx (\omega/\bar{a})^2 - i(2a\omega/\bar{a})$, since for small perturbations, the terms in brackets in (2.25) are small, and therefore $a \ll \omega$. With only the flow turning loss included, (2.25) may now be written

$$\left(\frac{\omega}{a}\right)^2 - i\left(\frac{2a\omega}{\bar{a}^2}\right) = k_l^2 + i \frac{q/S_c}{E_l^2} \frac{1}{\bar{\rho}\bar{a}k_l} \int_0^L \bar{m}_b \left(\frac{d\hat{p}_l}{dz} \right)^2 dz \quad (2.27)$$

This formula can be split into real and imaginary parts, the real part showing that the frequency is unchanged by the perturbations, $\omega = \bar{a}k_l$, and the imaginary part giving the formula for the decay constant due to the flow turning loss,

$$a_{ft} = -\frac{q}{2S_c E_l^2} \int_0^L \frac{\bar{m}_b}{\bar{\rho}} \left(\frac{1}{k_l} \frac{d\hat{p}_l}{dz} \right)^2 dz \quad (2.28)$$

It is easier to remember this result if it is written in a different form. First, the constant E_l^2 is related to the time-averaged total

acoustic energy by the following:

$$\begin{aligned}
 \langle \delta \rangle &= \langle \iiint (\frac{1}{2} \rho |u'|^2 + \frac{1}{2} \frac{|p'|^2}{\rho a^2}) dV \rangle \\
 &= \langle S_c \int_0^L \frac{|p'|^2}{\rho a^2} dz \rangle \\
 &= \frac{1}{2} \frac{S_c}{\rho a^2} \int_0^L \hat{p}_\ell^2 dz \\
 &= \frac{1}{2} \frac{S_c E_\ell^2}{\rho a^2} \tag{2.29}
 \end{aligned}$$

We have used the fact that the time-averaged kinetic and potential energies are equal. Now for the unperturbed acoustic field, with phases measured with respect to the pressure, so \hat{p}_ℓ is real, we have

$$\left(\frac{d\hat{p}_\ell}{dz}\right)^2 = \left|\frac{d\hat{p}_\ell}{dz}\right|^2 = |i\bar{\rho}\omega\hat{u}_\ell|^2 = (\bar{\rho}\bar{a}k_\ell)^2 |\hat{u}_\ell|^2$$

Thus the integral in (2.28) can be written, with $\bar{m}_b = \bar{\rho}\bar{u}_b$,

$$\int_0^L \bar{u}_b \left(\frac{1}{k_\ell} \frac{d\hat{p}_\ell}{dz}\right)^2 dz = \int_0^L \bar{u}_b (\bar{\rho}\bar{a})^2 |\hat{u}_\ell|^2 dz$$

After this relation and (2.29) have been substituted into (2.28) we have

$$2a_{ft} = - \frac{1}{\langle \delta \rangle} \int_0^L \bar{u}_b \left(\frac{1}{2} \bar{\rho} |\hat{u}_\ell|^2\right) dS_b \tag{2.30}$$

where $dS_b = qdz$ is the element of area on the lateral boundary.

The time-averaged value of the acoustic kinetic energy density is $\bar{\rho} |\hat{u}_\ell|^2 / 4$, the factor 1/4 composed of 1/2 from the definition of the kinetic energy and 1/2 from the time averaging. Thus the integral represents twice the time-averaged rate at which the incoming

flow acquires acoustic kinetic energy. It is twice because energy is dissipated (i.e. is associated with entropy production) at exactly the same rate at which the incoming flow gains its acoustic kinetic energy. Hence, the acoustic field within the chamber suffers a fractional rate of energy loss, represented by (2.30) which is twice the rate at which mechanical energy is gained by the gas flowing in at the boundary. This marvelous factor of two is explained in Ref. 15 for a problem of elementary mechanics and is verified by computation of the rate at which entropy is produced (Ref. 1).

The experimental work now to be described is intended to provide values of a_{FT} which will then be compared with the values calculated with the formula (2.28).

2.2 Analysis of the Apparatus

The resonance tube is sketched in Figure 1. Much of the hardware is that used in earlier work (Refs. 4 and 5) to determine the influence of the exhaust vent on acoustic waves. The new portions are the cylindrical porous tubes - the "lateral flow elements" - installed as a means of introducing flow in at the lateral boundary. Thus, flow in the tube enters through both the pistons at the ends, which serve to excite acoustic waves, and through the cross flow elements. In Figure 2, the various flow and geometrical parameters are defined.

In all the tests reported here, the resonance tube was driven, in its fundamental mode, by the oscillating pistons. The acoustic pressure then has a node at the center and is maximum at the ends of the tube. When the frequency of the driving mechanism is swept through the resonant frequency, the amplitude of the pressure oscillation

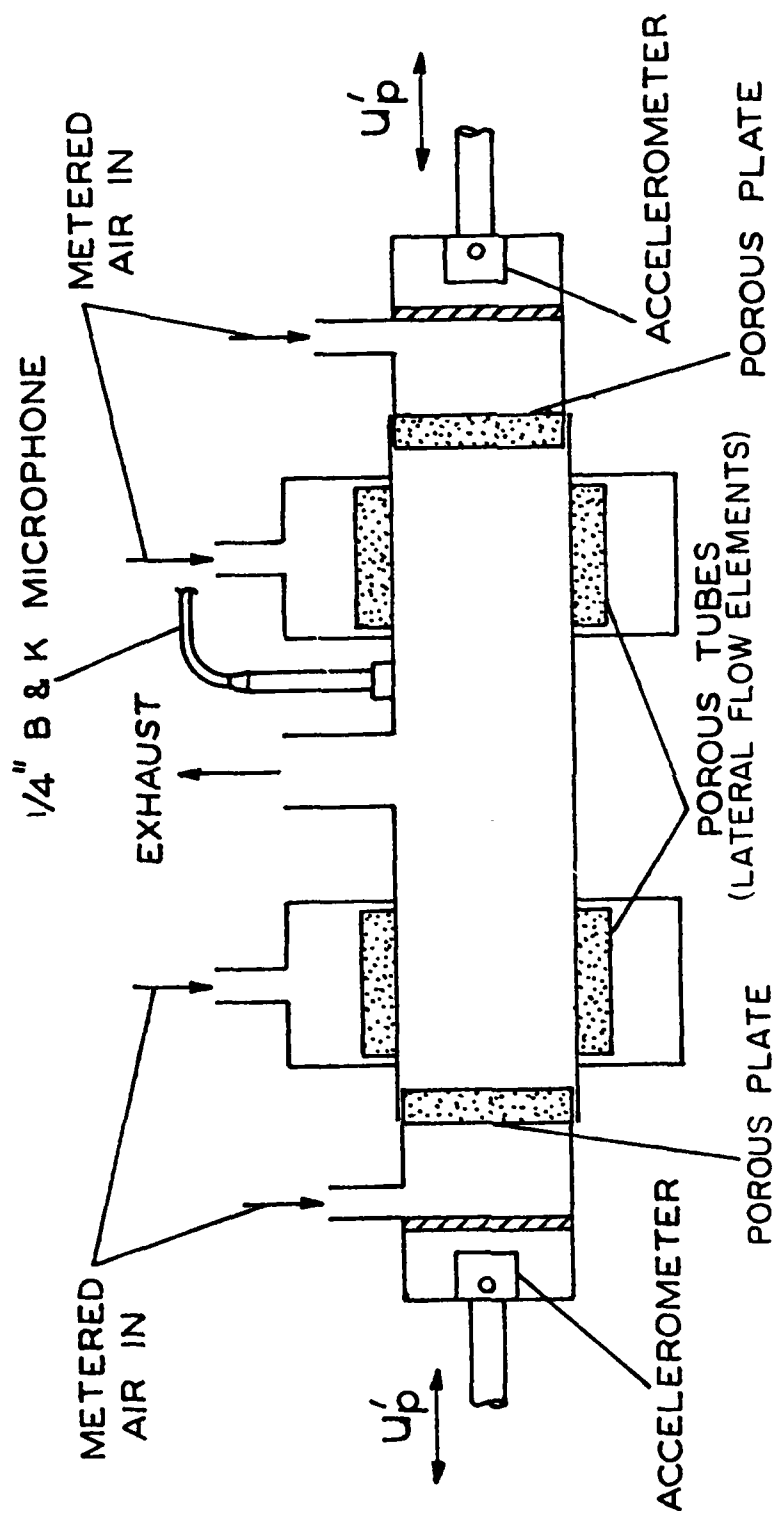
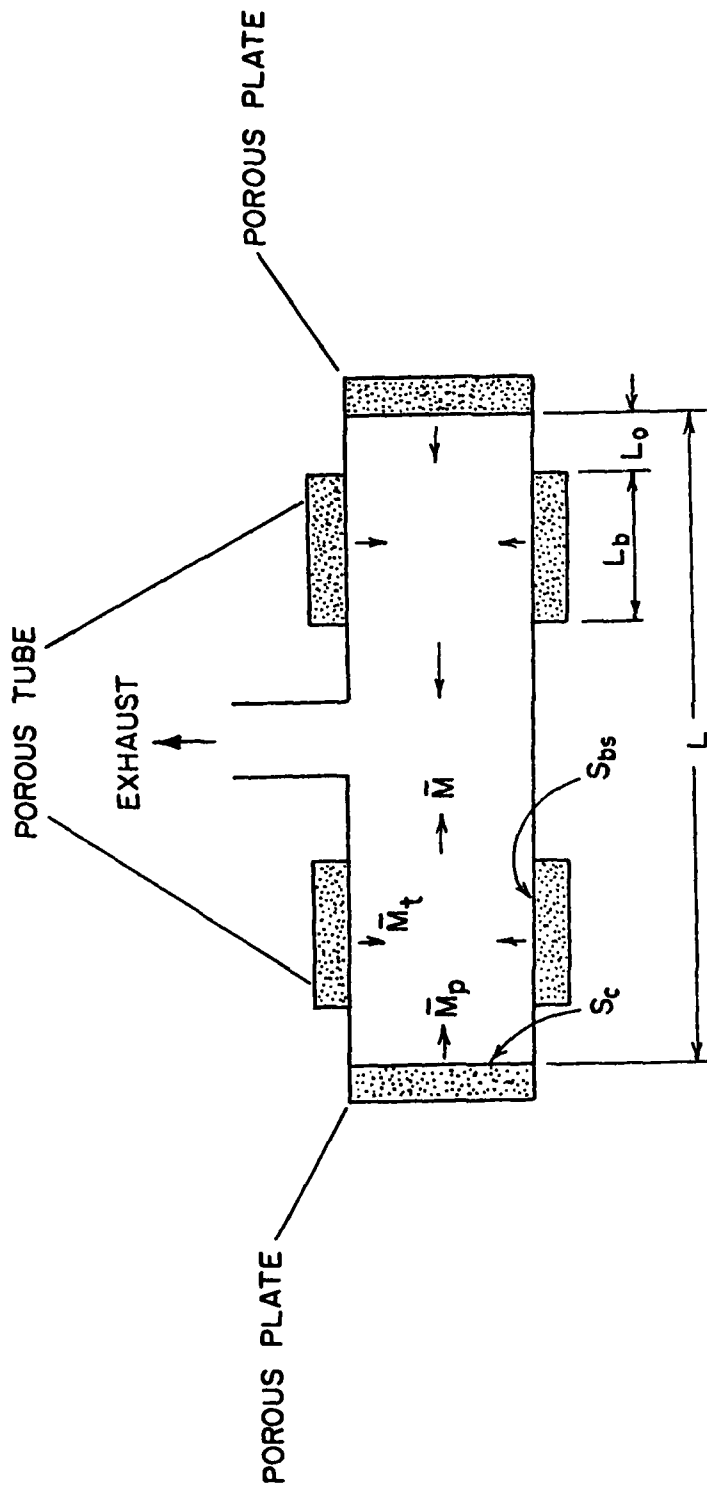


Figure 1. Resonance Tube with Piston Drivers and Lateral Flow Elements



$$f = \alpha_0 / 2L$$

$$\bar{M} = \bar{M}_p + \bar{M}_t \frac{S_{bs}}{S_c}$$

$$\beta = 2L_b / L$$

$$\beta_o = 2L_o / L$$

Figure 2. Sketch Showing Definitions for the Resonance Tube

describes a bell-shaped curve with maximum very closely at the resonant frequency. Thus the system appears to behave as a simple mass/spring/dashpot system.

It is therefore possible to relate the width of the resonance curve to the losses in the system. The analysis supporting that assertion has been given in Ref. 4 and need not be repeated here. The main result is that if $\Delta\omega$ is the width of the curve at the "half-power points", the frequencies at which the amplitude is reduced by $1/\sqrt{2}$ from its maximum value, then the net value of the attenuation coefficient is

$$a = \frac{1}{2} \Delta\omega_{1/2} \quad (2.31)$$

This formula is the basis for the testing procedure. Because a is the sum of many contributions, a sequence of tests is necessary to determine the separate parts until finally the desired quantity, in this case a_{ft} , can be determined.

The sequence of tests required is the same as that used in Refs. 4 and 5 to determine the influence of the vent, with one additional test to obtain the contribution from the lateral flow. From linear analysis of the configuration shown in Figure 1, the decay constant* a consists of five parts,

$$a = a_p + a_t + a_{ft} + a_v + a_d \quad (2.32)$$

where the terms on the right hand side represent the following contributions:

a_p : attenuation constant associated with the admittance and flow for the faces of the piston drivers;

$$a_p = 4f(A_p^{(r)} + \bar{M}_p) \quad (2.33)$$

*In the remainder of this report we use the sign convention that energy losses are represented by positive values of the decay constant a .

a_t : attenuation constant associated with the admittance and flow
for the cylindrical lateral flow elements;

$$a_t = 4f(A_t^{(r)} + \bar{M}_t) C_\ell \frac{S_{bs}}{S_c} \quad (2.34)$$

a_{ft} : attenuation constant associated with the flow turning losses, to
be determined;

a_v : attenuation constant associated with the influence of the exhaust
vent;

a_d : attenuation constant associated with other losses, mainly radiation
and viscous losses at the lateral boundary.

The formula (2.33) is a direct consequence of the one-dimensional analysis, Ref. 1. In subsequent work, Refs. 13 and 17, the result (2.34) was obtained in an analysis of a variable area T-burner; C_ℓ is a geometrical factor accounting for the finite extent of the region through which flow enters at the lateral boundary. For the single configuration tested in the present work, $C_\ell = 0.51$.

All of the terms on the right hand side of (2.32) are determined experimentally. The admittance functions, $A_p^{(r)}$ and $A_t^{(r)}$ are measured by using an impedance tube, and the Mach numbers M_p and M_t are found by measuring the flow rates through the porous samples. We have chosen experimental conditions such that the attenuation constant due to the vent can be taken from our earlier work, Refs. 4 and 5. Finally, a_d is determined as part of the present tests with the resonance tube used to obtain a_{ft} .

17. Culick, F.E.C. "Linear Analysis of One-Dimensional Oscillations in a Variable Area T-Burner", 9th JANNAF Combustion Meeting (1972).

2.3 Description of the Apparatus and Instrumentation

2.3.1 Cold Flow Resonance Tube

Figure 1 shows the configuration of the resonance tube. The tube itself is made of brass, having inside diameter equal to 3.81 cm, and 0.32 cm wall thickness; for the tests at 445 Hz, the length is 38.65 cm. The circular exhaust vent is of brass, having 0.32 cm wall thickness, inside diameter equal to 1.27 cm, and is 3.30 cm long. It has a plug, machined so that when inserted the vent is closed by a surface smoothly fitting the inside surface of the main resonance tube. Further details of the tube and the dimensions are given in Figure 2. The dimensions were chosen to give $\beta = 0.22$, $\beta_0 = 0.38$, $S_{bs}/S_c = 4.53$ and constant axial flow Mach number, for flow through the porous pistons,
 $\overline{M}_p = 4.43 \times 10^{-1}$.

The lateral flow was introduced through two porous tubes having inside diameter equal to 3.81 cm and fitted in manifolds. Each manifold has three series of orifices which help distribute the flow uniformly around the periphery of the tube.

The instrumentation used has been described in Refs. 3-5, and illustrated in Figure 3. The major addition here is the cross-flow supply and the related monitoring instrumentation which is similar to that for the axial flow supply and its monitoring instrumentation. To avoid interference from airborne noise and local reflections within the room, the resonance tube was placed in an anechoic chamber. The air supply and the instrumentation were located outside the chamber.

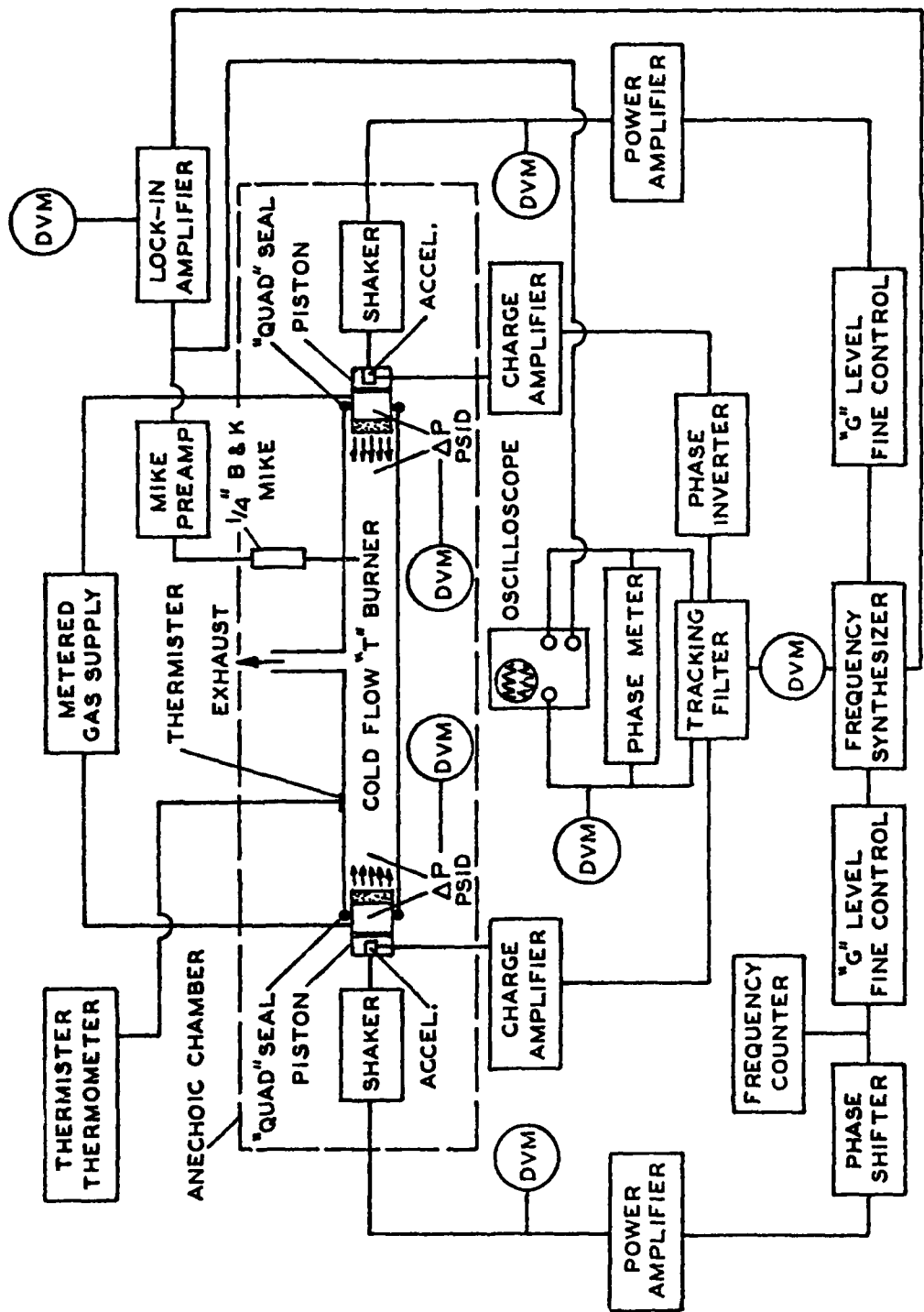


Figure 3. Schematic Diagram of the Resonance Tube and Associated Apparatus

2.3.2 Impedance Tube

The impedance tube is a modification of the Brüel & Kjaer (B&K) standing wave apparatus. A brass tube, 100 cm long having inside diameter of 3.81 cm is fitted to the speaker assembly. At one end the threaded cup type of sealed fixture is rigidly mounted to the tube; see Figure 4. This fixture accommodates various porous plates whose impedance is to be determined. The tube and ancillary apparatus are shown in Figure 5. The detailed description of the equipment required to drive the waves in the tube and the instrumentation for measuring the waves in the tube is provided in Refs. 2-5.

2.4 Calibration Procedures and Estimates of Errors

The flow turning losses to be determined are small and the indirect method of measuring them requires considerable care and good instrumentation to achieve the required accuracy. References 3 and 4 contain detailed descriptions of the calibration of the gas supply system, extended here for the lateral flow; calibration of microphones and sources; and estimates of errors for both the resonance and impedance tubes. However, the major source of error in the present work seems to be associated with measurement of the admittance functions of the circular tubes, which required extrapolation of the admittance function data for various porous plates. This problem is discussed in the following section.

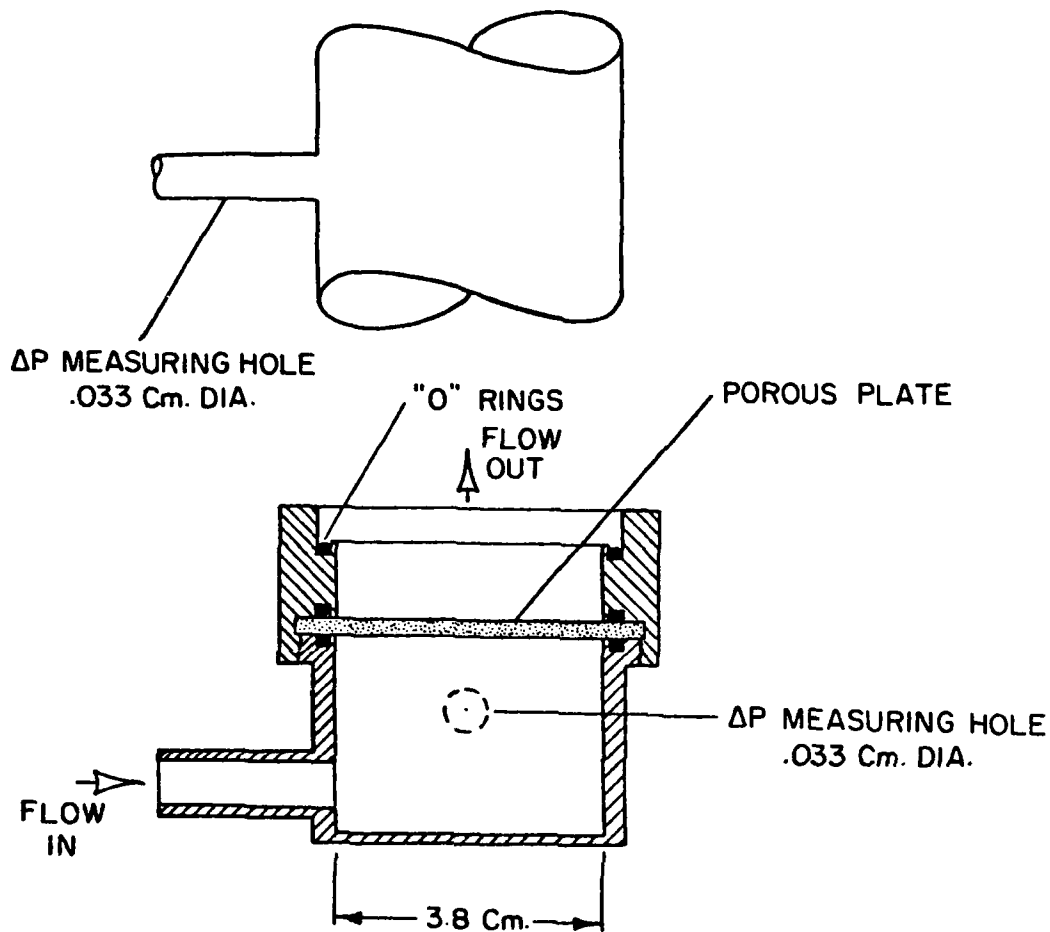


Figure 4. End Fixture for the Impedance Tube

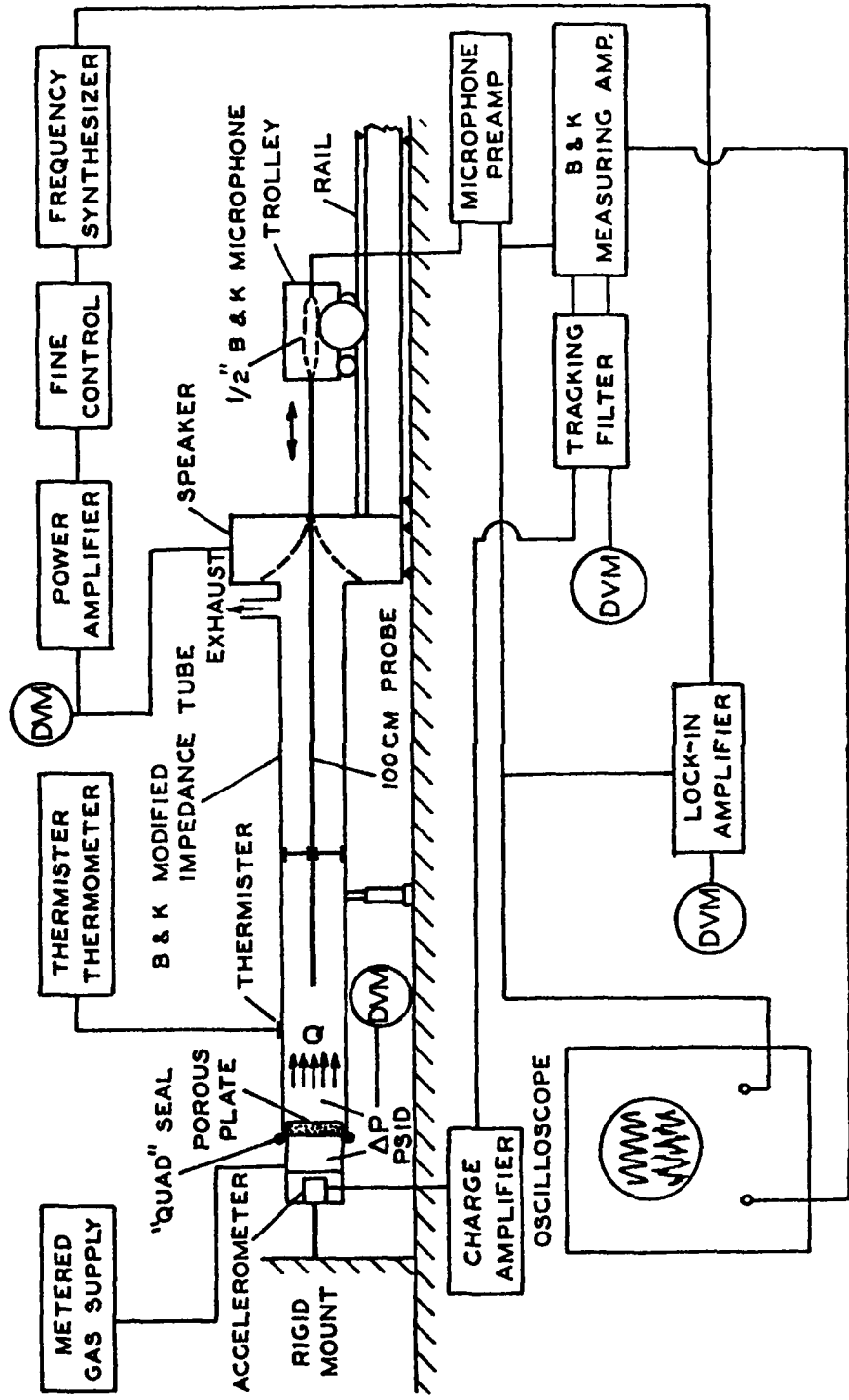


Figure 5. Schematic Diagram of the Impedance Tube and Associated Apparatus

2.5 Measurement of the Admittance Functions for Cylindrical Porous Tubes

This part of the program became a much larger problem than we had foreseen. There is one essential difficulty, namely measuring the admittance or impedance of a curved surface. An impedance tube is useful for measuring the characteristics of flat surfaces only. Intrinsic constraints set by the geometry prevent direct measurements for a curved surface by directing waves upon the sample and measuring the reflections.

For application to the apparatus used here we require the response of the curved elements to pressure fluctuations imposed by waves travelling parallel to the surface. The admittance function is required for conditions when mean flow is entering through the surface. A direct measurement is conceivable. The sample may be mounted in a tube at one end of which an acoustic driver excites travelling waves. The tube is terminated at the other end with an anechoic vent through which both the mean flow and the acoustic waves are exhausted. Measurement of the pressure on the upstream and downstream sides of the porous sample should then give the reduction of amplitude in the travelling wave and therefore a direct determination of the energy change of the wave. The energy change (loss) can be theoretically related to the admittance function of the lateral surface.

There are several difficulties, the main one being the very small losses involved. The influence of the surface, represented by its admittance function, is not substantially different from apparent losses caused by other interactions with the non-uniform flow field issuing

from the curved sample. That is, there are necessarily gradients of the average velocity in the axial direction along the tube. These produce internal losses and scattering of the acoustic waves. Furthermore, it is extraordinarily difficult to construct an anechoic termination sufficiently effective for our purposes. For reasonable lengths of lateral surfaces, the changes in amplitude of the travelling waves are so small as to be practically very difficult to measure with reproducible precision in this kind of arrangement. Because of reflections from the termination of the tube, waves travelling in both directions are present, obscuring the data. And finally, the damning characteristic - the flow turning loss is necessarily present.

Consequently, we have no choice* but to measure the admittance function for a flat surface with waves incident in the normal direction and assume that the results are applicable to a curved surface exposed to waves moving in the parallel direction. An unavoidable practical difficulty, unforeseen, then arose: we have been unable after considerable effort and time to obtain flat samples having the same porosity - and therefore flow characteristics - as the curved samples. It happens to be a consequence of the manufacturing processes that the cylindrical tubes have much lower porosity than any standard flat samples.

We have therefore made the additional assumption that the acoustical properties of the porous plates are defined uniquely by the steady-flow characteristic, flow rate as a function of pressure drop. The admittance functions for the curved surfaces (cylindrical lateral flow elements) were determined by extrapolation in the following way.

Three porous plates, referred to as grades F, G and H, were

*In order to minimize costs, we used as much as possible equipment from the preceding work (Ref. 4); we therefore continued using the circular resonance tube.

obtained from the manufacturer, Pall Western Company. These were first calibrated, by measuring the variation of flow rate with pressure drop across a plate. The results, and the results for the two lateral flow elements are shown in Figure 6.

The admittance functions for the three flat samples were then measured, using an impedance tube as described in Refs. 3-5. Repeated tests were made in order to determine the experimental uncertainty. The data for the real part of the admittance function for the three plates are given in Table 1 and plotted in Figures 7-9 for the frequency equal to 445 Hz. The solid lines in the figures are least squares fits to the data. Table 2 is a summary of the data for the three flat samples. These data were then plotted, as shown in Figure 10, as the real part of the admittance versus pressure drop for several values of the average Mach number of flow through the plates.

We then make the crucial assumption that the results may be extrapolated, as indicated in Figure 10. The real part of the admittance for a cylindrical element is supposed to lie on the same line of constant Mach number (or flow speed, or flow rate) but at the value of pressure drop measured and shown in Figure 6. Table 3 is a summary of values of the real parts of the admittance functions for the two lateral flow elements. These results are plotted in Figures 11 and 12.

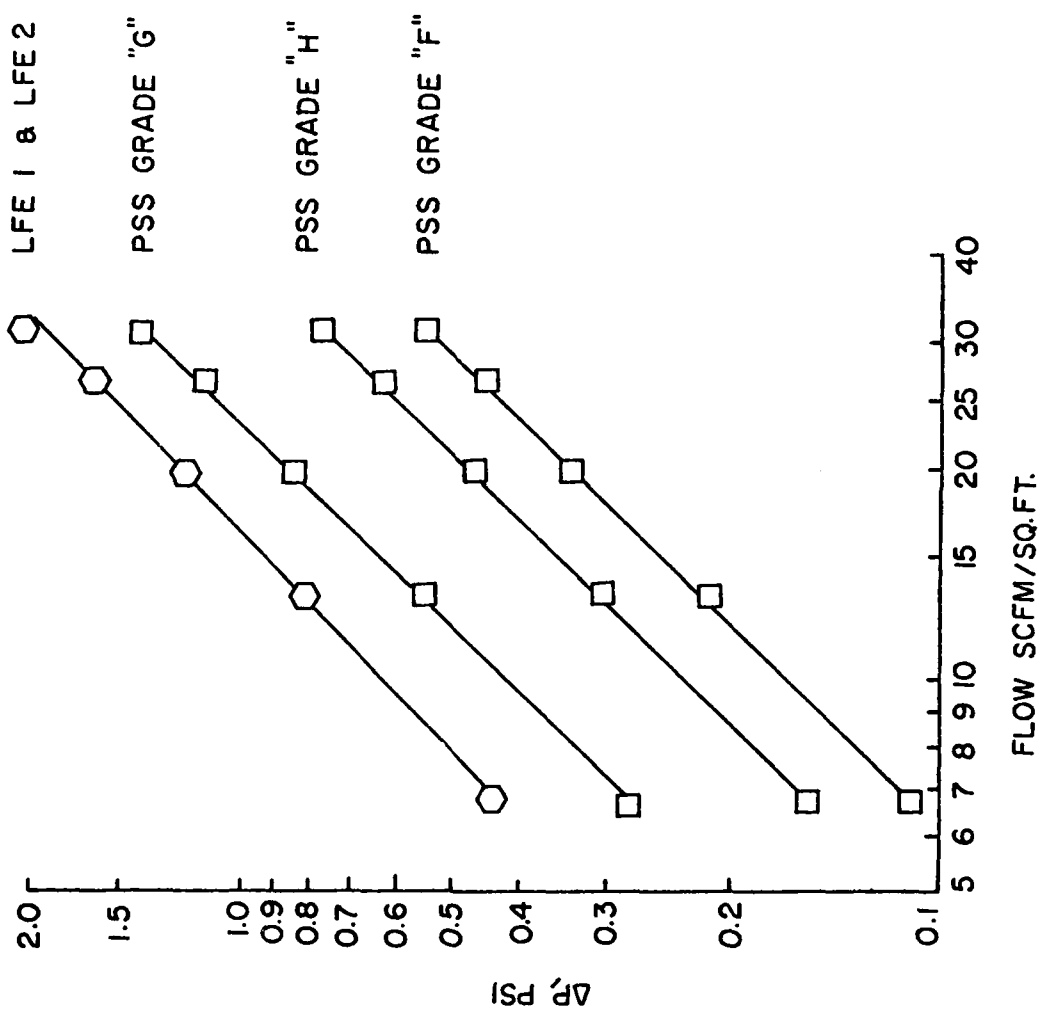


Figure 6. Flow Characteristics of Porous Flat Platen and Cylindrical Samples

TABLE 1

Data for the Admittance Functions of the Porous Plate

Grade F ($f = 445$ Hz)

$\bar{M}_b \times 10^4$	$A_b^{(r)} \times 10^2$	$\bar{A}_b^{(r)} \times 10^2$	$\sigma \times 10^6$
0	2.4984		
	2.4405	2.4724	240
	2.4783		
0.97	2.2246		
	2.2379	2.2230	129
	2.2064		
1.95	1.9224		
	1.9262	1.9103	199
	1.8822		
2.92	2.2200		
	2.1502	2.1926	320
	2.2275		
3.90	2.0549		
	2.0055	2.0237	222
	2.0106		
4.87	2.2569		
	2.2211	2.2289	204
	2.2088		

TABLE 1 (Cont'd.)

Data for the Admittance Functions of the Porous Plate

Grade G ($f = 445$ Hz)

$\bar{M}_b \times 10^4$	$A_b^{(r)} \times 10^2$	$\bar{A}_b^{(r)} \times 10^2$	$\sigma \times 10^6$
0	0.6719		
	0.6079	0.6488	290
	0.6665		
0.97	0.6939		
	0.6953	0.6985	55
	0.7062		
1.95	0.7060		
	0.6854	0.6911	106
	0.6819		
2.92	0.6784		
	0.6861	0.6839	39
	0.6872		
3.90	0.7083		
	0.6935	0.6845	240
	0.6516		
4.87	0.6295		
	0.6012	0.6104	135
	0.6006		

TABLE 1 (Cont'd.)

Data for the Admittance Functions of the Porous Plate

Grade H ($f = 445$ Hz)

$\overline{M}_b \times 10^4$	$A_b^{(r)} \times 10^2$	$\overline{A}_b^{(r)} \times 10^2$	$\sigma \times 10^6$
0	1.2504	1.2408	252
	1.2657		
	1.2063		
0.97	1.2340	1.2370	40
	1.2344		
	1.2627		
1.95	1.3958	1.3860	114
	1.3909		
	1.3702		
2.92	1.3283	1.3538	180
	1.3657		
	1.3673		
3.90	1.4445	1.4380	63
	1.4400		
	1.4294		
4.87	1.4373	1.4622	225
	1.4918		
	1.4576		

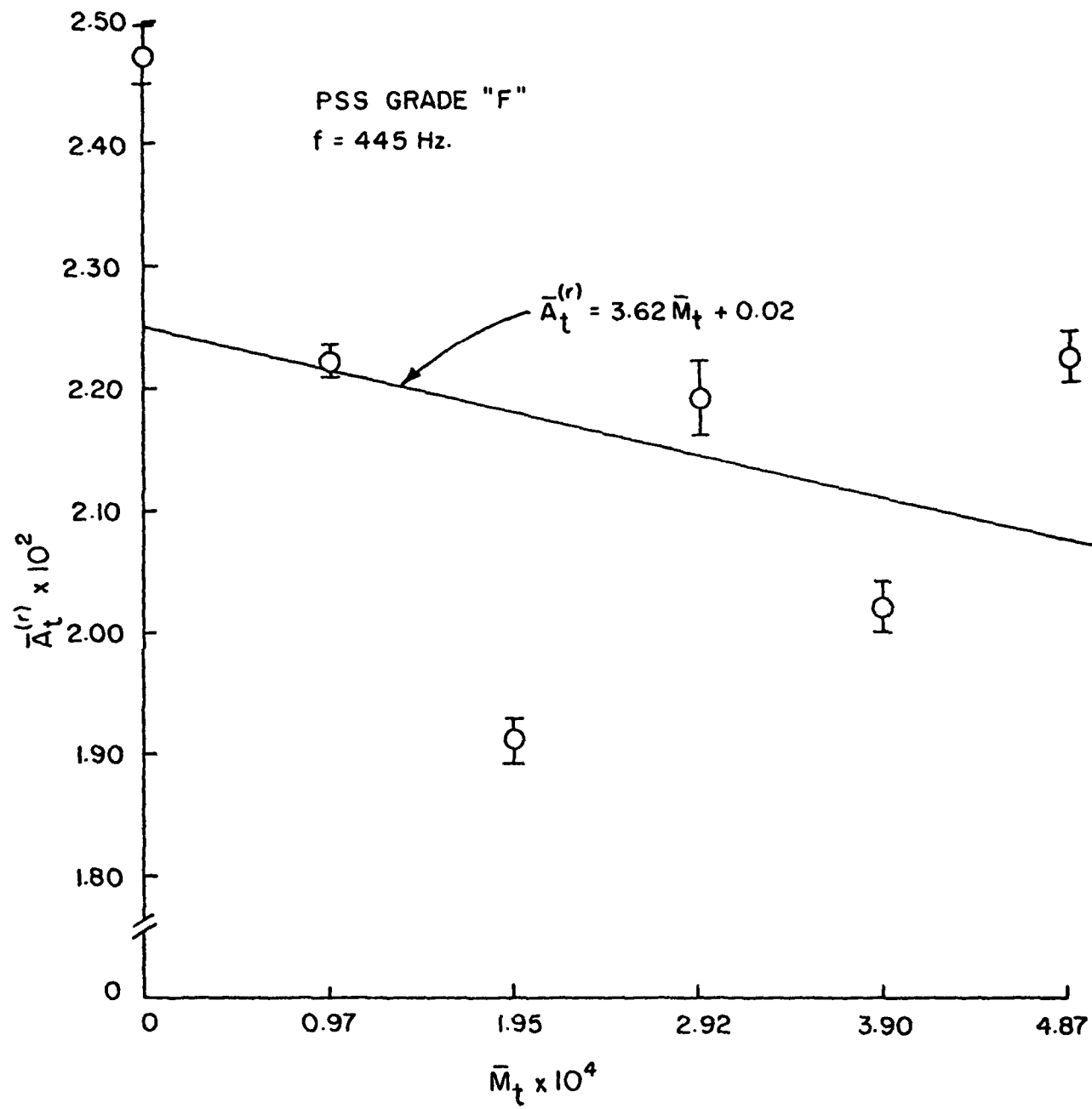


Figure 7. Real Part of the Admittance Function, Plate F

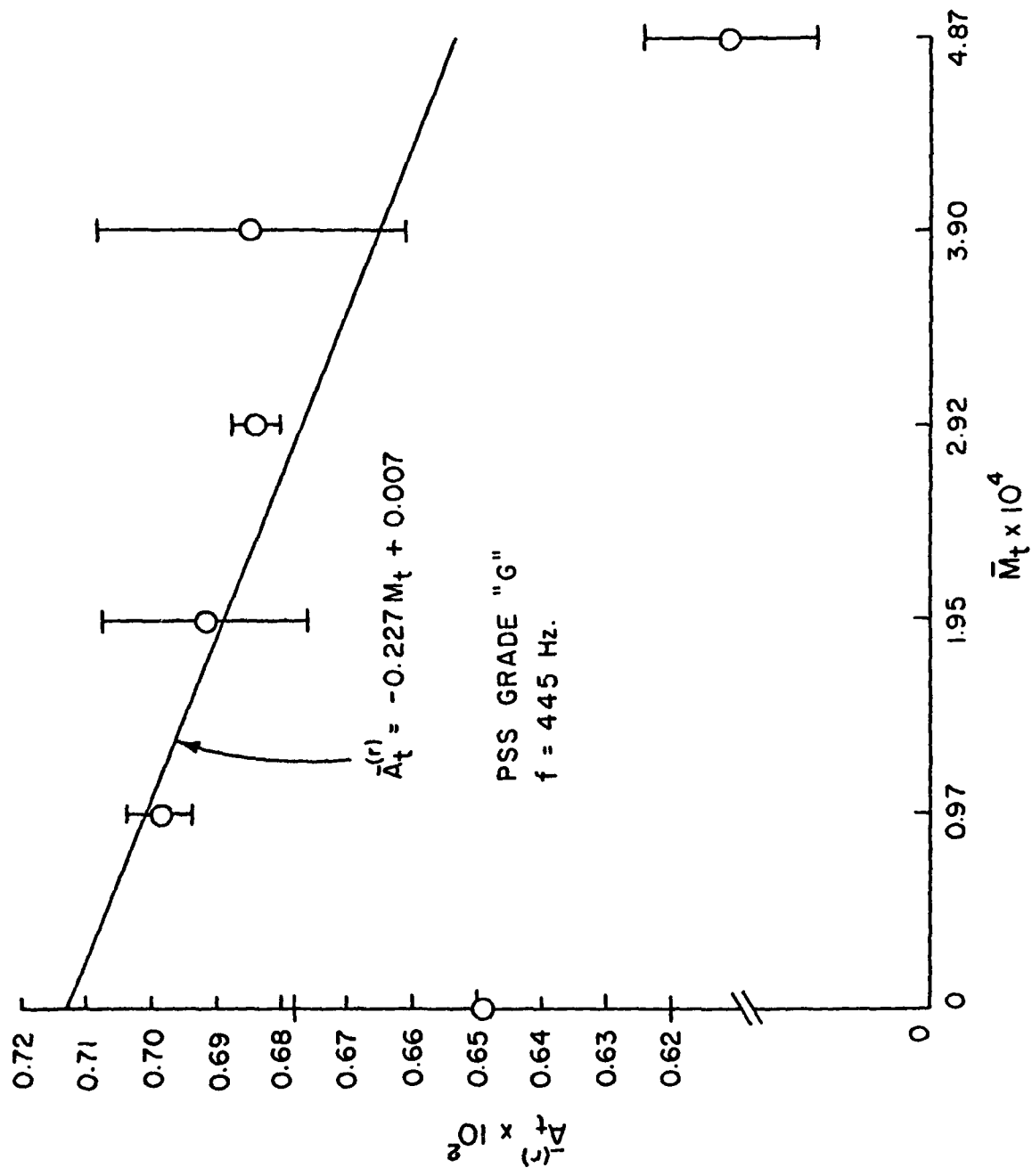


Figure 8. Real Part of the Admittance Function, Plate G

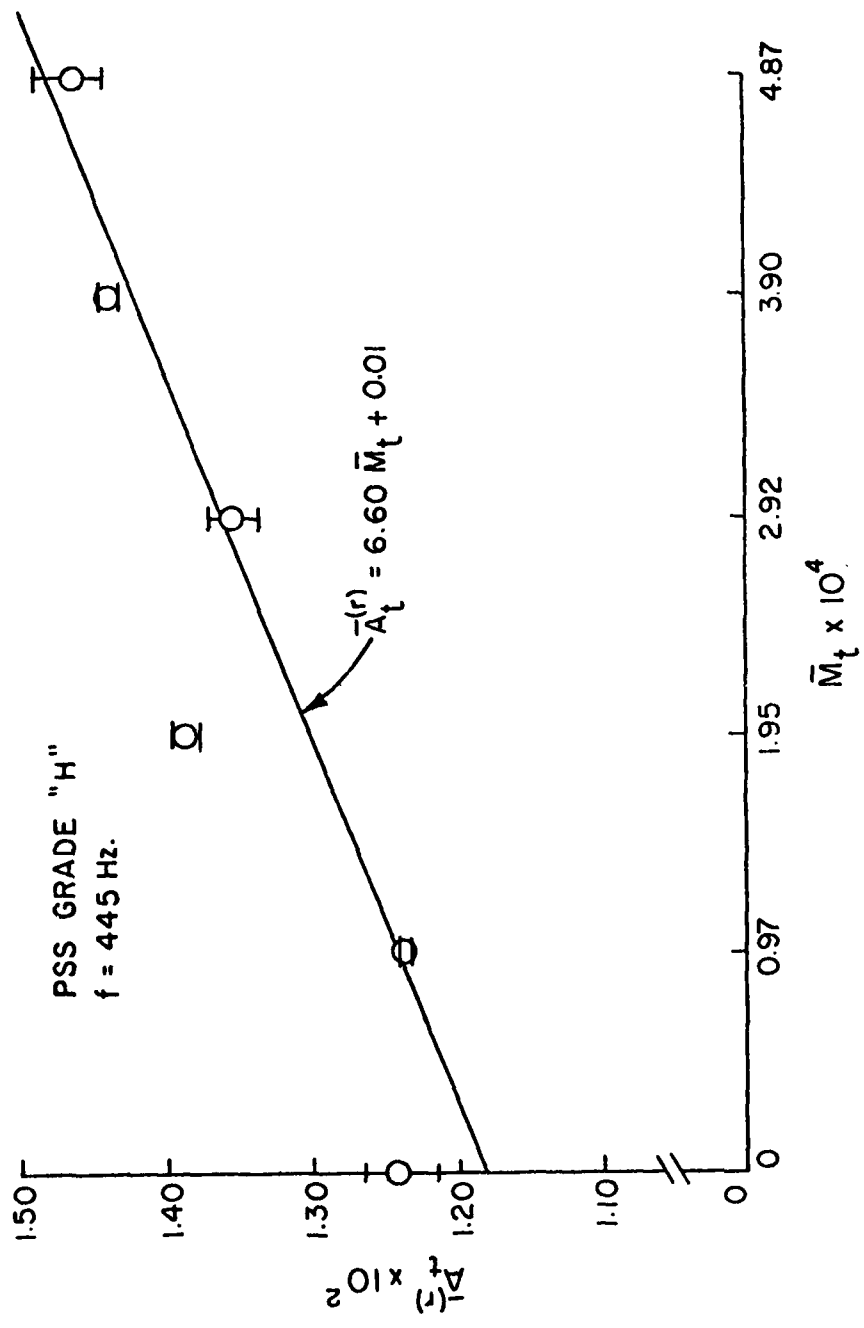


Figure 9. Real Part of the Admittance Function, Plate H

TABLE 2
Summary of Results for the Porous Plates

Flow Mach No. $\frac{M_t}{M_t} \times 10^4$	PSS Grade F			PSS Grade G			PSS Grade H		
	$\Delta P, \text{Psi}$	$\bar{A}_t^{(r)} \times 10^2$	$\sigma \times 10^5$	$\Delta P, \text{Psi}$	$\bar{A}_t^{(r)} \times 10^2$	$\sigma \times 10^5$	$\Delta P, \text{Psi}$	$\bar{A}_t^{(r)} \times 10^2$	$\sigma \times 10^5$
0	0	2.4724	24	0	0.6488	29	0	1.2408	25
0.97	0.110	2.2230	13	0.279	0.6985	6	0.155	1.2370	4
1.95	0.214	1.9103	20	0.548	0.6911	11	0.302	1.3860	11
2.92	0.335	2.1926	32	0.853	0.6839	4	0.468	1.3538	18
3.90	0.445	2.0237	22	1.146	0.6845	24	0.627	1.4380	6
4.87	0.549	2.2289	20	1.411	0.6104	14	0.768	1.4622	23

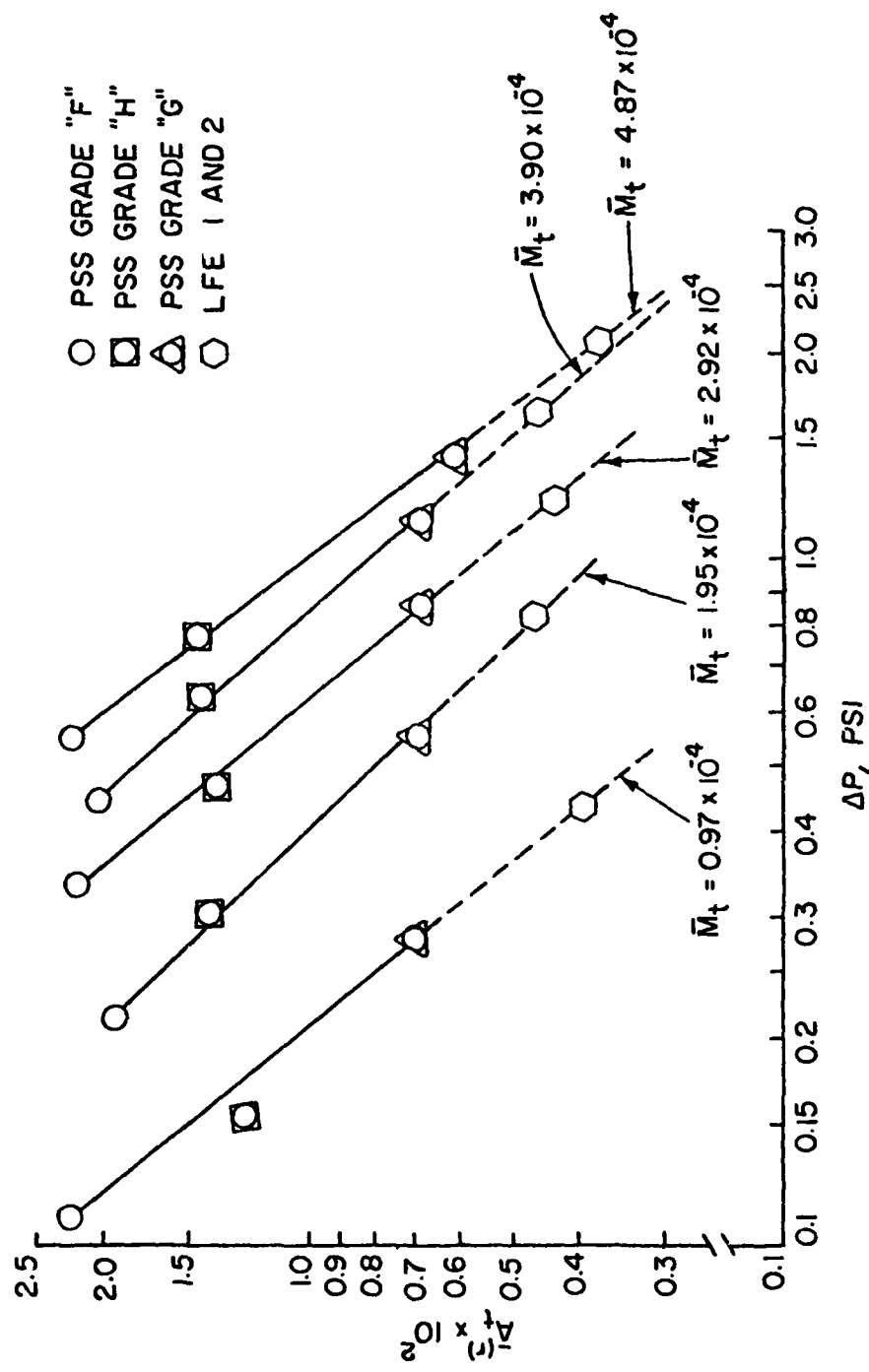


Figure 10. Real Parts of the Admittance Functions versus Pressure Drop

TABLE 3
Final Results for the Admittance Functions
for the Lateral Flow Element

Flow Mach No. $\bar{M}_t \times 10^4$	<u>CFE 1</u> $A_{t1}^{(r)} \times 10^2$	$\sigma_\ell \times 10^6$	Flow Mach No. $\bar{M}_t \times 10^4$	<u>CFE 2</u> $A_{t2}^{(r)} \times 10^2$	$\sigma_\ell \times 10^6$
0	0.536	610	0	0.538	590
0.97	0.388	135	0.97	0.385	133
1.95	0.453	23	1.95	0.449	23
2.92	0.434	20	2.29	0.427	20
3.90	0.459	17	3.90	0.459	17
4.87	0.363	11	4.87	0.360	11

Least squares fit to these data:

$$A_{t1}^{(r)} = (.00536 \pm .00061) + (-3.277 \pm 1.883) \bar{M}_t$$

$$A_{t2}^{(r)} = (.00538 \pm .00059) + (-3.143 \pm 1.825) \bar{M}_t$$

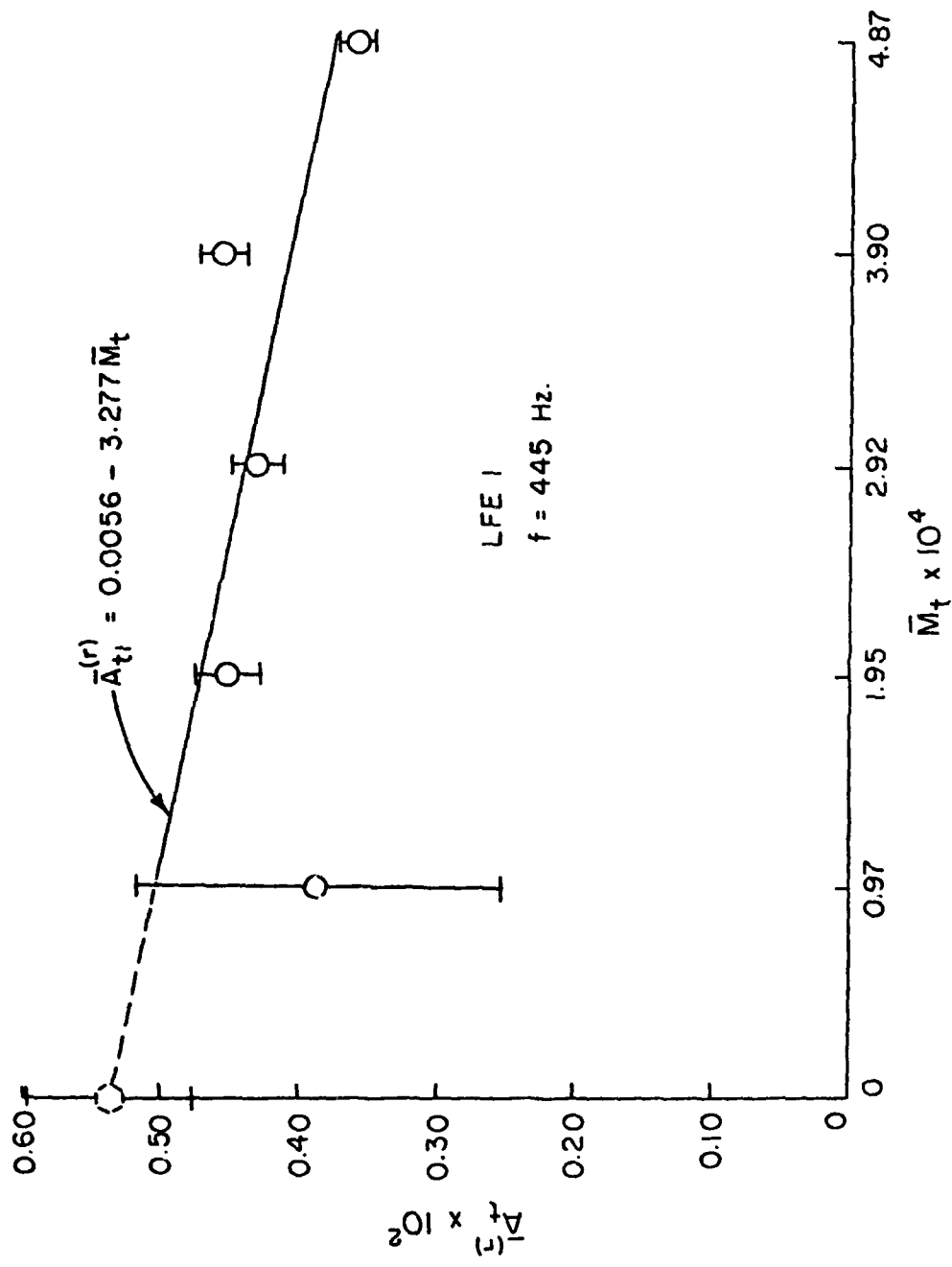


Figure 11. Admittance Function Measured for Lateral Flow Element 1

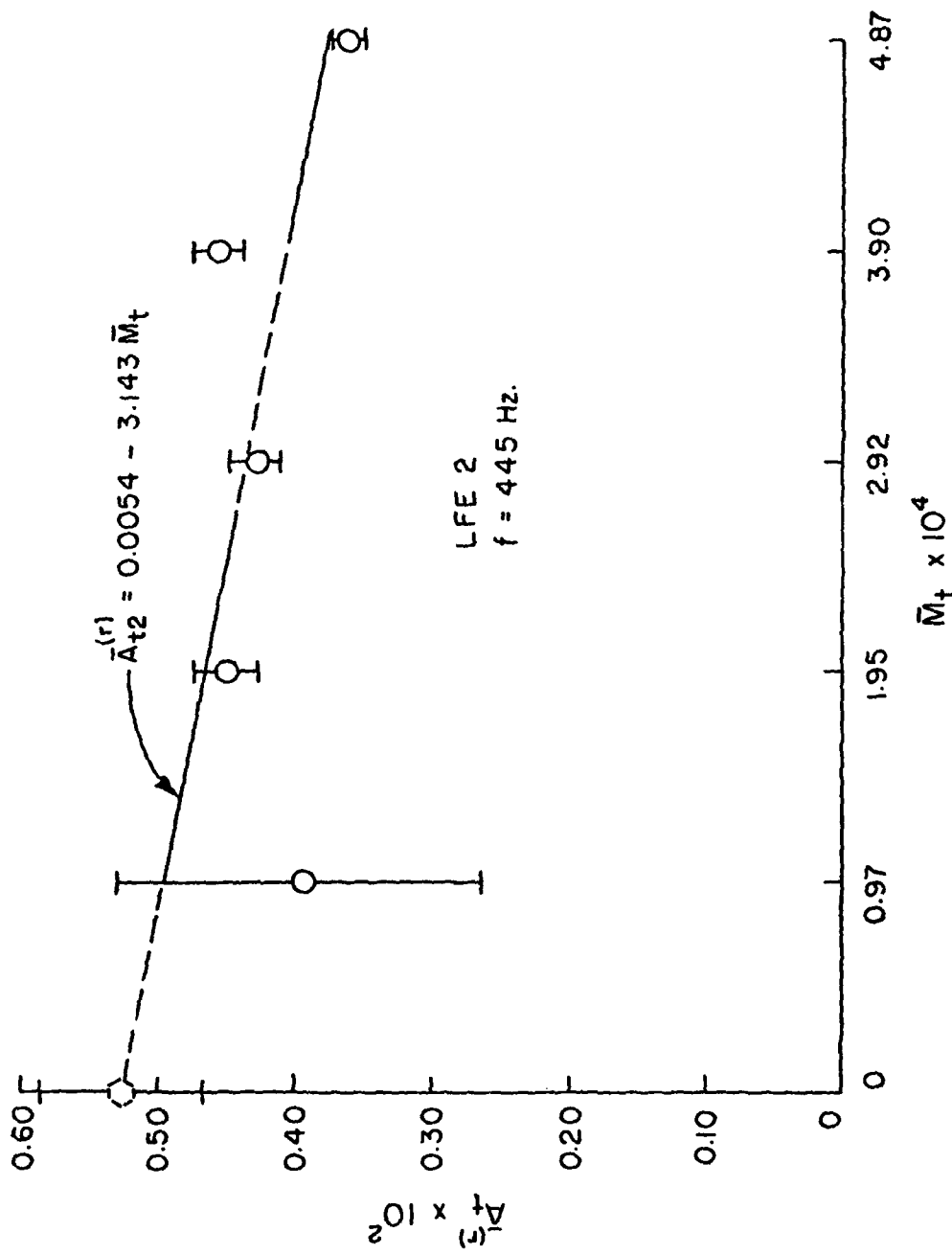


Figure 12. Admittance Function Measured for Lateral Flow Element 2

2.6 Measurements of the Flow Turning Loss

With the results of Refs. 3-5 and the preceding section, we have the values of a_p , a_t and a_v in eq. (2.32), all as functions of the appropriate Mach number. Before a_{ft} can be measured it is necessary to measure the contribution from other losses, denoted by a_d . The series of tests carried out to achieve this result also serve as an important check of the experimental procedures by providing a means of assessing the self-consistency of the data. It is during this portion of the experimental work that many faults with the apparatus have been found and corrected (see also Refs. 3 and 4). We discuss here only the final series of tests.

Table 4 contains data taken for three series of tests performed at each Mach number \bar{M}_t for the average flow through the lateral boundary. The average values and standard deviations of both the net attenuation constant and resonance frequency are also given.

Figure 13 shows the variation of the average values of the net attenuation constant with respect to the mean cross-flow Mach number \bar{M}_t at the resonance frequency near 445 Hz. The solid line in the figure represents the least squares fit, assuming that \bar{a}_{net} varies linearly with \bar{M}_t .

Two series of tests, as shown in Table 4, were carried out with no flow: one series with the vent open and one with the vent closed. The difference in the attenuation constants should represent the effects of radiation losses. Here, the difference is $-0.01 \pm 0.02 \text{ sec}^{-1}$, representing a small average gain, although it could (as it should be) be a loss within the experimental uncertainty.

TABLE 4

Data for the Attenuation Coefficient with Lateral Flow

(1/2" vent, $f = 445$ Hz.)

$\bar{M}_p \times 10^4$	$\bar{M}_t \times 10^4$	a_{net} (sec $^{-1}$)	f Hz	\bar{a}_{net} (sec $^{-1}$)	σ_a (sec $^{-1}$)	f Hz	σ_f Hz
0	0	63.99	446.00	64.21	0.16	446.40	0.28
		64.27	446.60				
		64.36	446.50				
4.43	0	64.22	445.90	64.25	0.03	445.97	0.05
		64.24	446.00				
		64.30	446.00				
4.43	0.97	64.69	445.40	65.87	0.14	445.80	0.50
		65.90	445.50				
		66.03	446.50				
4.43	1.95	66.21	446.20	66.50	0.21	447.03	0.69
		66.69	447.90				
		66.61	447.00				
4.43	2.92	66.65	445.00	66.53	0.13	445.33	0.24
		66.60	445.50				
		66.35	445.50				
4.43	3.90	66.79	446.00	66.94	0.12	446.33	0.24
		67.08	446.50				
		66.95	446.50				
0	0 (vent closed)	64.04	445.00	64.22	0.13	445.33	0.24
		64.25	445.50				
		64.35	445.50				

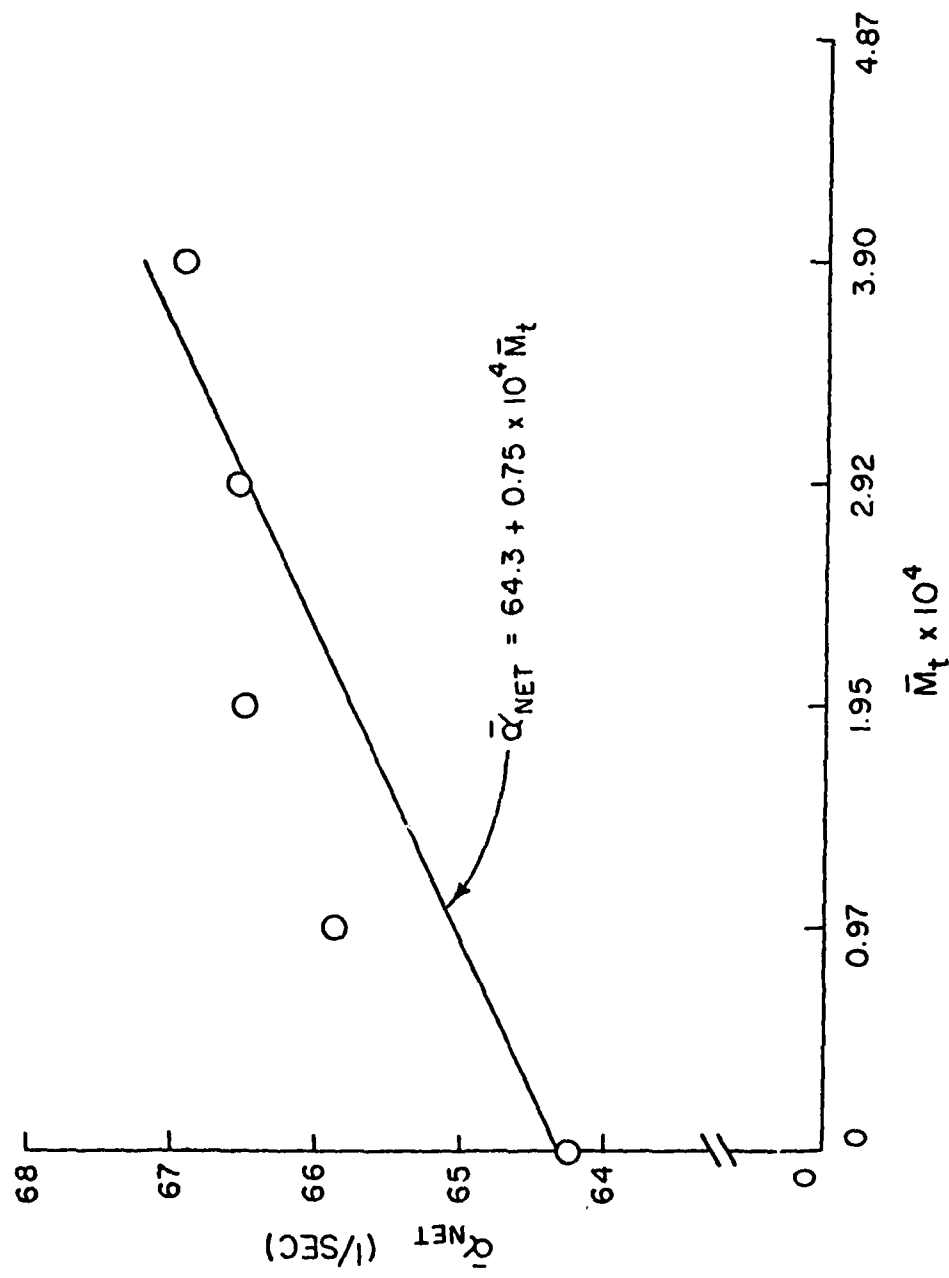


Figure 13. Net Attenuation Coefficient Measured with Lateral Flow

Because of the experimental difficulties discussed at greater length in Refs. 3 and 4, the numerical value of the measured radiation loss is necessarily uncertain.

The consistency of the data and losses through the lateral boundary have been determined with no flow and the vent closed, using the equation

$$a = a_p + a_t + a_d \quad (2.35)$$

The value of a was measured, and with a_p and a_t given by previous results, we have found

$$a_d = 14.90 \pm 2.75 \text{ sec}^{-1} \quad (2.36)$$

The theoretical value for viscous and heat transfer losses calculated according to classical formulas for laminar flow is 11.20 sec^{-1} . The difference, $3.70 \pm 2.75 \text{ sec}^{-1}$, represents other contributions, probably located mainly at the driver pistons, with a small radiation loss through the lateral boundary. The relatively small size of these other contributions is a result of the care taken to perfect the apparatus.

According to the analysis described in Section 2.1, the decay constant associated with the flow turning losses is expected to vary linearly with the Mach number of the average flow entering the boundary. For the configuration shown in Figure 2, the formula (2.28) gives

$$a_{ft} = 2f\bar{M}_t \frac{S_{bs}}{S_c} \beta_l \quad (2.37)$$

where β_l is a geometrical factor, evaluated in Refs. 13 and 17, which is equal here to 0.97. We therefore assume, in correlating our data, that $a_{ft} \sim \bar{M}_t$ and we shall compare the slope $da_{ft}/d\bar{M}_t$ computed for the data with that given by (2.37).

We assume that the Mach numbers and frequency are given with no error, so that eq. (2.32) can be written to show explicitly the average values and standard deviations, after (2.33) and (2.34) have been used:

$$\begin{aligned} a_{ft} \equiv \bar{a}_{ft} \pm \Delta a_{ft} &= (a \pm \Delta a) - [4f(\bar{A}_p^{(r)} \pm \Delta A_p^{(r)} + \bar{M}_p) \\ &+ 4f(\bar{A}_t^{(r)} \pm \Delta A_t^{(r)} + \bar{M}_t) \frac{S_{bs}}{S_c} C_l \\ &+ (\bar{a}_v \pm \Delta a_v) + (\bar{a}_d \pm \Delta a_d)] \end{aligned} \quad (2.38)$$

The values for $\bar{A}_p^{(r)}$, $\Delta A_p^{(r)}$, $\bar{A}_t^{(r)}$, $\Delta A_t^{(r)}$ are averages for the components in the two sides of the resonance tube. All of the quantities in the square brackets on the right hand side of (2.38) are known from the previous experimental work described above. These are summarized in Tables 5-7 for direct use in (2.38).

Equation (2.38) may now be used with the data summarized in Tables 4-7 to infer the values of a_{ft} . These are given in Table 8 and plotted in Figure 14. The solid line in Figure 14 represents a least squares fit to the data using the equation

$$a_{ft} = (\bar{a}_{ft})_{\bar{M}_{t=0}} + \bar{M}_t \left(\frac{da_{ft}}{d\bar{M}_t} \right) \quad (2.39)$$

The least squares fit was done without imposing the physical requirement that the linear fit should pass through origin, using a library routine in its primitive form. Note that the experimental uncertainty in a_{ft} at $\bar{M}_t = 0$ encompasses $a_{ft} = 0$; the average of the measured values is slightly negative.

The derivative $da_v/d\bar{M}_t$ of equation (2.38) can be used with the date to provide an independent result:

TABLE 5 Values of the Admittance Function for the Faces of the Driver Pistons, $f = 442$ Hz. (Ref. 4)

\bar{M}_p	$\bar{A}_p^{(r)}$	σ
0	.01544	.00009
4.43×10^{-4}	.01550	.00019

TABLE 6 Values of the Attenuation Coefficient for the 1/2" Circular Vent, $f = 442$ Hz. (Ref. 4)

$\bar{M}_v \times 10^4$	\bar{a}_v	Δa_v
0	0.06	0.70
4.43	-0.59	0.85
8.86	-0.90	0.78
13.29	-1.15	0.72
17.72	-2.39	1.00
22.15	-3.15	0.73

TABLE 7 Values of the Admittance Function for the Lateral Flow Elements, $f = 445$ Hz (Average of values in Table 3)

$\bar{M}_t \times 10^4$	$\bar{A}_t^{(r)}$	σ
0	0.5320	.0006
0.97	0.3862	.0013
1.95	0.4512	.0002
2.92	0.4307	.0002
3.90	0.4576	.0002

TABLE 8 Values of the Attenuation Coefficient for Flow Turning Losses,
 $f = 445$ Hz.

$\overline{M}_t \times 10^4$	$\overline{a}_{ft} (\text{sec}^{-1})$	$\Delta a_{ft} (\text{sec}^{-1})$
0	-0.33	6.42
0.97	+7.23	9.48
1.95	+5.04	4.95
2.92	+6.75	5.01
3.90	+6.42	4.64

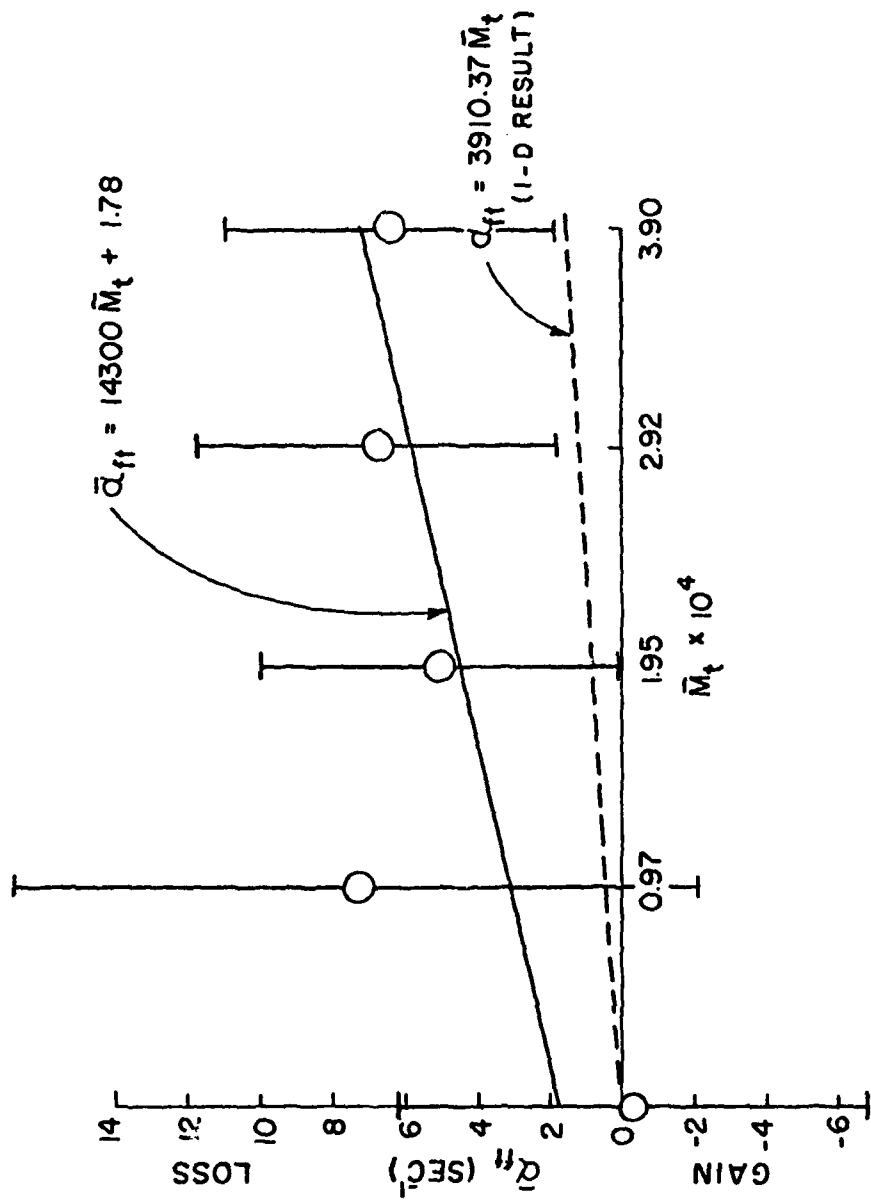


Figure 14. Measured Attenuation Coefficient for Flow Turning Losses

$$\begin{aligned}\frac{\bar{da}_{ft}}{\bar{dM}_t} \pm \Delta \left(\frac{\bar{da}_{ft}}{\bar{dM}_t} \right) &= \frac{\bar{da}}{\bar{dM}_t} \pm \Delta \left(\frac{\bar{da}}{\bar{dM}_t} \right) \\ - 4f \left\{ \frac{dA_t^{(r)}}{\bar{dM}_t} \pm \Delta \left(\frac{dA_t^{(r)}}{\bar{dM}_t} \right) + 1 \right\} \\ - \left\{ \left(\frac{\bar{da}_v}{\bar{dM}_v} \right) \pm \Delta \left(\frac{\bar{da}_v}{\bar{dM}_v} \right) \right\} \frac{\bar{dM}_v}{\bar{dM}_t}\end{aligned}\quad (2.40)$$

The value using the data discussed above is

$$\frac{\bar{da}_{ft}}{\bar{dM}_t} \pm \Delta \left(\frac{\bar{da}_{ft}}{\bar{dM}_t} \right) = 23000 \pm 11000 \text{ sec}^{-1} \quad (2.41)$$

This is five times as large as the theoretical value 4000 sec^{-1} calculated using eq. (2.37).

There is little doubt that there is indeed a loss of acoustic energy associated with the flow in at the lateral boundary, and that it increases with flow rate, or Mach number. Unfortunately, owing to the large experimental uncertainty associated with these results, it is not possible to state with any degree of confidence how closely the one-dimensional approximation represents the actual losses.

We emphasize in conclusion that there are two major sources of uncertainty: the necessity to obtain the admittance function for the curved lateral flow elements by extrapolation from the data taken for flat elements; and the problem of obtaining the desired quantities as small differences of large numbers. The only way to overcome the second difficulty is to use a larger scale apparatus, requiring a larger gas supply not available to us. If a sufficiently large, high pressure supply is available, all porous elements should be operated choked to

prevent spurious coupling between the acoustic field in the chamber and the system upstream of the porous elements. We believe that those losses have been minimized in our tests, although we have been able to provide choked flow only through orifices further upstream.

III. MEASUREMENTS OF THE ADMITTANCE FUNCTION OF A CHOKED NOZZLE

The objective of this portion of the program was to develop a technique for measuring the admittance function of a choked nozzle, including the effects of mean flow and nozzle submergence. The approach taken involved adaptation of a continuously operating supersonic tunnel. This approach was expected to have several advantages over use of the blow-down facility used in the most recent previous work (Refs. 9-12): the capital investment in measuring equipment and instrumentation is considerably less; it is easier to study the flow field, for example, to determine whether the field is really one-dimensional as required by the usual theory; reduction of data is often simpler; and tests to obtain comparable information should be less expensive to conduct.

During the early part of the work, we carried out tests to determine the severity of contamination of the test section by noise and oil from the compressors running the tunnel. The amount of oil present was a serious problem, prompting the decision to operate the tunnel as an open circuit. A diagram of the entire facility is given in Figure 15, and the open-circuited test section is shown in Figure 16. Air is drawn in from the room and flows through the test section which terminates in the choked nozzle to be tested.

Acoustic waves are generated at the entrance to the test section by an acoustic driver, an Atlas sound driver, Model 5D-370. The test section then serves as an impedance tube and the primary measurements are taken to determine the distributions of amplitude and phase for the standing acoustic field within the test section. In principle, the technique is sound and is essentially that used previously in Refs. 9-12. In practice there are substantial difficulties which we had not foreseen. It appears that they can be overcome for a broad range of conditions and the

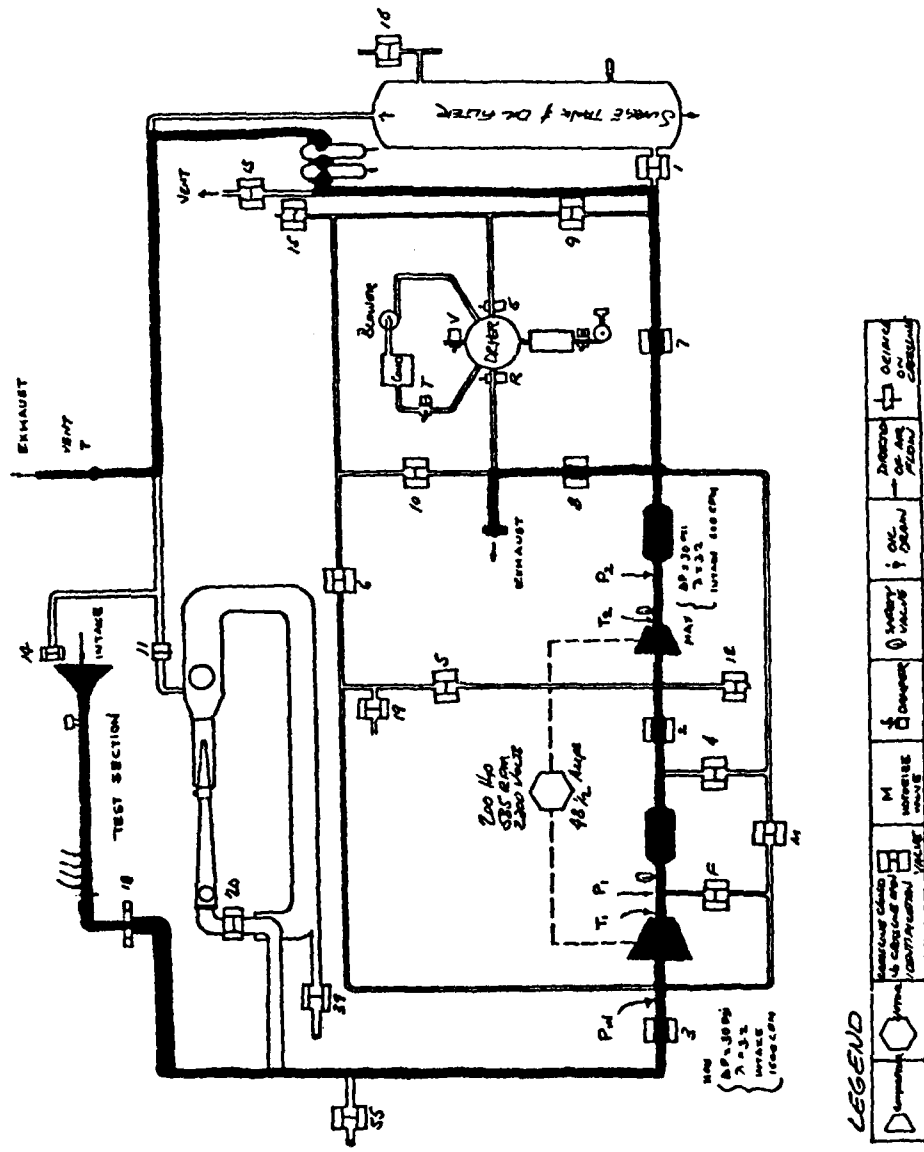


Figure 15. Schematic of the GALCIT Supersonic Wind Tunnel

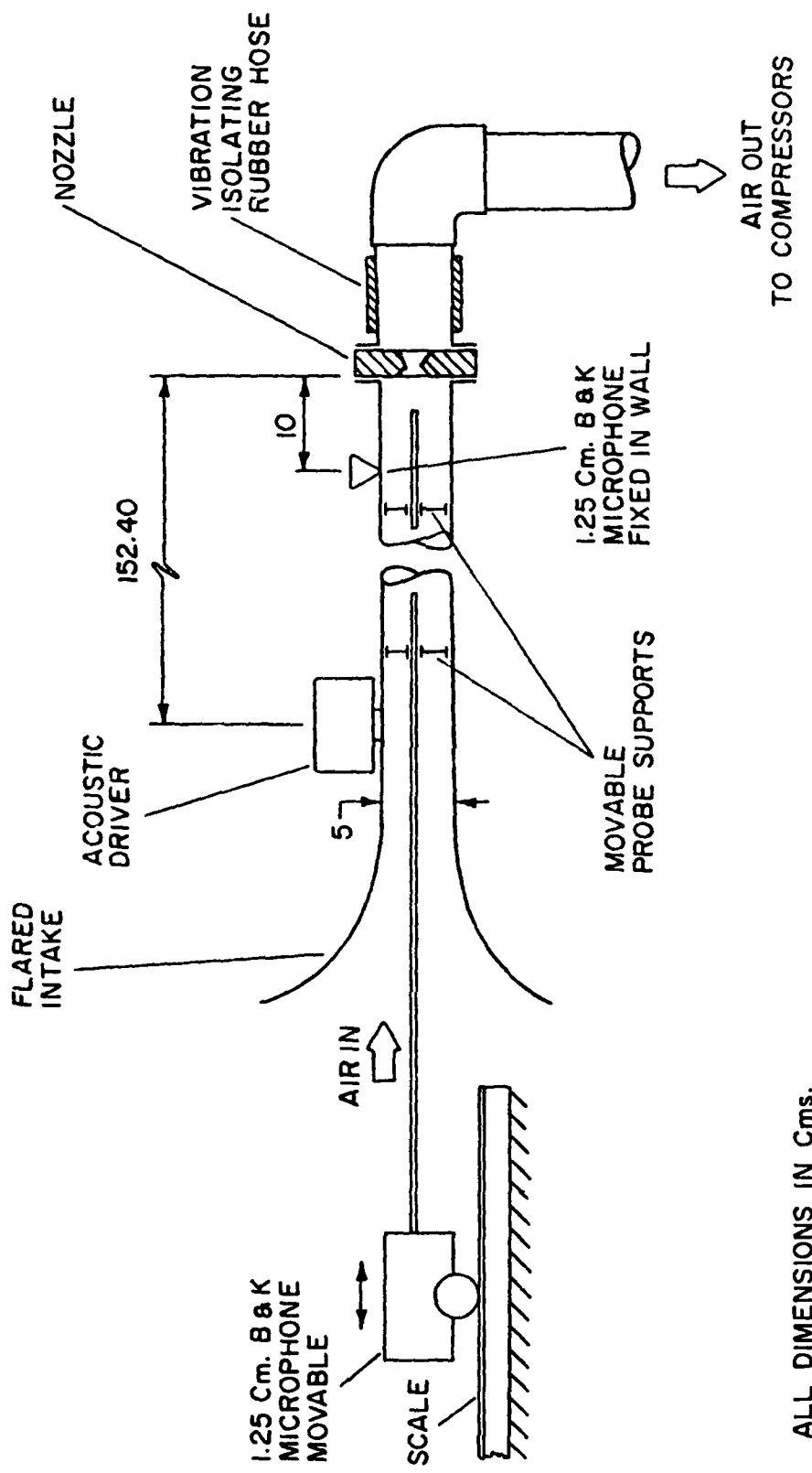


Figure 16. Sketch of the Test Section in the Supersonic Wind Tunnel

method should be regarded as a promising technique for obtaining the admittance functions for choked nozzles. There are some important improvements which are evident from the present work; these will be noted in the following sections and summarized in the concluding remarks.

3.1 Analysis of the Impedance Tube

The traditional applications of the impedance tube have two important characteristics: there is no average flow through the tube; and the loss of acoustic energy at the test sample are generally quite large, producing relatively large changes in the pressure amplitude in the acoustic field. Both of those characteristics are significantly changed in the present application.

Flow through the tube produces a boundary layer which in fact becomes quite thick for the lengths of tubes required. This must have some influence on the acoustic field, but we have not examined this problem in this work. We have assumed throughout that the acoustic field is one-dimensional, with phase fronts flat and normal to the axis of the tube. Some limited tests, described later in Section 3.3, have shown that the assumption is quite good, for the apparatus used in these experiments, if the frequency is less than 1000 Hz. and the Mach number of the average flow is less than 0.20.

The procedures eventually used for reducing the data are described in Section 3.4. Here we describe the simplest analysis of the impedance tube with flow. As sketched in Figure 17, the stationary acoustic field may be represented as the superposition of two travelling waves. Let the nozzle be located at $z = 0$, with the test section stretching over $z > 0$. With a uniform flow, in the negative z -direction, the governing equations

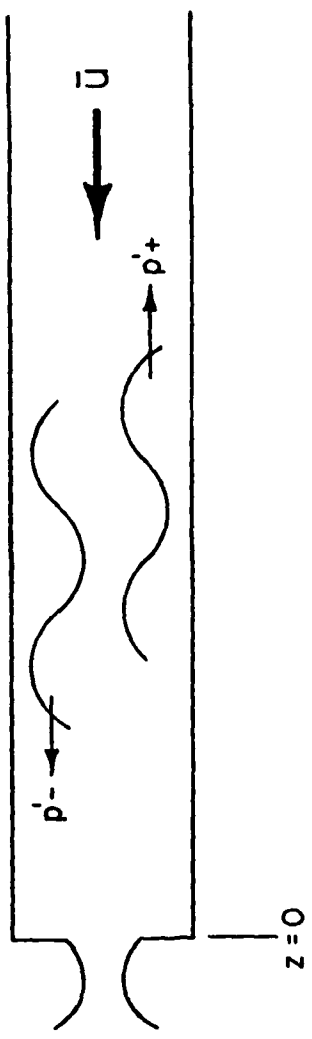


Figure 17. Sketch of an Impedance Tube with Flow

are (2.11) and (2.12) without the sources:

$$\bar{\rho} \frac{\partial u'}{\partial t} + \bar{\rho} \bar{u} \frac{\partial u'}{\partial z} + \frac{\partial p'}{\partial z} = 0 \quad (3.1)$$

$$\frac{\partial p'}{\partial t} + \bar{u} \frac{\partial p'}{\partial z} + \gamma \bar{p} \frac{\partial u'}{\partial z} = 0 \quad (3.2)$$

The field in the tube consists of a wave travelling to the right, incident upon the nozzle, and the reflected wave travelling to the left; in steady state the superposition of the two waves forms a stationary wave pattern.

Appropriate solutions to (3.1) and (3.2) are

$$p' = [P_+ e^{ik_+ z} + P_- e^{-ik_- z}] e^{-iwt} \quad (3.3)$$

$$u' = [U_+ e^{ik_+ z} + U_- e^{-ik_- z}] e^{-iwt} \quad (3.4)$$

Waves to the right (left) are denoted by + (-). Substitution of (3.3) and (3.4) into (3.1) and (3.2) leads to four equations for the coefficients P_+ , P_- , U_+ , U_- . The condition for non-trivial solutions gives the formulas

$$k_+ = \frac{k}{1 - \bar{M}} ; \quad k_- = \frac{k}{1 + \bar{M}} \quad (3.5)$$

where here $k = \omega/a$ is the real wavenumber because no losses have been accounted for. The equations may then be used to relate the coefficients:

$$U_+ = \frac{1}{\bar{\rho} a} P_+ ; \quad U_- = \frac{1}{\bar{\rho} a} P_- \quad (3.6)$$

Then (3.3) and (3.4) may be written

$$p' = [P_+ e^{iKz} + P_- e^{-iKz}] e^{-i(\omega t - MKz)} \quad (3.7)$$

$$u' = \frac{1}{\rho a} [P_+ e^{iKz} - P_- e^{-iKz}] e^{-i(\omega t - MKz)} \quad (3.8)$$

with

$$K = \frac{k}{1 - M^2} \quad (3.9)$$

The admittance function of the nozzle is defined as

$$A = \frac{1}{\rho a} \frac{u'}{p'} \quad (3.10)$$

Substitution of (3.7) and (3.8) into this formula leads to the relation between P_- and P_+ :

$$P_+ = \delta P_- ; \quad \delta = \frac{1-A}{1+A} = |\delta| e^{i\varphi} \quad (3.11)$$

The reflection coefficient, δ , has amplitude and phase given by the formulas

$$|\delta| = \left[\frac{1 - |A|^2}{(1 + A^{(r)})^2 + (A^{(i)})^2} \right]^{1/2} ; \quad \tan \varphi = \frac{-2A^{(i)}}{(1 + A^{(r)})^2 + (A^{(i)})^2} \quad (3.12)$$

The pressure field may be written in the form

$$\begin{aligned} p' &= P_- [e^{iKz} + \delta e^{-iKz}] e^{-i(\omega t - MKz)} \\ &= Pe^{-i(\omega t - MKz - \psi)} \end{aligned} \quad (3.13)$$

where, with $P_- = 1$,

$$P = 1 + |\delta|^2 + 2|\delta| \cos(2Kz + \varphi) \quad (3.14)$$

$$\tan \psi = \frac{-\sin Kz + |\delta| \sin(Kz + \varphi)}{\cos Kz + |\delta| \cos(Kz + \varphi)} \quad (3.15)$$

Equation (3.13) shows explicitly how the pressure field may be written in terms of its amplitude and phase. A similar form may be

constructed with viscous losses included, but there is no reason here to do so. The purpose of the preceding is to display as simply as possible the structure of the acoustic field, particularly the way in which the amplitude and phase depend on the admittance function. The experimental procedure is based on the idea that data for the amplitude and phase can be interpreted with an analytical result, such as (3.13) to give the real and imaginary parts of the admittance function. The details will be pursued further in Section 3.4 where the method of data reduction is discussed.

3.2 Description of GALCIT Supersonic Wind Tunnel and Experimental Apparatus

The schematic of the GALCIT (Guggenheim Aeronautical Laboratory, California Institute of Technology) supersonic wind tunnel is given in Figure 14. The tunnel is designed to operate continuously. The compressors (maximum compression ratio of 3.2 each) were run in series with a 200 HP electric motor. In the present work, one of the test sections was disconnected from the main flow line and the other was run open circuit. The open circuit arrangement makes it possible to use the room air which, after expanding through the nozzle, is compressed by the compressors and then exhausted back into the atmosphere. This passage of air helps reduce the flow noise otherwise transmitted to the test section from the running of the compressors. Also, it prevents the deposition of the compressor lubricating oil to the surface of the microphones.

The stagnation pressure in the test section is therefore maintained to be atmospheric. The compressed air from the compressor passes

through an aftercooler, one for each compressor. The heat from this compressed air is exhausted by cooling water which in turn is cooled by the cooling tower on the roof of the laboratory. To maintain the compression ratio within the desired limits, the valve settings for the various valves were adjusted for each flow Mach number. With appropriate cooling, test run times of approximately 2 hours were easily obtained.

The impedance tube used to measure the admittance of the nozzles is sketched in Figure 16. The test section is an aluminum tube 150 cm long having an internal diameter of 5 cm and wall thickness of 0.64 cm. At one end, a radiating horn shell is connected which serves as the flared intake for incoming air, while at the other end a nozzle is mounted. The flow through the nozzle is carried to the suction end of the compressors for the supersonic wind tunnel. A 1.25 cm B&K microphone, Model 4133, is mounted on the tube wall at a distance of 10 cm from the entrance plane of the nozzle. Another microphone is mounted on elastic supports within the microphone trolley. The microphone probe is 275 cm long, open at one end and connected to the microphone trolley at the other end.

The probe is supported at four different locations within the tube using teflon tipped spider supports. The trolley slides on a graduated scale fitted with its own bernier. The major advantage of this arrangement is the accuracy with which the acoustic minima can be located. The trolley is filled with cotton balls to aid insulation against both external air-born noise and structural vibrations. Near the flare intake, a 100 Watt Atlas sound acoustic driver Model SD-370 is mounted on the tube wall. This driver imposes acoustic oscillations on the main flow of air.

Table 9 Summary of the Characteristics of Nozzles Used for Admittance Measurements

Mach Number of the Main Flow	Secondary Flow, % of Main Flow	Throat Diameter, d* (cm)	Submersion (cm)
0.04	--	1.25	small conical nozzles in plates
0.10	--	2.11	
0.20	--	2.95	
0.30	--	3.66	
0.35	--	3.91	
<hr/>			
0.04	0	1.25	0.48 4.29
0.04	2.5	1.25	0.48 4.29
0.04	5.0	1.25	0.48 4.29

Table 9 is a list of the different nozzles constructed for the experiments. One-dimensional compressible flow formulas were used to determine the throat diameters of the nozzles. For simplicity, both the convergent and divergent sections of the nozzles were conical, Figure 18. The nozzles are machined of aluminum. Only one of these nozzles was constructed to accommodate the secondary flow injection; see Figure 18. A grade "H" porous sintered steel plate (Pall Western Co.) 0.32 cm thick was glued to the front end of the nozzle manifold. This nozzle was fabricated with external threads. This arrangement with additional aluminum spacers permits variable submersion of the nozzle in the main flow.

In addition to the main air supply, the apparatus and the ancillary equipments shown in Figure 19 can be divided into three subsystems:

- (i) the equipment required to drive the acoustic waves in the tube
- (ii) instrumentation for measuring the waves in the tube
- (iii) secondary air flow supply and instrumentation necessary to measure and monitor the flow.

A Wavetek frequency synthesizer, Model 171, together with a McIntosh amplifier, Model MI-75, was used to excite the driver. The Mura power meter, Model APMG-18, was connected in series to monitor the electrical power input to the acoustic driver. A Monsanto counter timer, Model 101 B, was used to monitor the output frequency of the synthesizer. Pressure signals from the end of the probe tube at the wall were detected by 1.25 cm B&K microphones, Model 4133, as

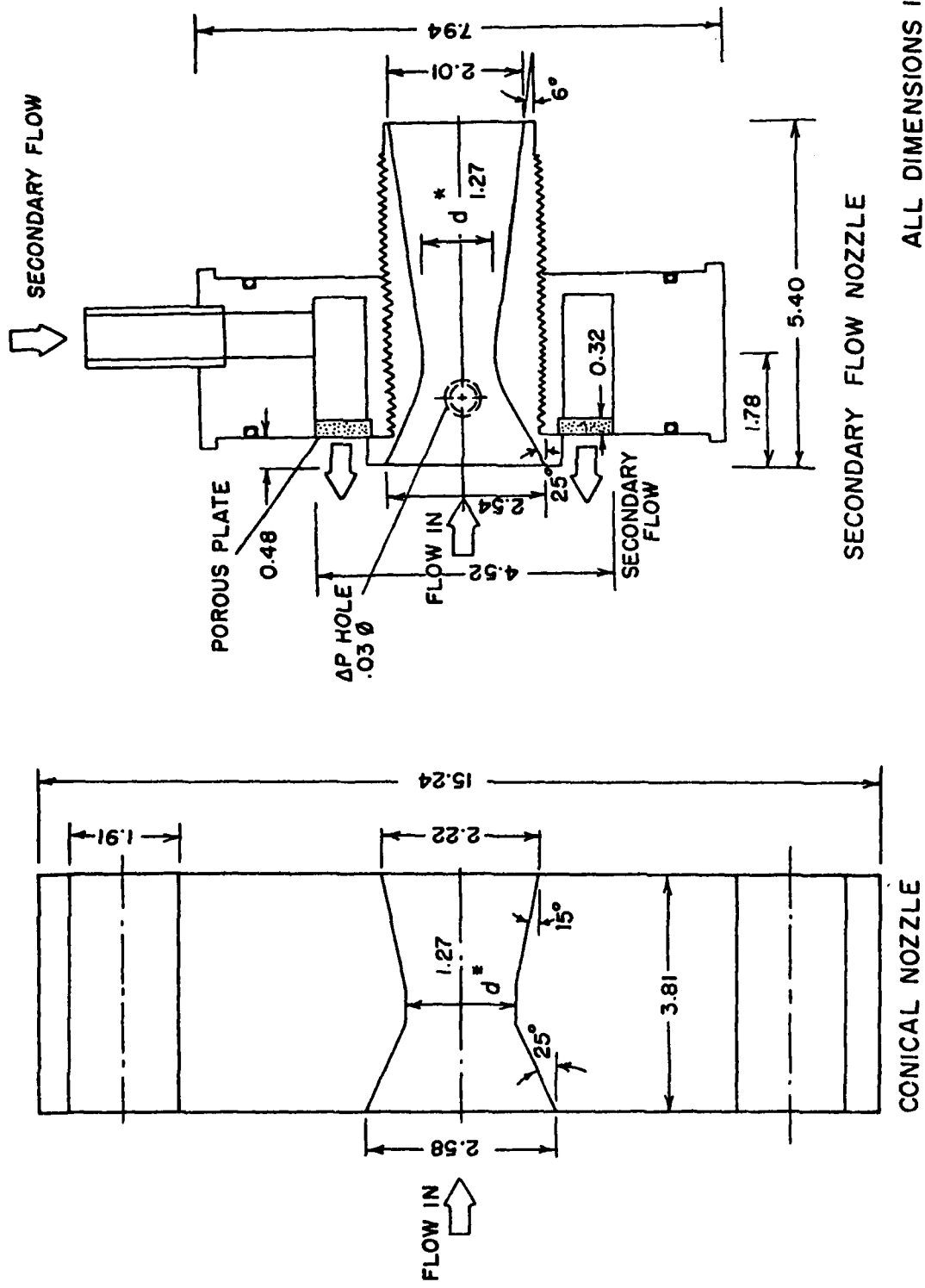


Figure 18. Drawings of the Nozzle Tested

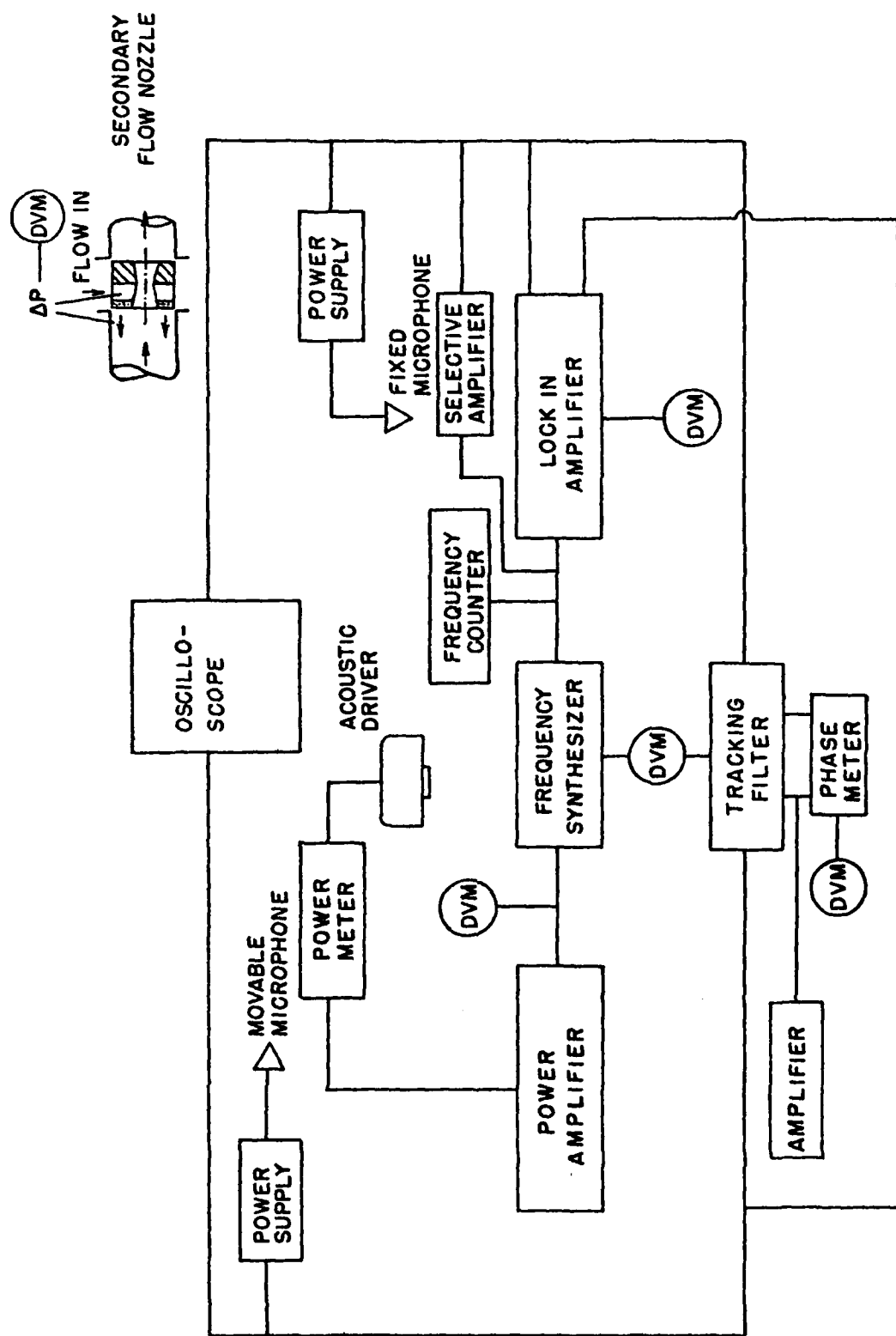


Figure 19. Instrumentation for Measurements of the Nozzle Admittance Function

described earlier. A track scale was used to measure the distance of the location of the front end of the probe tube from the nozzle face.

For a large majority of the experiments, both signals were filtered through a two channel unity gain tracking filter, Spectral Dynamics Model SD-122, with relative phase of 0° and 1 Hz. band pass filters driven by a carrier generator, Spectral Dynamics Model SD-120. The filtered output of the microphone in the trolley was amplified using a Hewlett-Packard amplifier, Model 465 A and was then used to measure the relative phase with respect to the wall microphones filtered signal using a Wavetek phase meter, Model 740. For some of the experiments the desired signal was extracted from the noise by using a Princeton Applied Research Lock-in Amplifier, Model 124 A with preamplifier, Model 117. The lock-in amplifier was externally tuned to a filtered signal from the wall microphone using a Princeton Applied Research selective amplifier, Model 189. For some experiments, the signal from the frequency synthesizer was used to tune the lock-in amplifier. The former technique of conditioning the signals using the tracking filter enabled us to measure the actual signal to noise ratio near the acoustic pressure minima. That information cannot successfully be obtained using the lock-in amplifier. The output of the lock-in amplifier and all other AC and DC outputs used for monitoring various parameters are measured with a 5-1/2 digit Data Precision Voltmeter, Model 3500.

The calibration of the secondary air flow supply was done as described in Ref. 3. The pressure drop across the porous plate was monitored with a Statham differential pressure gauge (0-50 psi). A Dynamic bridge supply, Model 6343 A was used with the pressure gauge.

The porous plate was chosen to provide very high acoustic impedance, which implies a relatively large pressure drop for a given secondary flow rate.

3.3 Preliminary Tests

A large number of preliminary tests were conducted during the early phase of this program to characterize

- (a) the flow noise
- (b) acoustic pressure symmetry in the tube, and
- (c) the influence of the support mount of the long probe on the acoustic pressure measurements.

Results from these experiments were used to guide the selection of appropriate parameters such as the flow Mach number and the strength of the acoustic pressure signal during the tests.

An earlier test was done with a thick plate orifice; the Mach number of the mean flow was approximately 0.20. The acoustic signal was measured at a fixed location from the orifice. It was found that the flow noise was $102 \text{ db} \pm 2 \text{ db}$ (reference pressure $2 \times 10^{-5} \text{ N/m}^2$) over a frequency range of 300 to 3000 Hz. It was subsequently determined that the flow noise is independent of the location of the probe. Numerous tests were conducted at flow Mach numbers of 0.10 or less. Those tests verified that the signal to noise ratio at the acoustic pressure minima was at least 2.8 db. This figure was measured and checked using a finely tuned tracking filter as described earlier.

Non-uniformities in the acoustic pressure over the cross-section of the tube may arise because of the presence of a non-uniform flow

distribution or because of the location of the sound source which is in the tube wall. A check of the symmetry of the acoustic pressure was considered essential for subsequent treatment of these data using the one-dimensional theory of an impedance tube. Some experiments were carried out to determine whether or not the phase fronts are flat. Two microphones were placed exactly opposite each other ten centimeters from the thick plate orifice (flow Mach number of approximately 0.20). There appears to be negligible asymmetry for frequencies below 750 Hz., but at 2000 Hz. a difference of about 20% was found between the amplitudes on opposite sides of the tube.

For the 2-inch diameter tube used here, the frequency of the lowest tangential mode is roughly 3500 Hz., so transverse modes are not excited directly by the acoustic driver. The asymmetry in the field is due to the location of the driver on one side of the tube. We were unsuccessful in some tests using two opposed drivers. The problem of obtaining a proper match of both amplitude and phase of the two drivers is a very difficult one and the fields we obtained in this way were not as uniform as those excited by a single driver. A single driver mounted on the axis at the inlet is the best arrangement, but that requires special hardware when the pressure probe is also located on the axis, as we chose here.

As discussed earlier, a long probe was used to measure the acoustic pressure distribution along the length of the tube. A large number of measurements are easily obtained, distributed along the axis in any desired manner. This improves the accuracy of the results obtained from the numerical scheme used to reduce the data. The long probe was supported at three to five different locations using sprocket type

supports. These supports move together with the probe tube sliding along the tube walls during measurements. Their locations, shape, size and the presence of the probe is bound to affect the acoustic pressure signal at the measuring positions downstream. The critical measure of this influence was characterized using the solid end plate and the condition of no flow in the tube. Two microphones, one at a distance 10 cm and the other at a distance of 20 cm from the solid end plate, were mounted in the wall of the tube. The test frequency was selected to be 425 Hz. so that the first acoustic pressure minimum was at the second probe, 20 cm from the end plate. For a fixed source excitation, the amplitude ratio and the phase difference between these two microphones were recorded as a function of the location of the probe. It was found that when the probe is at a distance of more than 25 cm from the end, the amplitude ratio and the phase difference, approximately 45° , are not affected by its presence. If the support is close to the end of the probe, both the amplitude ratio and phase are strongly affected when the probe is near the end wall.

This can be attributed to the presence of the sprocket support. In all the tests reported here, the support was therefore located at least 15 cm. from the end of the probe. This configuration minimizes the influence of the support and we have made no corrections to the data to account for the presence of the probe and its support.

3.4 Procedures for Data Reduction

When this program began, we anticipated that there should be no difficulty using the well-known procedure for determining the admittance

function from measurements of the pressure amplitude. The procedure is straightforward and had apparently been used successfully in the work reported in Refs. 9-12. However, we encountered severe difficulties which consumed considerable time before we realized their source.

In summary, the main conclusion is that measurements of the pressure amplitude only are adequate to determine accurately the real and imaginary parts of the admittance function providing the real part is relatively large. That is, the losses of acoustic energy incurred at the end of the tube must be sufficiently large - therefore making the real part of the admittance large - that the structure of the acoustic field is substantially perturbed from the ideal case. The losses at the end affect most significantly the structure of the field in the vicinity of the pressure minima, where the experimental error is greatest.

If, as happens to be the case for the influence of the choked nozzles used in the present work, the losses are not large enough, the traditional procedure leads to large errors and in many cases results having the wrong sign (i.e. a gain of energy may be inferred). Under these circumstances, it is absolutely essential that both the amplitude and the phase of the pressure field be measured and that both pieces of information be used in the data reduction.

The importance of phase measurements was earlier recognized by Baum (Ref. 18) and was brought to our attention while the present program was in progress. We had encountered difficulties while reducing data

18. Baum, J.D., Daniel, B.R. and Zinn, B.T. "Determination of Solid Propellant Admittances by the Impedance Tube Method", AIAA 18th Aerospace Sciences Meeting (Jan. 1980) AIAA Paper 80-0281.

taken primarily to check the apparatus, experimental technique and the procedures for data reduction. We then spent considerable effort examining the sensitivity of the traditional method using "data" calculated for idealized cases. It is quite clear now that a technique based on data for both amplitude and phase should always be used. We have adopted without change the numerical procedures suggested in Ref. 18 and have found them to be very accurate and easy to use.

3.4.1 Application of Analysis of the Impedance Tube

Before summarizing the techniques finally used, it is worthwhile demonstrating what goes wrong with the traditional method, the use of which can no longer really be justified.

With a uniform flow field, and distributed viscous losses along the tube accounted for, the leftward and rightward running waves sketched in Figure 16 and introduced in Section 3.1 can be written

$$\begin{aligned} p'_+ &= P_+ e^{-kz} e^{i(k_+ z - \omega t)} & u'_+ &= \frac{1}{\rho a} P_+ e^{-kz} e^{i(k_+ z - \omega t)} \\ p'_- &= P_- e^{kz} e^{-(k_- z + \omega t)} & u'_- &= \frac{1}{\rho a} P_- e^{kz} e^{-i(k_- z + \omega t)} \end{aligned} \quad (3.16)a, b$$

The boundary condition at $z = 0$ is satisfied in the form

$$P_+ = -P_- e^{2\psi} ; \quad \psi = \pi a_0 + i\pi\beta_0$$

and the stationary pressure field is the superposition of p'_+ and p'_- :

$$\begin{aligned}
 p' &= P_- e^{\psi} \left[-e^{-\kappa z + ik_+ z + \psi} + e^{+\kappa z - ik_- z - \psi} \right] e^{-iwt} \\
 &= -P_- e^{\psi} e^{i \frac{\bar{M}k}{1-\bar{M}^2} z} \left[e^{-\kappa z + i \frac{k}{1-\bar{M}^2} z + \psi} - e^{\kappa z - i \frac{k}{1-\bar{M}^2} z - \psi} \right] e^{-iwt} \\
 &= -2P_- e^{\psi + i\bar{M}kz} \frac{e^{-iwt}}{\sinh(-\kappa z + iKz + \psi)} e^{-iwt} \tag{3.17}
 \end{aligned}$$

Now define

$$\pi(a + i\beta) = -\kappa z + iKz + \psi = (\pi a_0 - \kappa z) + i(\pi \beta_0 + Kz) \tag{3.18}$$

and the pressure field is

$$\begin{aligned}
 p' &= -2P_- e^{\pi a_0} e^{i(\beta_0 + Kz - \omega t)} \frac{e^{-iwt}}{\sinh \pi(a + i\beta)} \\
 &= |\hat{p}| e^{i\theta} e^{-iwt} \tag{3.19}
 \end{aligned}$$

The amplitude and phase of the spatial distributions are

$$|\hat{p}| = 2P_- e^{\pi a_0} \left[\cosh^2 \pi(a_0 - \frac{\kappa z}{\pi}) - \cos^2 \pi(\beta_0 + \frac{2\kappa}{\lambda(1-\bar{M}^2)}) \right]^{1/2} \tag{3.20}$$

$$\theta = \beta_0 + Kz + \tan^{-1} \left[\coth \pi(a_0 - \frac{\kappa z}{\pi}) \tan \pi(\beta_0 + \frac{2\kappa}{\lambda(1-\bar{M}^2)}) \right] \tag{3.21}$$

where the wavelength is $\lambda = 2\pi/k$.

The formula (3.21) is the basis for the familiar method of treating data taken with an impedance tube, as for example, explained in Ref. 19. There are four parameters in eq. (3.21): a_0 , β_0 , κ , and the amplitude P_- . The real and imaginary parts of the admittance function are found

19. Morse, P. Vibration and Sound, McGraw-Hill Book Co., New York (1948), pp. 239-244.

from a_0 and β_0 by equating δ in (3.11) to $-\exp(2\psi)$, (3.16):

$$\delta = |\delta| e^{i\varphi} = -e^{2\pi a_0} e^{i2\pi\beta_0} = e^{2\pi a_0} e^{i2\pi(\beta_0 - \frac{1}{2})}$$

Hence,

$$|\delta| = \left[\frac{1 - |A|^2}{(1 + A(r))^2 + (A(i))^2} \right]^{1/2} = e^{2\pi a_0} \text{ and } \varphi = 2\pi(\beta_0 - \frac{1}{2}) \quad (3.22)$$

where $|\delta|$ and φ are given by eq. (3.12). The value of β_0 is not particularly sensitive to the admittance function, but a_0 is, and in particular is small when the admittance is small. Note that if $A = 0$, then $a_0 = a$ as well. More conveniently, one can show that the admittance is related to a_0 and β_0 by

$$A = \coth \pi(a_0 + i\beta_0) \quad (3.23)$$

In principle, four values of $|\hat{p}|$ determined at four different locations can be used with (3.20) to determine the four parameters listed above. If many measurements are taken, the data can be used in sets of four, providing corresponding sets of the four parameters. The results could then be averaged over a number of sets of four.

A better way of taking advantage of many data points is to use a nonlinear regression technique to fit the data with the four-parameter representation (3.20). A measure of the difference between the measured and predicted distributions is

$$E = \sum [|\hat{p}(z_i)|_{\text{exp}} - |\hat{p}(z_i; a_0, \beta_0, \kappa, P_-)|]^2 \quad (3.20)$$

where the sum is over all data points. The nonlinear regression technique may be used to determine numerically those values of a_0 , β_0 , κ , P_- which minimize E . This seems to have been the technique used in Refs. 9-12.

Both of those methods have been tried with test problems defined by specifying the four parameters first and then using (3.20) to calculate "data points". Not surprisingly, numerical errors are small, and the parameters specified initially can be recovered with great precision.

The problem is revealed when one follows the same tact, but adds a bit "error" to the specified data points. For the sorts of values one would expect in the experiments, a 1% error applied to the data can produce as large as 100% errors in the values of a_0 (or the real part of the admittance function) and κ . Moreover, it is possible even to extract values of a_0 having the wrong sign.

Several alternative procedures have been tried, including one based on the integral of the amplitude distribution and one based on a correlation coefficient. In the course of those calculations, an analysis of the sensitivities of the results to errors in the input data was also carried out. That served mainly to verify that indeed we should have the troubles we had encountered, although one useful conclusion was that the inferred values of the parameters should be less uncertain if good data is taken near the minima of the pressure field. That too is not a startling result; it follows simply from examining the influence of the losses on the pressure distribution: the influence is greater in the vicinity of the minima as shown by Figure 20.

Two examples serve to show the difficulties; for simplicity, $\bar{M} = 0$. Figures 20 and 21 show the influence of changing a_0 by a factor of three, from -.01 to -.03 representing losses at the nozzle. The value of κ is given by the formula for viscous losses associated with the classical acoustic boundary layer (Ref. 13, p. 219)

$$\kappa = 2\sqrt{\pi\nu} \left[1 + \frac{\gamma - 1}{\sqrt{Pr}} \right] \frac{f^{1/2}}{D} = 5.88 \times 10^{-5} \frac{f^{1/2}}{D} \quad (3.24)$$

where D is the diameter of the tube and the constant is the value for air at one atmosphere and room temperature. Note that with all other parameters fixed, changing the value of a_0 by a substantial amount affects the amplitude and phase distributions only near pressure minima.

Figures 22 and 23 constitute a striking demonstration of the crucial importance of measuring the phase. In this case, for fixed values of κ , β_0 and a small change of amplitude, changing the sign of a_0 causes essentially no discernable shift in the pressure distribution but the phase is qualitatively as well as quantitatively very different. Even a crude measurement of the phase distribution serves to distinguish between a loss and gain of energy at the end of the tube.

Finally, Figures 24 and 25 show how insensitive both the amplitude and phase distributions are to the value of κ except in narrow regions immediately near the minima. It follows, as indeed we shall see later, that it is relatively difficult to obtain precise values for the distributed losses from data taken with an impedance tube.

The reasons for the awkward behavior described here can be traced to the form of the amplitude distribution (3.20). Suppose $\kappa = 0$; then the formula is

$$|\hat{p}| = 2P_e e^{\pi a_0} [\cosh^2 \pi a_0 - \cos^2 \pi \beta_0]^{1/2}$$

When data is fitted numerically, the amplitude is $2P_e \exp(\pi a_0)$, so a_0 has no influence. It then appears only in $\cos^2 \pi a_0$ which is insensitive to the sign of a_0 , explaining the behavior in Figure 22.

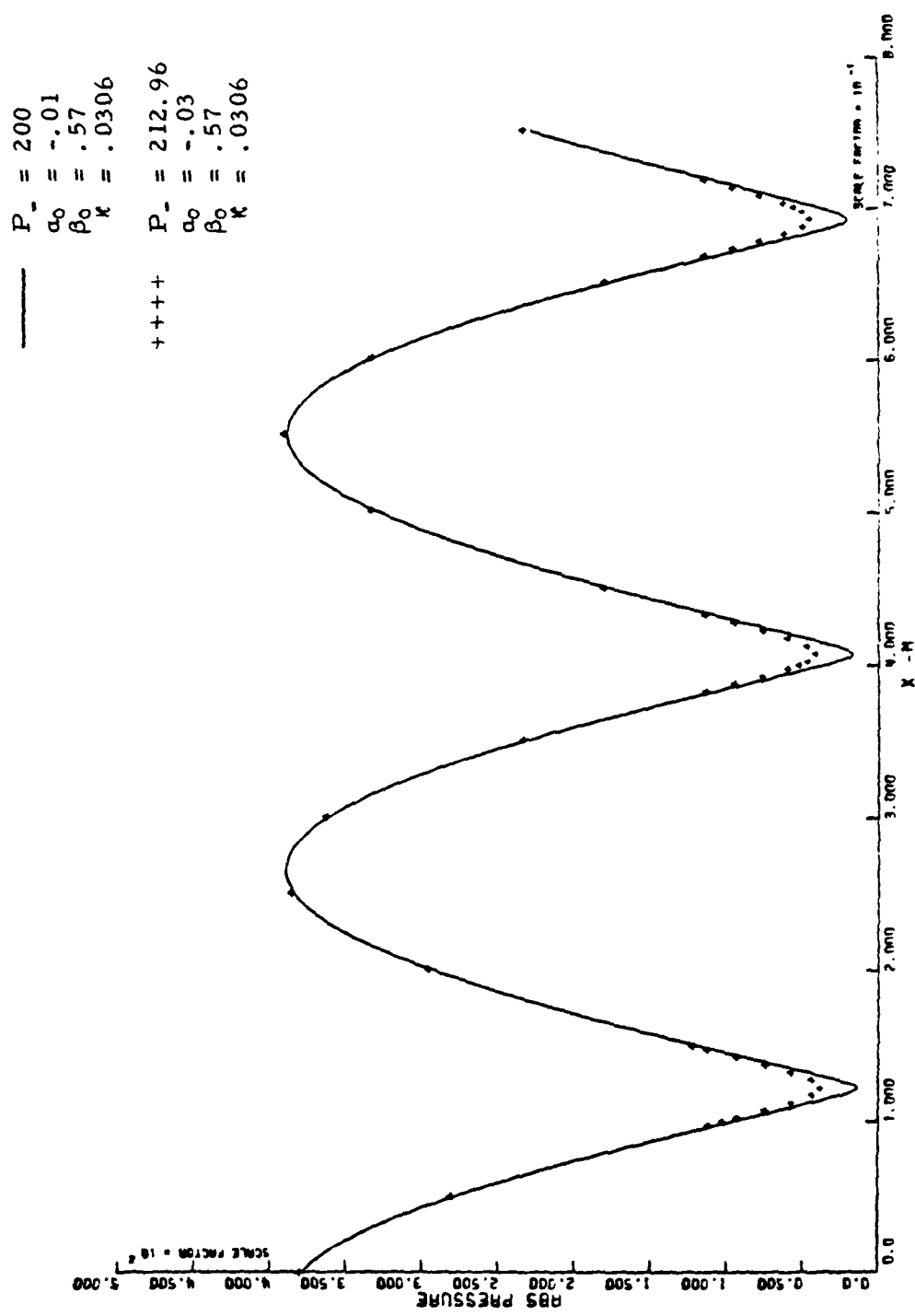


Figure 20. Calculated Amplitude Distribution, Showing the Influence of α_0

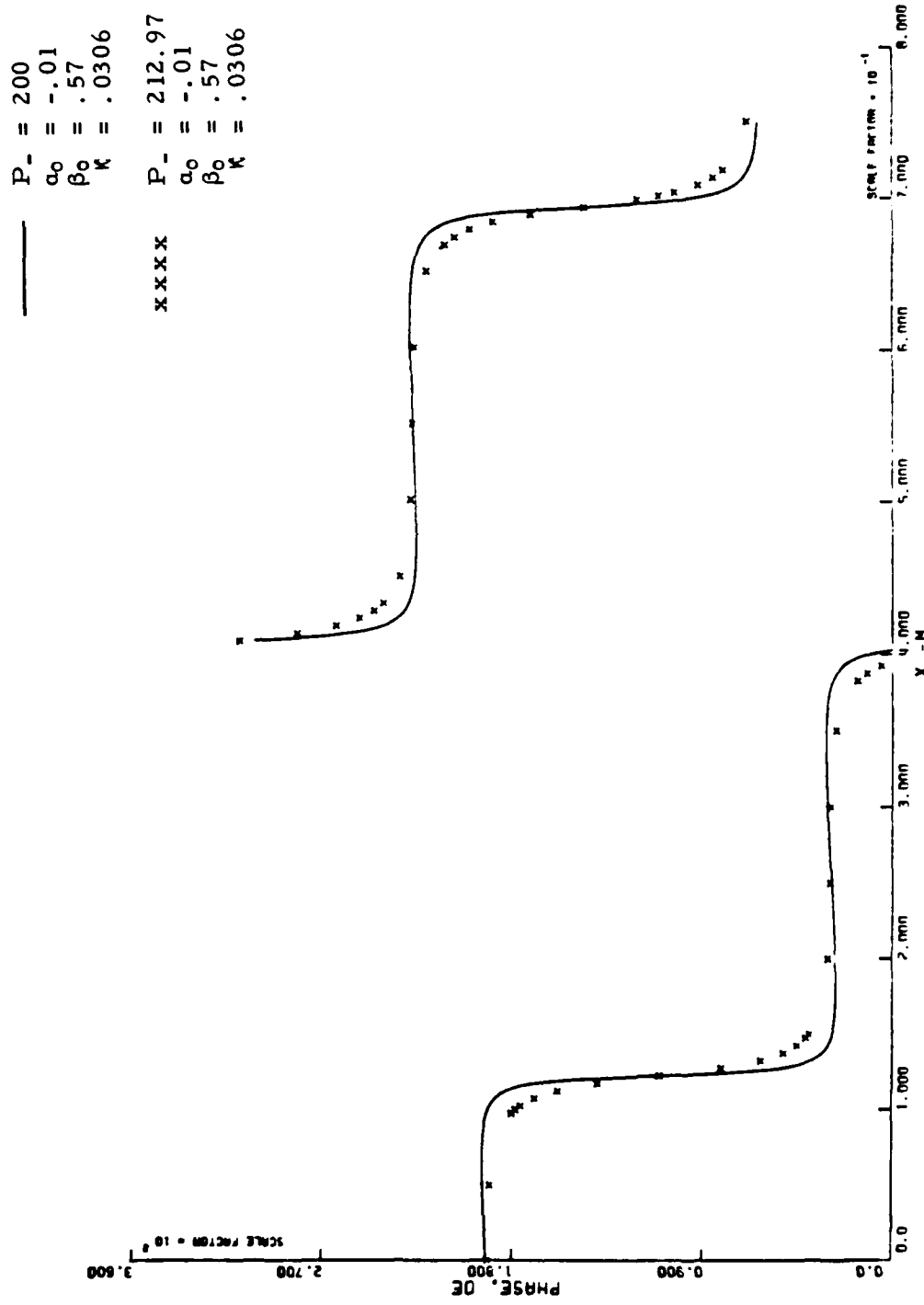


Figure 21. Calculated Phase Distribution, Showing the Influence of α_0

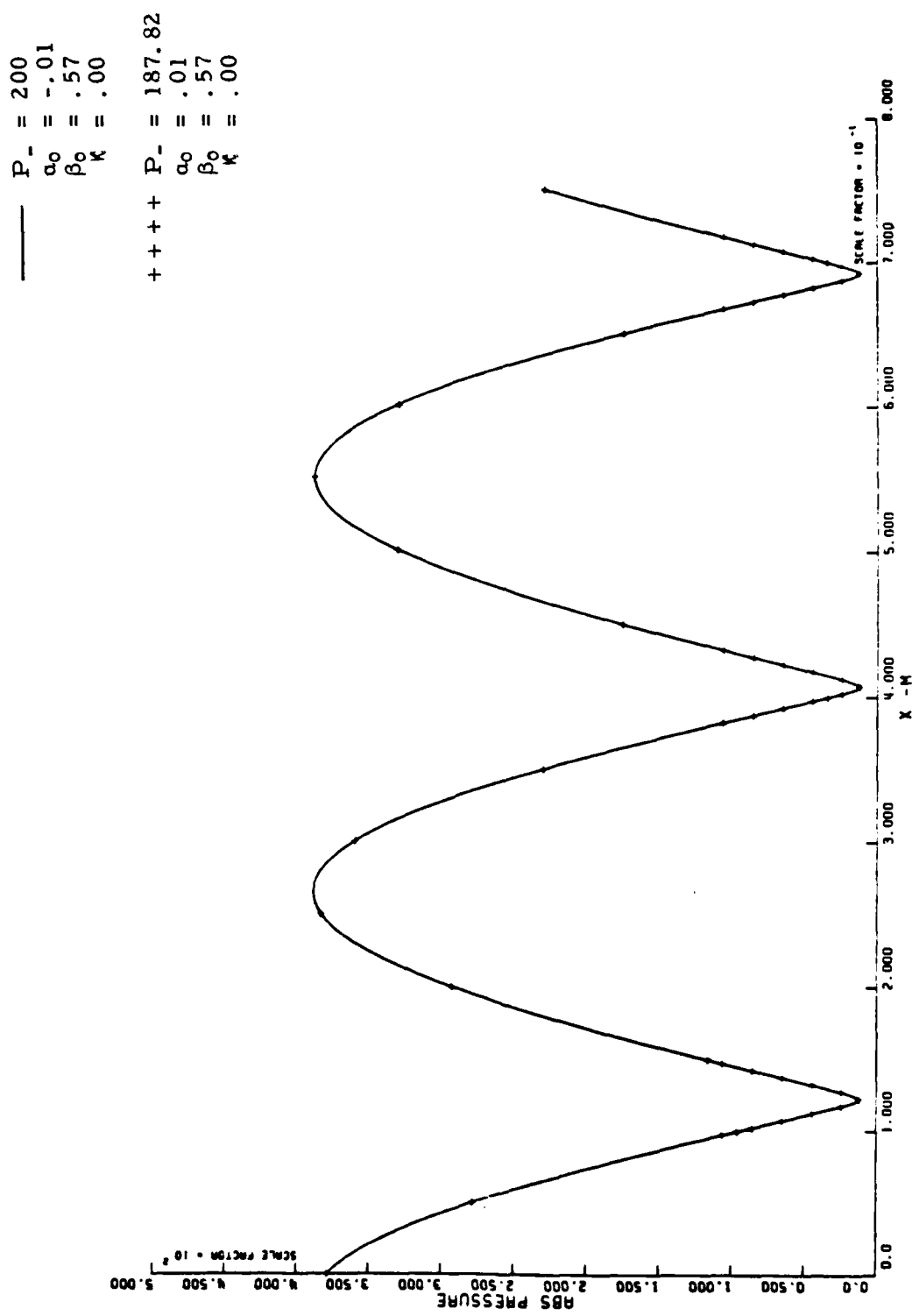


Figure 22. Calculated Amplitude Distribution, Showing the Influence
of the Sign of α_0

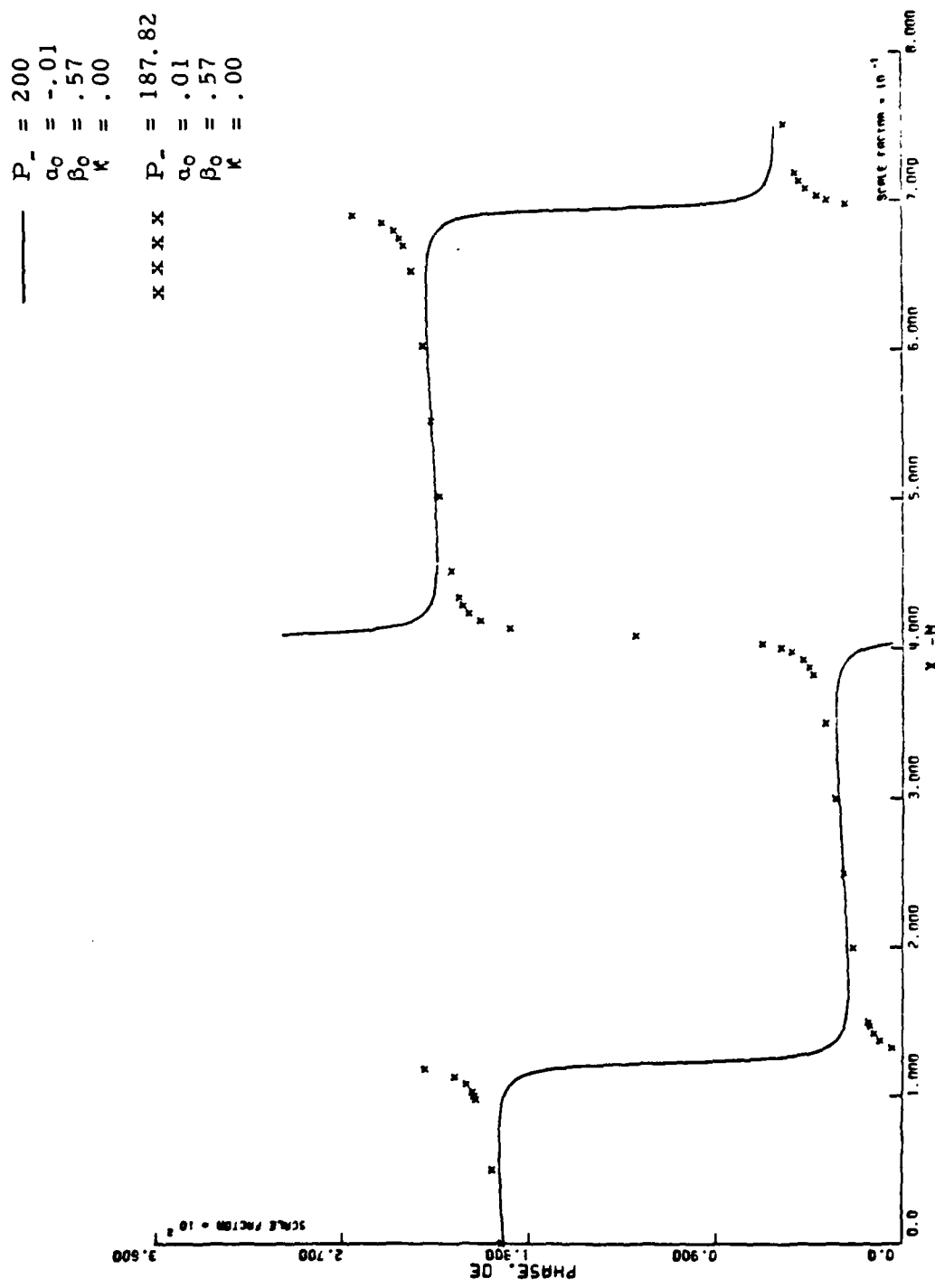


Figure 23. Calculated Phase Distribution, Showing the Influence of the Sign of α_0

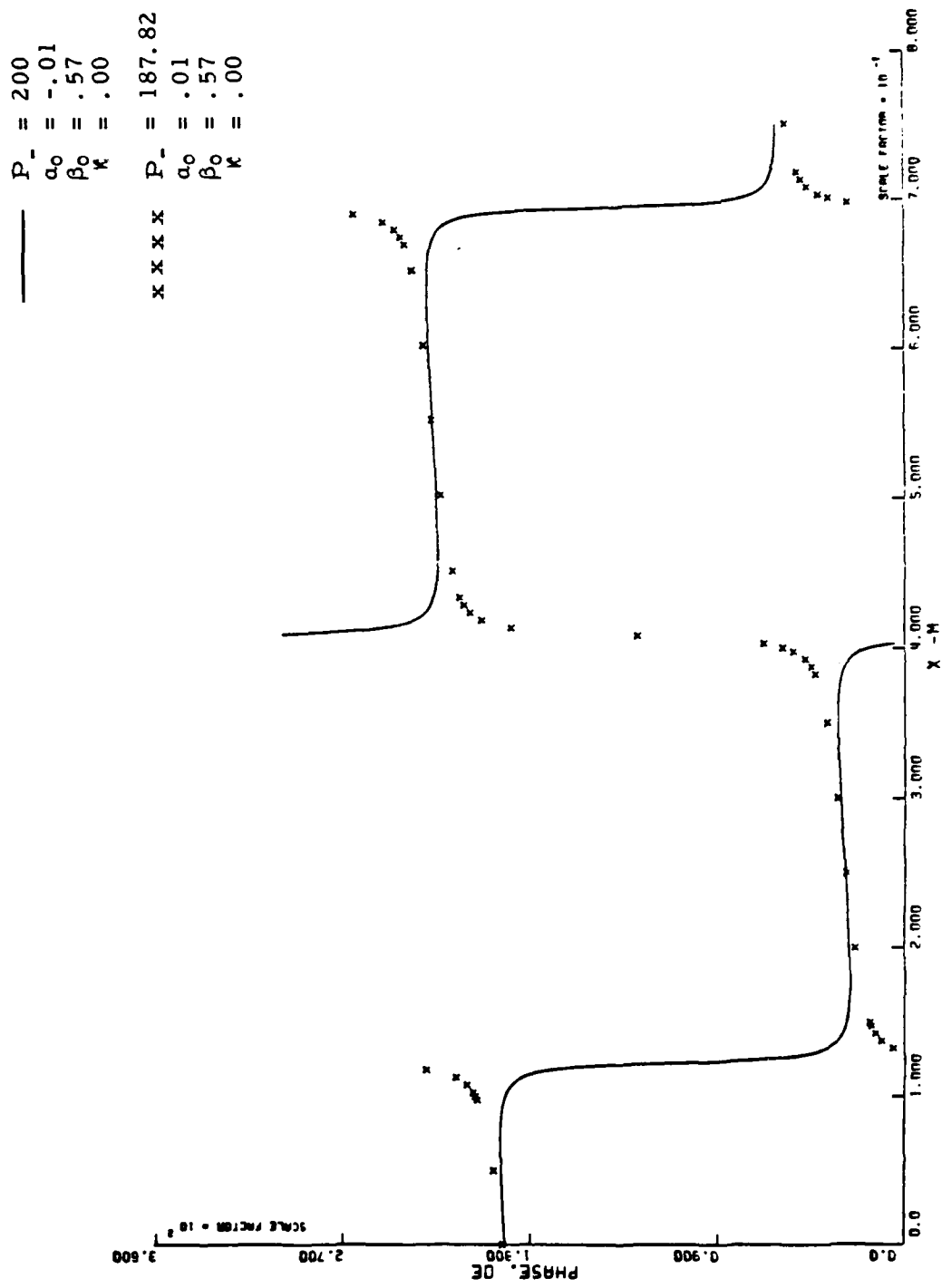


Figure 23. Calculated Phase Distribution, Showing the Influence of the Sign of α_0

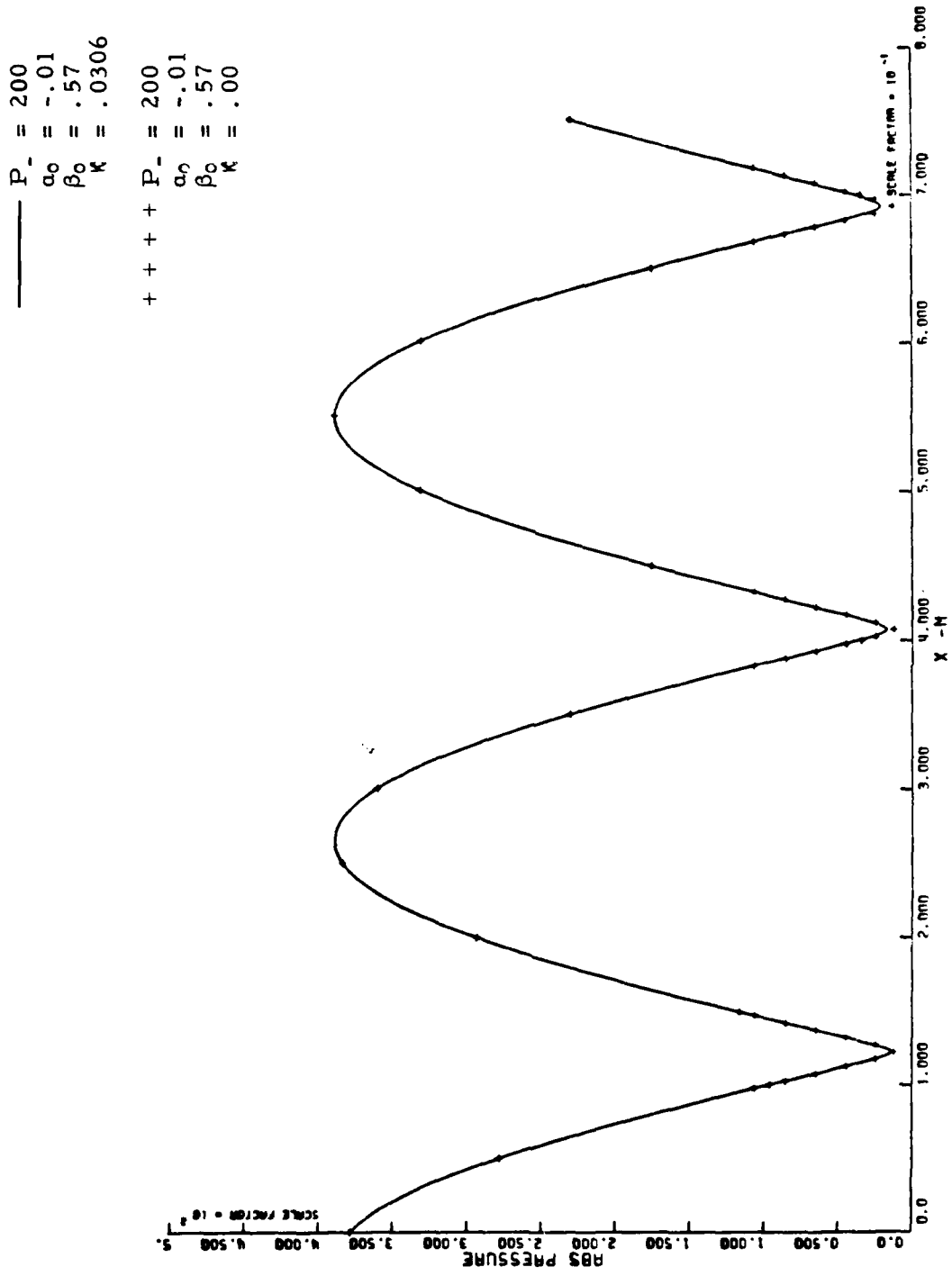


Figure 24. Calculated Amplitude Distribution, Showing the Influence of κ

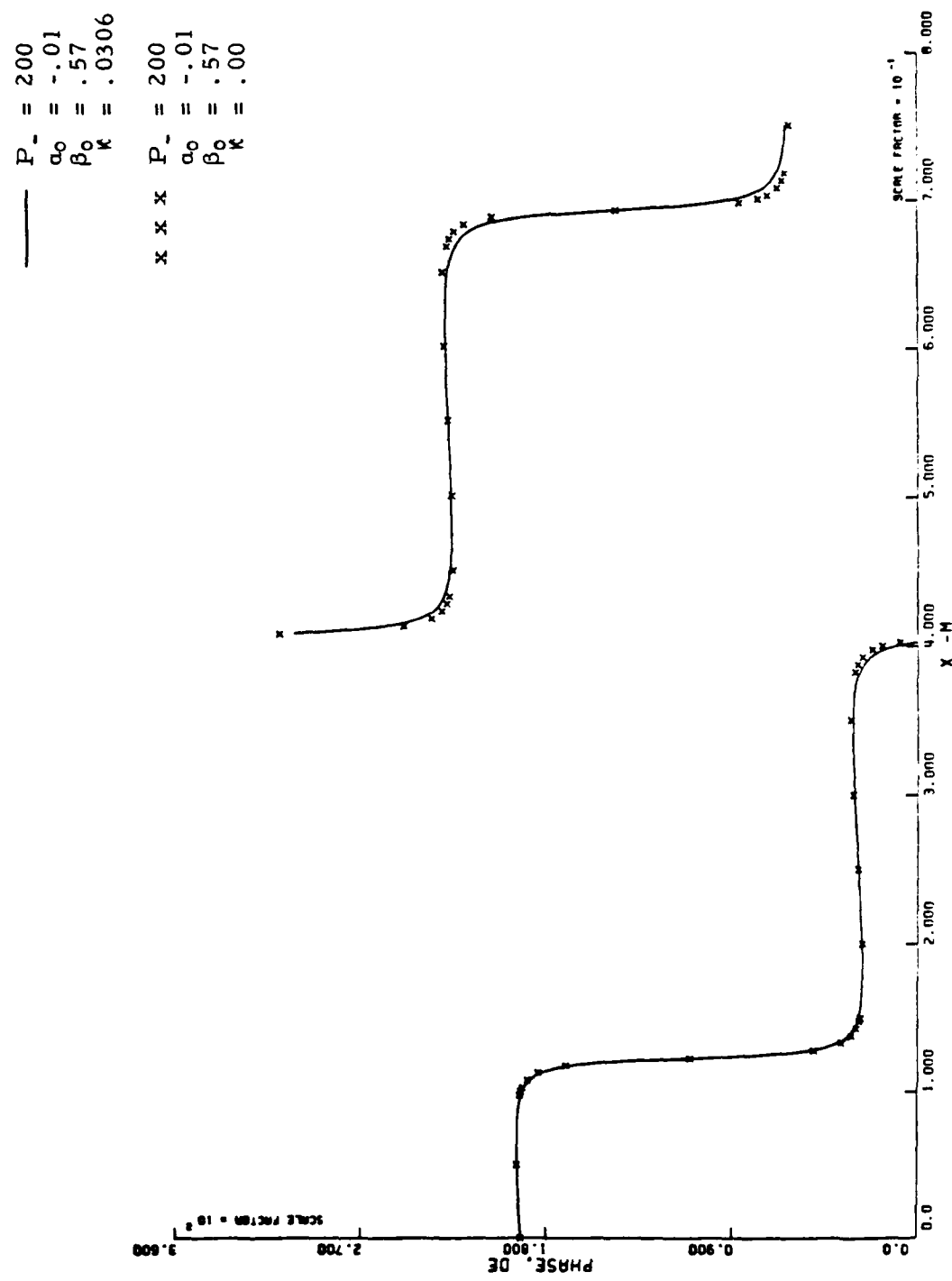


Figure 25. Calculated Phase Distribution, Showing the Influence of κ

The sensitivity may be estimated by choosing $\kappa = 0$, $\beta_0 = 0.5$, so $|\hat{p}| \sim \cosh \pi a$. Then the small change of a due to a small change of $|\hat{p}|$ is roughly

$$\delta a_0 = \frac{\partial a_0}{\partial |\hat{p}|} \delta |\hat{p}| \sim \frac{1}{\pi \sinh \pi a_0} \delta |\hat{p}|$$

so $\delta a \sim |\hat{p}| / \pi^2 a_0$ for a_0 small. If $a \sim .01$, $\delta a_0 \sim 10 |\hat{p}|$ and a small error in the pressure amplitude is amplified ten fold in its influence on the value of a_0 . It is this behavior which blocks effective use of data for the amplitude distribution only.

3.4.2 Numerical Reduction of Data for the Amplitude and Phase Distributions

The technique we have used to reduce the data discussed later in Section 3.7 is exactly that reported in Ref. 18. In these sections we summarize the procedure and give the results of several test cases which serve to verify the precision and efficiency of the method.

We now take the average flow to be from left to right towards the nozzle. Although we can use the exact representation in terms of plane waves, we follow Ref. 18 and base the procedure on numerical integrations of the linearized conservation equations, written for harmonic motions,

$$iw\hat{\rho} + \bar{\rho} \frac{d\hat{u}}{dz} + \bar{u} \frac{d\hat{\rho}}{dz} = 0 \quad (3.25)$$

$$iw\hat{u} + \bar{u} \frac{d\hat{u}}{dz} + \frac{1}{\bar{\rho}} \frac{d\hat{\rho}}{dz} = - G\hat{u} \quad (3.26)$$

$$iw\hat{p} + \bar{u} \frac{d\hat{p}}{dz} + \frac{-1}{\bar{\rho}} a^2 \frac{d\hat{u}}{dz} = 0 \quad (3.27)$$

The parameter G is used to introduce viscous losses. It is not difficult to show, by substituting the earlier formulas (3.16)a,b in these

equations that for $G/\omega \ll 1$, G and κ are simply related:

$$G = 2\bar{a} \left(\frac{1 - \bar{M}}{1 + \bar{M}} \right) \kappa \quad (3.28)$$

Because the density fluctuation appears only in (3.25), the other two equations can be integrated as a pair. These may be rearranged and written in the matrix form,

$$\frac{d}{dz} \{Z\} = [A]\{Z\} \quad (3.29)$$

where

$$\{Z\} = \begin{Bmatrix} \hat{p} \\ \hat{u} \end{Bmatrix} \quad (3.30)$$

$$[A] = \begin{bmatrix} -\frac{i\omega}{\bar{u}} & \frac{\bar{p}}{\bar{M}^2} (i\omega + G) \\ \frac{i\omega}{\bar{u}^2} & -\frac{1}{\bar{u}} (i\omega + G) \end{bmatrix} \quad (3.31)$$

Terms of order \bar{M}^2 have been dropped.

Now suppose that the boundary conditions are specified at $z = 0$:

$$\{Z\}_0 = \{Z(0)\} = \begin{Bmatrix} \hat{p}(0) \\ \hat{u}(0) \end{Bmatrix} \quad (3.32)$$

Integration of (3.29) will lead to the form

$$\{Z(z)\} = [T(z)]\{Z(0)\} \quad (3.33)$$

To find the transfer matrix $[T]$, differentiate (3.33) and compare with (3.29) to give

$$\frac{d}{dz} [T] = [A][T] \quad (3.34)$$

with the initial condition on $[T]$:

AD-A104 185

CALIFORNIA INST OF TECH PASADENA GUGGENHEIM JET PROP--ETC F/6 21/2
MEASUREMENTS OF ENERGY LOSSES ASSOCIATED WITH INTERACTIONS BETW--ETC(U)
JUL 81 F E CULICK, K MAGIAWALA, J WAT, E AWAD F04611-80-X-0013
AFRPL-TR-81-22 NL

UNCLASSIFIED

2 OF 2
AC-4
D-4-P

END
DATE
FILED
10-81
DTIC

$$[T(0)] = \begin{bmatrix} 1 & 0 \\ 0 & 1 \end{bmatrix} \quad (3.35)$$

The transfer matrix is then found by integrating the pair of equations represented by (3.34). This will then produce the formulas for the pressure and velocity fields from (3.33):

$$\hat{p}_{th} = T_{11}(z) \hat{p}(0) + T_{12}(z) \hat{u}(0) \quad (3.36)$$

$$\hat{u}_{th} = T_{21}(z) \hat{p}(0) + T_{22}(z) \hat{u}(0) \quad (3.37)$$

The solution \hat{p}_{th} depends on the parameters G , $\hat{p}(0)$, $\hat{u}(0)$. First G is fixed and $\hat{p}(0)$ and $\hat{u}(0)$ are determined so as to minimize the complex quantity Δ , analogous to the error E defined in connection with the nonlinear regression method:

$$\Delta = \sum (\hat{p}_{th} - \hat{p}_{exp})^2 \quad (3.38)$$

The sum is again over all locations where data are taken. For Δ to be minimum with respect to $\hat{p}(0)$ and $\hat{u}(0)$,

$$\frac{\partial \Delta}{\partial \hat{p}(0)} = 0 \quad \frac{\partial \Delta}{\partial \hat{u}(0)} = 0 \quad (3.39)$$

These are two linear equations which can be solved to give $\hat{p}(0)$, $\hat{u}(0)$ explicitly in terms of the elements of the transfer matrix and the experimental values for the pressure:

$$\hat{p}(0) = \frac{1}{D} [(\sum p_e T_{11})(\sum (T_{12})^2) - (\sum p_e T_{12})(\sum T_{12} T_{11})] \quad (3.40)$$

$$\hat{u}(0) = \frac{-1}{D} [(\sum p_e T_{11})(\sum T_{11} T_{12}) - (\sum p_e T_{12})(\sum (T_{11})^2)] \quad (3.41)$$

where

$$D = (\sum (T_{11})^2)(\sum T_{12})^2 - (\sum T_{11} T_{12})(\sum T_{12} T_{11}) \quad (3.42)$$

Note that p_e , standing for p_{exp} , the measured pressure, is complex. With (3.40) and (3.41), the theoretical pressure field may now be computed by using (3.36).

The error given by (3.38) is still a function of the parameter G which is determined by iteration, using Muller's method (Ref. 20) to minimize $|\Delta|$.

3.4.3 Some Test Cases

(a) Sensitivity of the Numerical Technique

The numerical scheme described above reproduces specified exact input to within less than one part in 10^5 . That is, the values of the pressure field calculated for a given admittance function at the end, are used as "data", then the calculated admittance is within 10^{-5} of the input values both real and imaginary parts. This conclusion is true over the entire useful range of values.

More importantly, the technique is relatively insensitive to errors or uncertainties in the data. This was checked by specifying the viscous parameter G and the admittance function and then using as data the calculated values of the pressure field. Nine cases have been examined; the results are shown in Table 10. The first column lists the pairs of a_0, β_0 used and the second column displays the corresponding real and imaginary parts of the admittance function. The remaining four columns show the computed values of the admittance when the theoretical "data" are composed of the exact values plus varying amounts of random

20. Muller, D. A. "A Method for Solving Algebraic Equations Using an Automatic Computer", Mathematical Tables and Other Aids to Computation (1956) pp. 208-215.

Table 10

Results of Calculations for the Sensitivity to Random Errors

Boundary Conditions	Theoretical Admittance	Maximum Value of Random Error			
		$\pm 0.5\% P_{max}$	$\pm 1.5\% P_{max}$	$\pm 2.5\% P_{max}$	$\pm 3.5\% P_{max}$
$\alpha_0 = 0.005$	-0.02004	-0.02095	-0.01933	-0.01843	-0.01603
$\beta_0 = 0.25$	-0.99980	-0.10005	-0.10054	-0.99720	-0.99483
$\alpha_0 = 0.005$	-0.01570	-0.01583	-0.01537	-0.01555	-0.01431
$\beta_0 = 0.5$	-0.00018	-0.00053	-0.00310	-0.00172	-0.00017
$\alpha_0 = 0.005$	-0.04276	-0.04268	-0.04236	-0.04245	-0.04175
$\beta_0 = 0.75$	+0.99895	+0.99817	+0.99680	+0.99680	0.99434
$\alpha_0 = 0.01$	-0.05139	-0.05240	-0.05080	-0.04951	-0.04701
$\beta_0 = 0.25$	-0.99855	-0.99940	-1.0040	-0.99610	-0.99326
$\alpha_0 = 0.01$	-0.03140	-0.03153	-0.03120	-0.03126	-0.02954
$\beta_0 = 0.5$	-0.00036	-0.00072	-0.00313	-0.00193	-0.00038
$\alpha_0 = 0.01$	-0.07408	-0.07398	-0.07369	-0.07355	-0.07265
$\beta_0 = 0.75$	0.99711	0.99637	0.99499	0.98920	0.99237
$\alpha_0 = 0.015$	-0.08233	-0.08374	-0.08223	-0.08053	-0.07819
$\beta_0 = 0.25$	-0.99645	-0.99774	-1.0017	-0.99459	-0.99102
$\alpha_0 = 0.015$	-0.04708	-0.04722	-0.04697	-0.04697	-0.04488
$\beta_0 = 0.5$	-0.00054	-0.00090	-0.00382	-0.00213	-0.00598
$\alpha_0 = 0.015$	-0.10526	-0.10513	-0.10489	-0.10449	-0.10348
$\beta_0 = 0.75$	0.99430	0.99360	0.99220	0.98662	0.98940

Upper values are real parts and lower values are imaginary parts of the admittance function.

errors distributed over the pressure distribution. Even for uncertainties as large as 3.5% of the maximum pressure, the errors in the calculated admittance function are less than 2%. Thus, the amplification of uncertainties which accompanies the technique based on the pressure amplitude only, is entirely absent.

(b) Results for a Rigid Flat Plate

A flat plate was installed as the end condition and the impedance tube operated without flow. In this case, the admittance function is ideally zero because the velocity normal to the surface must vanish. Table 11 shows the results. Although small, the admittance doesn't vanish, a consequence of the impossibility of providing an absolutely rigid mounting.

Also included in Table 11 are the inferred values of the attenuation constant κ and those calculated using the formula (3.24). Note that while the admittance function varies only weakly with frequency, as it should, the inferred values of κ do not agree particularly well with the predicted values, $\kappa \sim \sqrt{f}$. The main reason for this has been remarked upon earlier: the distributed losses have mainly a relatively small influence near the minima in the pressure field, where the experimental errors are greatest. Hence, one should not expect to be able to infer good values for κ . Fortunately, as discussion in Section 3.7 will clarify further, the values inferred for the admittance function are very insensitive to the value for κ .

Table 11 Results for Measurements with a Rigid Flat Plate

Frequency	Admittance		κ_{exp} (cm^{-1})	κ_{th} (cm^{-1})	% Error, κ
	$A^{(r)}$	$A^{(i)}$			
500	-0.0056	0.05902	0.0245	0.0256	- 4.4%
700	-0.0059	0.068	0.015	0.0301	-100%
1050	-0.0048	0.081	0.065	0.0381	+100%

(c) Examples Showing Importance of Obtaining Data Near Pressure Minima

The numerical calculations discussed in Section 3.4.1 show very clearly the importance of obtaining good data near pressure minima. This implies that best use is made of a given number of data points if they are in some sense concentrated near the minima. Several examples have been calculated to show the truth of this conclusion, and to demonstrate that one must have data near two minima; good definition of only one minimum is insufficient. Both the end losses and the distributed losses affect variations in the stationary acoustic field along the axis and good results are obtained only if one has some measure of the gradients.

Table 12 shows the results of one such exercise. A large number of data - measurements of pressure at many axial locations - were taken. The first two rows show the results for the admittance function and the attenuation constant κ obtained with two different sets of 32 points.

The third row shows the results of a calculation using only half as many data, but chosen from the regions near two minima. The point is clear, and generally true for use of the classical impedance tube: it is best to take data near minima, and at least two minima must be well-defined.

Table 12 An Example Showing the Importance of Data Near Pressure Minima

Data Set	$A^{(r)}$	$A^{(i)}$	κ_{exp}	κ_{th}
(a) 32 points	-.0497	-.1786	.043	.038
(b) 32 points	-.0475	-.1824	.053	.038
(c) 16 points near minima	-.0510	-.1833	.049	.038

3.5 Summary of Tests Conducted

Table 13 shows the tests conducted with the two types of nozzles illustrated in Figure 18. Because the nozzle entrances do not fair smoothly with the lateral boundary of the impedance tube, we have no possibility of comparing the results unambiguously with the well-known one-dimensional theory given in Refs. 6 and 7.

Each test entered in Table 12 means the acquisition of data for both the amplitude and phase of the pressure at various locations along the tube, sometimes as many as 32.

We encountered considerable problems with the flow noise for higher Mach numbers, so most tests are for $\bar{M} \leq 0.04$. A total of 100 tests are entered in Table 13. There are of course many not included here because they were carried out to check the apparatus and procedures for data reduction or otherwise were of an exploratory nature.

3.6 Calibration Procedures and Estimates of Errors

The quantities to be determined, the real part of admittance function of the nozzles, are relatively small and their variation with respect to flow Mach numbers and nozzle configurations are also relatively small. Thus, the measurements require considerable care and good instrumentation to obtain the highest possible accuracy. Considerable effort was devoted to achieve the necessary level of accuracy.

3.6.1 Calibration of the Secondary Air Supply System

A Brooks full view rotometer was used for the calibration of secondary flow. As part of this calibration, the rotometer was

Table 13 Summary of Tests Conducted for Measuring the Nozzle Admittance

Tests with Conical Nozzles

$\frac{f}{M}$.3 kHz	.4 kHz	.5 kHz	.6 kHz	.7 kHz	.8 kHz	1. kHz	2. kHz
.04	1	1	1	1	6	4	4	2
.10	1			1			1	1

Tests with Secondary Flow ($\bar{M} = 0.04$)

Submergence	f	.3 kHz	.5 kHz	.6 kHz	1. kHz	1.5 kHz	2. kHz
	2nd Flow						
Minimum Submergence	0.0%	1	3	1	4	3	4
	2.5%	1		1	1		3
	5.0%	1	3	1	4	3	6
Maximum Submergence	0.0%	1	3	1	4	3	4
	2.5%	1		1	1		1
	5.0%	1	3	1	4	3	4

separately calibrated using a Precision wet test meter. The flow circuit and further details for the calibration of the secondary flow are given in Refs. 3 and 4. The supply pressure and flow rate are controlled and maintained constant by a series of coarse and fine regulators and a fine metering needle valve. The pressure drop across the porous plate in the secondary flow system was measured with a Statham differential pressure gauge. The calibration of the wet test meter was provided by Precision Scientific Company, while the pressure gauge was calibrated at the Standards and Calibration Laboratory of the Jet Propulsion Laboratory.

The results for flow rate vs. pressure drop across the porous plate obtained in Refs. 3 and 4 were adopted here. These porous plates were chosen to provide very high acoustic impedance, which implies a relatively large pressure drop for a given flow rate. The data obtained are within the tolerances ($\pm 30\%$) quoted by the manufacturer.

3.6.2 Calibration of Microphones and Other Instruments

The values of the sensitivities and the frequency response curves for the microphones were provided by the manufacturer. Periodic verifications were made on the sensitivity by using a B&K piston phone microphone calibrator, Model 4220, used together with a B&K measuring amplifier, Model 2607.

The Princeton Applied Research lock-in amplifier Model 124 A, Wavetek synthesizer Model 171, Wavetek phase meter Model 740 and the Data Precision digital voltmeter Model 3500 were sent periodically to the calibration laboratories of the respective manufacturers for calibration. The spectral Dynamics tracking filter Model SD-122 and

carrier generator Model SD-120 were calibrated only once at the calibration laboratory of the manufacturer.

3.6.3 Sources and Estimates of Errors

Estimates of errors were carried out with the best available information and some laboratory experiments.

- (a) The driver speaker was mounted on one side of the tube entrance. Best results were obtained by lengthening the impedance tube so that plane waves would be achieved in the test section. As mentioned earlier, the serious asymmetries were encountered for frequencies above 750 Hz., but they have not been accounted for in the data reduction.
- (b) Determination of the acoustic pressure is affected by the flexibility and mounting of the long probe. Spurious room noise also has some influence. Neither of these errors is known.
- (c) The spacial resolution of the pressure measurements is ± 0.1 mm.
- (d) The amplitude linearity of the lock-in amplifier enters in determining the absolute values of the signals. Here, the internal calibrator of the instrument was used to estimate the error. A practical difficulty arises because we need to measure signals ranging from 1% to 80% of the full scale sensitivity on a single sensitivity of the lock-in amplifier. When the signal was only 1% of the full scale sensitivity

setting, the error in amplitude was determined to be $\pm 0.1\%$, and for signals greater than 30% of the full scale it was almost impossible to detect the very small error.

- (e) Day to day changes in temperature were ignored. They are small in the basement laboratory used for this work.
- (f) The discharge coefficient of the nozzles was assumed to be unity. The error in flow rate should be less than 1%.

3.7 Results for Measurements of the Admittance Function

Tests were conducted with the two types of nozzles shown in Figure 18; the test program covering 100 tests has been summarized in Table 13. We shall discuss the results in three groups for the following configurations:

- (i) conical nozzles with no secondary flow ($\bar{M} = 0.04$ and 0.1)
- (ii) a nozzle with secondary flow, minimum submergence ($\bar{M} = 0.04$)
- (iii) a nozzle with secondary flow, maximum submergence ($\bar{M} = 0.04$)

3.7.1 Conical Nozzles, No Secondary Flow

The inferred values for the real and imaginary parts of the admittance function are given in Table 14 for $\bar{M} = 0.04$ and in Table 15 for $\bar{M} = 0.1$. Figures 26 and 27 are plots of the real parts. Repeated tests for $\bar{M} = 0.04$ gave the standard deviations listed and indicated by the error bars drawn in Figure 26. The experimental uncertainty is of the order of 10% except for the series

Table 14 Results of Tests of a Conical Nozzle ($\bar{M} = 0.04$)

Frequency (Hz)	$A^{(r)}$	$\bar{A}^{(r)}$	σ_r	$A^{(i)}$	$\bar{A}^{(i)}$	σ_i
300	-0.0485			-0.129		
350	-0.043			-0.08		
500	-0.0510			-0.129		
600	-0.0567			-0.157		
700	-0.0455 -0.048 -0.0479 -0.055	-0.0491	0.004	-0.08 -0.085 -0.103 -0.102	-0.0925	0.0117
800	-0.059 -0.0527 -0.0437	-0.0518	0.007	-0.0980 -0.0986 -0.006	-0.067	0.053
1050	-0.055 -0.053 -0.0497 -0.0475	-0.0513	0.0033	-0.147 -0.151 -0.1785 -0.1824	-0.1647	0.0183
2100	-0.56 -0.046	0.051	0.007	-0.326 -0.326	-0.326	0

Table 15 Results of Tests of a Conical Nozzle ($\bar{M} = 0.1$)

Frequency (Hz)	$A^{(r)}$	$A^{(i)}$
2100	-0.086	-0.96
1050	-0.089	-0.37
600	-0.095	-0.187
300	-0.084	-0.072

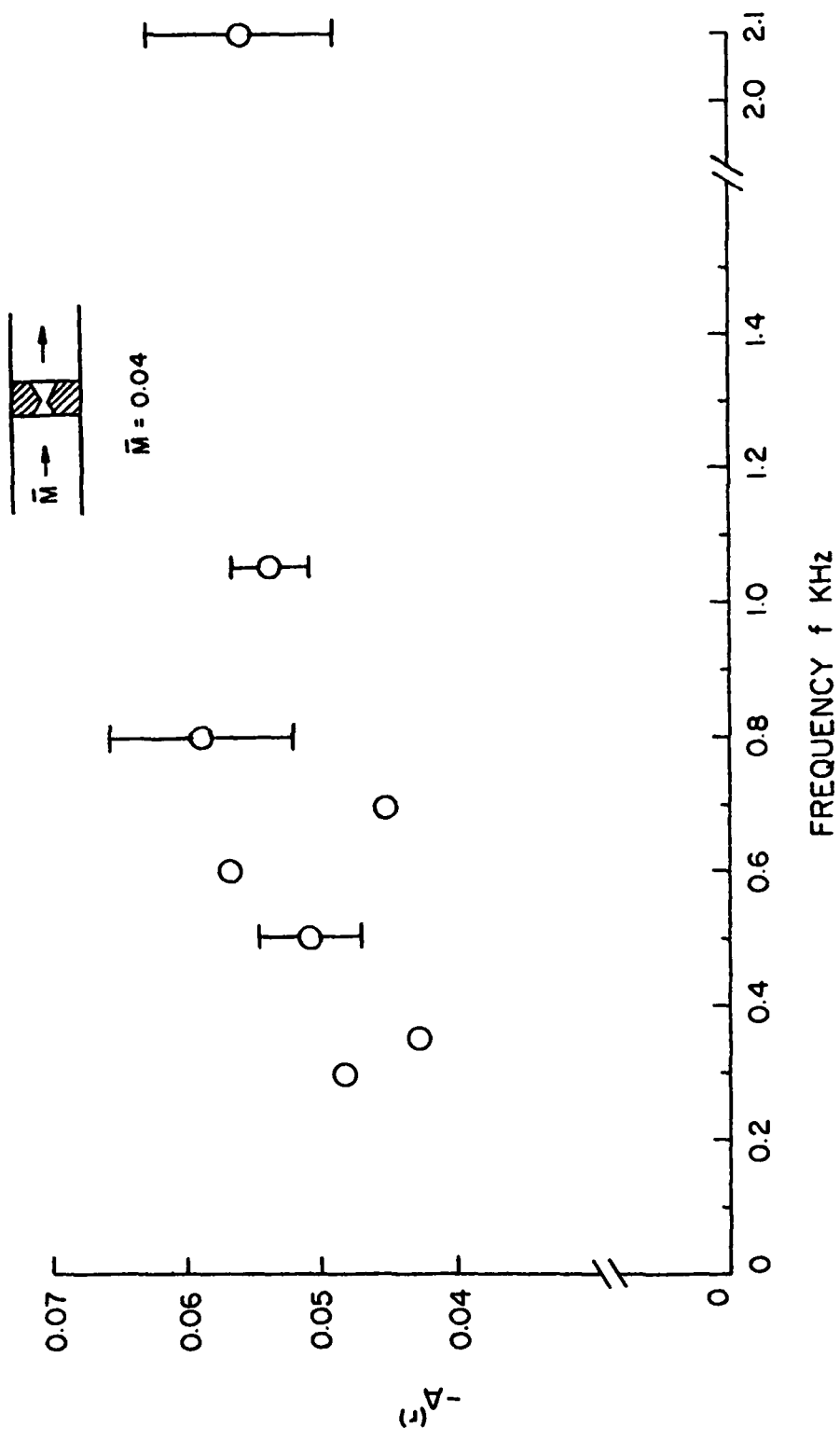


Figure 26. Admittance Function Measured for a Conical Nozzle, $\bar{M} = 0.04$

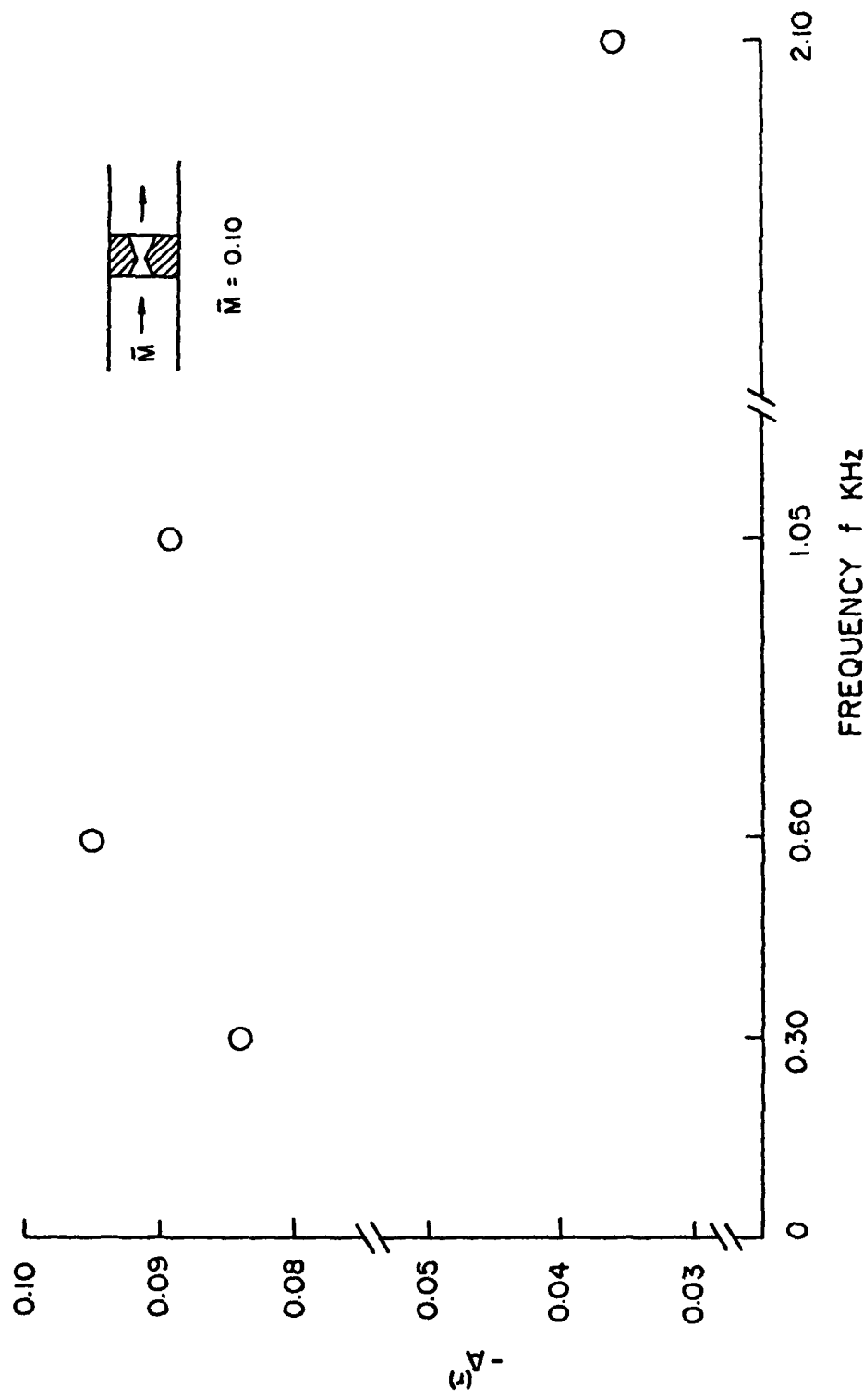


Figure 27. Admittance Function Measured for a Conical Nozzle, $\bar{M} = 0.1$

at 800 Hz., for which one of the tests appears to be seriously in error, for an unknown reason; given the other results one might guess that that test is likely invalid.

If a choked nozzle behaves quasi-statically, the admittance function is real and given by the formula

$$A = \overline{M}_n \frac{\gamma-1}{2} \quad (3.43)$$

where \overline{M}_n is the Mach number of the average flow entering the nozzle.

This is the ideal result, valid in the limit of very low frequencies.

For the nozzles used in this program, the diameter of the nozzle entrance (see Figure 18) is 2.58 cm, while the diameter of the test section is 5 cm. Hence, for incompressible flow, with Mach number \overline{M} in the test section, $\overline{M}_n = \overline{M} (5.0/2.58)^2 = 3.76 \overline{M}$. The formula (3.43) then gives for this short or compact nozzle approximation,

$$A = \begin{cases} 0.150 & (\overline{M} = 0.04) \\ 0.376 & (\overline{M} = 0.1) \end{cases} \quad (3.44)$$

The values measured at 300 Hz. are roughly 0.05 for $\overline{M} = 0.04$ and 0.085 at $\overline{M} = 0.10$. While the measurements show the expected increase with Mach number, the variation is less than linear and the values are smaller than predicted by the simple theoretical result.

The most obvious reason for the discrepancy is the influence of separation of the flow upstream of the entrance. This must obviously happen, producing an effective nozzle having entrance larger than the physical orifice actually used.

We have noted earlier, we chose these nozzles because of the closer resemblance to those used for the measurements with secondary

flow. If a short nozzle is used with entrance fairing smoothly to the test section, the theoretical values for the admittance would be given directly by (3.43), producing the values 0.008 for $\bar{M} = 0.04$ and 0.02 for $\bar{M} = 0.01$. The measured results lie between these and the values (3.44), a reasonable conclusion.

That there is considerable interaction between the acoustic field and the regions of separation is shown also by the large measured values for the imaginary parts, Tables 14 and 15. There is presently no way to predict the imaginary parts.

The results therefore seem reasonable so far as we can determine, and serve to provide an estimate of the experimental errors one can achieve with this technique. No discussion of experimental errors was given in Refs. 9-12; we therefore have no basis for comparison of the accuracy of our results with those obtained using a blow-down facility.

In general it is better to report the admittance as a function of the dimensionless frequency $s = \omega l/a$ where l is a characteristic length. The usual choices for l in the absence of separation are the length of the convergent section or the radius of the inlet section. Using the latter, we have ($r_i = 1.29$ cm) for the range of dimensionless frequency corresponding to the range of real frequency $300 < \omega < 2000$ Hz.

$$0.013 < s < 0.85 \quad (3.45)$$

Because of the smaller scale of our apparatus, we have been able to reach values of s somewhat less than half those covered by the work in Refs. 9-12.

Measurements of the sort taken in this program should ultimately provide a basis for assessing computations reported in Ref. 21. Detailed

calculations of the unsteady velocity and pressure fields have been performed but the results are presently unavailable. In principle, it should be possible to compute the admittance function averaged over any chosen plane upstream of the nozzle, for comparison with experimental measurements. (See Section 3.8 below for further remarks.) This will be a particularly important exercise for cases in which the flow is smooth everywhere. If separation occurs, as may happen with secondary flow, the analysis is less reliable.

3.7.2 Submerged Nozzles with Secondary Flow

Tables 16 and 17 contain the values for the admittance functions obtained with secondary flow and two values of submergence, very small but not zero, and the maximum value possible with our apparatus. The real parts of the admittance functions are plotted in Figures 28 and 29.

The experimental errors for these tests increase greatly with frequency; the results at 2000 Hz. are very doubtful indeed. With the caveat that there are large uncertainties attached to the results, we may offer the following observations:

- (i) For frequencies less than 1500 Hz. there seems to be no enormous influences of secondary flow, up to 5% of the main flow.
- (ii) There also seems to be no large effect of submergence, below 1500 Hz. However, the maximum submergence is 4.3 cm and at 1500 Hz., the wavelength is roughly 20 cm, so the nozzle spans less than one-quarter of a wavelength.

Table 16 Results of Tests of Nozzles with Secondary Flow (Maximum Submergence, $\bar{M} = 0.04$)

Frequency (Hz)	No Secondary Flow			2.5% Secondary Flow			5% Secondary Flow		
	$A(r)$	$\bar{A}(r)$ σ_r	$A^{(i)}$	$\bar{A}(r)$	$A^{(i)}$	$A(r)$	$\bar{A}(r)$ σ_r	$A^{(i)}$	$\bar{A}(r)$ σ_i
300	-0.028		-0.169		-0.027	-0.17	-0.0257		-0.168
500	-0.047 -0.043 -0.047	-0.046 0.0025	-0.309 -0.314 -0.313	-0.312 0.0026			-0.0477 -0.0499 -0.047	-0.0479 0.0016	-0.310 -0.308 -0.304
600	-0.0322		-0.369		-0.025	-0.366	-0.0127		-0.359
1050	-0.0179 -0.018 -0.0043 -0.033	-0.0183 0.0117	-0.785 -0.782 -0.782 -0.787	-0.784 0.0025	-0.032	-0.784	-0.032 -0.035 -0.028 -0.076	-0.042 0.022	-0.756 -0.756 -0.74
1500	-0.0382 -0.026 -0.0487	-1.3818 -0.0376 0.0116	-1.839 -1.678 -1.819	-1.839 0.258			+0.0072 +0.047 -0.066	-0.0039 0.0573	-1.87 -1.97 -1.90
2100	-0.65 +2.05 -5.21 +0.727	17.09 +0.77 3.15 5.12	16.7 13.95 5.12 5.89		+0.40	5.199	+0.145 -0.766 +2.577 1.412	+0.681 15.6 14.2 +0.770	14.2 15.6 12.17 5.04

Table 17 Results of Tests of a Nozzle with Secondary Flow (Minimum Submergence, $\bar{M} = 0.04$)

Frequency (Hz)	No Secondary Flow			2.5% Secondary Flow			5% Secondary Flow		
	$A(r)$	$\bar{A}(r)_{\sigma_r}$	$A^{(i)}$	$\bar{A}^{(i)}_{\sigma_i}$	$A(r)$	$A^{(i)}$	$\bar{A}(r)_{\sigma_r}$	$A(r)$	$\bar{A}^{(i)}_{\sigma_i}$
300	-0.0324		-0.0739		-0.031	-0.081	-0.0305		-0.0833
500	-0.039	-0.120	-0.131	-0.132			-0.0112	-0.137	
	-0.013	-0.0197	-0.0169	-0.0047			-0.036	-0.020	-0.133
	-0.0072	-0.0169	-0.138				-0.013	0.0138	-0.131
600	-0.037		-0.178		-0.045	-0.183	-0.0375		-0.1801
	-0.046	-0.318	-0.336	-0.322	-0.027	-0.332	-0.045	-0.036	-0.322
1050	-0.0344	-0.0381	-0.0053	-0.009			-0.041	-0.041	-0.328
	-0.0360	0.0053	-0.318	0.009			-0.036	0.008	-0.328
	-0.0360	-0.318	-0.318				-0.0252		0.008
	-0.072	-0.459	-0.484	-0.471			-0.039	-0.052	-0.3418
1500	-0.068	-0.064	-0.010	-0.471	0.012		-0.046	-0.0457	-0.48
	-0.053	-0.471					-0.052	-0.0457	-0.47
	-0.053	-0.471					-0.046	-0.006	0.01
	-0.110	-0.730	-0.728	-0.755	+0.0188	-0.79	-0.084	-0.095	-0.733
2100	-0.096	-0.066	-0.065	-0.045			-0.095	-0.0335	-0.729
	-0.086	0.065	-0.741	0.045			-0.102	0.0666	-0.716
	+0.0317	-0.822					+0.041	+0.021	0.035
							+0.021	-0.797	-0.701
								+0.018	-0.706

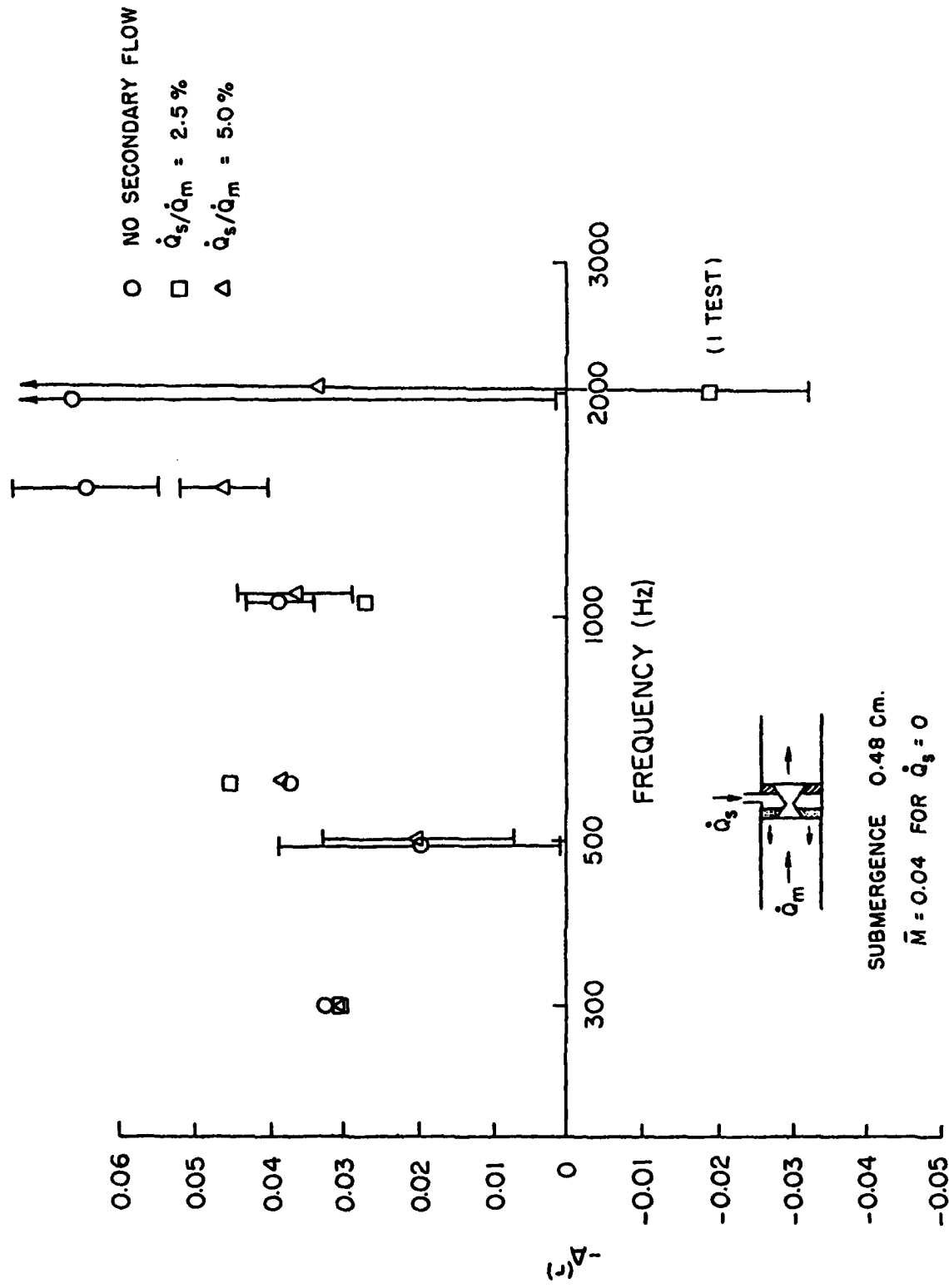


Figure 28. Admittance Function Measured for a Nozzle with Secondary Flow
No Submergence, $\bar{M} = 0.04$

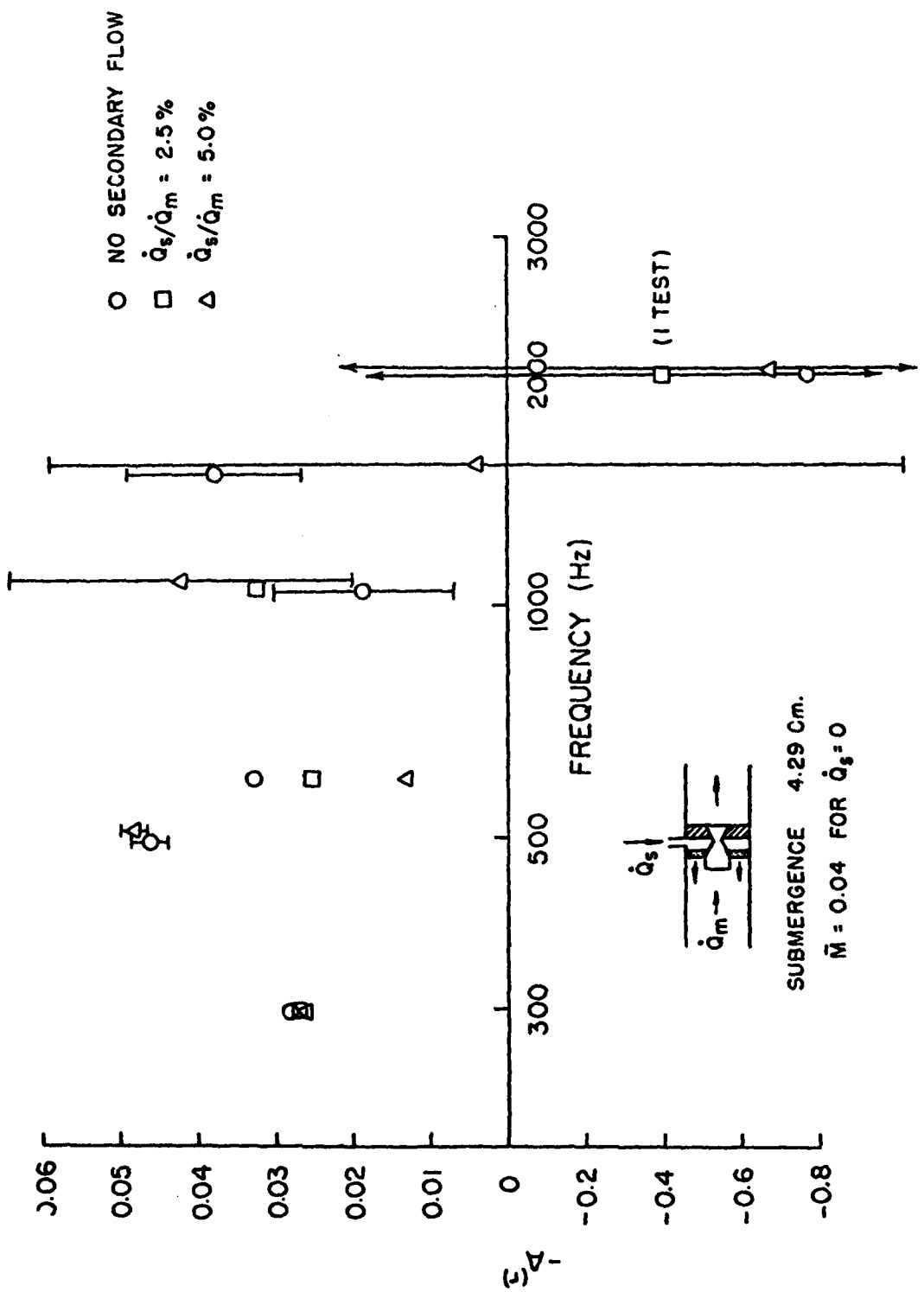


Figure 29. Admittance Function Measured for a Nozzle with Secondary Flow.
Maximum Submergence, $\bar{M} = 0.04$

(iii) There is only a vague suggestion in the data that the real part of the admittance is increased by submergence when the nozzle is submerged by more than one-quarter of a wavelength. The values of the real parts at 2000 Hz. are, on the average, less for maximum submergence.

The large experimental uncertainties prevent us from claiming these to be credible conclusions. They are at best very qualitative and tentative.

In all cases for these tests, the imaginary part of the admittance has been determined to be larger than the real part. This conclusion is true for all frequencies, independently of the submergence and value of secondary flow. Unfortunately, the most likely source of this result is not the nozzle or flow field, but rather the system used to provide the secondary flow.

As for the flow-turning measurements discussed in Section II, we have been unable to choke the porous plate surrounding the nozzle. The plenum chamber is therefore not perfectly isolated from the acoustic field in the test section of the tunnel. A grade H sintered steel plate was used to pass the flow. Its measured admittance has been shown earlier in Figure 9. For the conditions used in these tests, the real part of its admittance is of the order of .013, roughly 1/3 to 1/5 the values measured for the nozzle. The imaginary parts of the admittance for the plate have not been determined, although there is no reason to believe that they are larger than the real parts. Thus, the large imaginary parts measured in the nozzle tests are almost certainly not only a consequence of the behavior of the nozzle itself, but also the system used for the gas supply. We cannot separate the one from the other with the data we have acquired in the present work.

The major source of difficulty in acquiring data has been flow noise. This is of course most troublesome near pressure minima, exactly in the regions where it is most important to obtain good data. The problem is more serious with the measurements of phase: that measurement carries with it larger experimental error even under the best of conditions. Above Mach number 0.1 it appears that the tracking filter, even with a bandwidth of 0.5 Hz., is inadequate. One would be forced to use machine processing of the data, using, for example, correlation techniques or signal averaging. However, our experience suggests that with secondary flow this becomes a very difficult problem. The noise we observed is so severe that, according to brief conversations with personnel at JPL, very extensive signal averaging would be required to produce the necessary effective bandwidth.

An obvious help is to use a stronger signal, obtainable only with pneumatic drivers. Since we did not have one at our disposal, we have been unable to verify the extent to which this helps solve the problem. Judging by the reports in Refs. 9-12, this should help considerably.

Just as for the measurements of the flow turning losses, the relative experimental errors can be reduced by working with larger scale apparatus. The disadvantage is of course the increased expense, arising from many sources. The advantages of using as small a facility as possible are: low cost; ease of operation; and increased flexibility. However, if good data cannot be obtained, these advantages are of little value.

Another possible means of solving the problem of data acquisition near pressure minima is simply not to do so. With the impressive advances in laser-Doppler-anemometry (or velocimetry) during the past

several years, it may well be best to return to the more direct method first used in Ref. 8. The admittance function can in principle be determined from data for the pressure and velocity fluctuations taken at a position just upstream of the nozzle. This technique offers a reasonable opportunity for concentrating on acquiring data over one plane, thereby allowing one to form the averaged quantity which is required as the boundary condition for stability analysis. The signal/noise problem still exists, but because the data should be taken near the nozzle, it may be possible in some cases to take data at locations not near velocity or pressure minima. The signal is greater and there is no need to define pressure minima.

3.8 Remarks on the Plane of Definition for an Admittance Function

When data taken in an impedance tube is reduced to obtain values of the admittance function, the plane to which the function applies is defined by the origin of the coordinate system used. This is an immediate consequence of the idealized analysis described in Section 3.1 and of the more general method summarized in Section 3.4.2. The locations of the pressure minima and maxima; for example, are measured with respect to some origin chosen in the experiments.

The origin can of course be shifted, and the same data used to infer the admittance function for any other plane. If there are no losses in the volume between two transverse planes, then the admittance functions must be identical. We have verified this property in one simple example. The major practical consequence is that the plane chosen in the experimental work must be such as to allow application of the results more generally. Care is required that the plane selected should

include downstream all influences which one anticipates finding in other circumstances to which the results will be applied. But if there are losses upstream, they must be accounted for in the data reduction.

For example, consider the case of a small conical nozzle in a plate, such as that shown in Figure 18. If the origin ($z=0$) is chosen at the face of the plate, influences of flow separation upstream should not affect the admittance function. But they certainly do affect the acoustic upstream where measurements will be made. They must therefore be accurately represented in the data reduction. In this case they cannot be modelled well. It is therefore necessary to place the origin far enough upstream of the face of the plate that the influences of the separated region is downstream. The major losses upstream are then the viscous losses in the acoustic boundary layer. The admittance function inferred will then reflect the behavior of the nozzle and interactions between incident waves and the separated regions.

It is especially important to be aware of these matters when dealing with nozzles exposed to secondary flow. Because it is not possible to analyze such situations with any confidence, it is essential that the model used for testing be a faithful rendition of the entire aft end of the motor, and that the plane for which the admittance function is defined be carefully specified. The location of that plane must then be correctly incorporated in the analysis of the stability of oscillations in the motor.

IV. SUMMARY AND CONCLUSIONS

4.1 Flow Turning Losses

The results of this experimental program have supported the main qualitative characteristics of the flow turning loss as predicted by the one-dimensional analysis. There is indeed a loss of acoustic energy associated with average inward flow at the boundary, and the loss increases with the Mach number of the average flow. There are very large uncertainties associated with the data, and the results suggest that the losses are several times greater than those predicted.

Owing to those uncertainties which reflect many difficulties arising in the performance of the experiments, it is not possible to conclude unequivocally that the actual losses are in fact significantly greater than those deduced from the approximate analysis. Consequently, one should really conclude that at the present time, theory has predicted and experiment has confirmed the existence of the losses, but their quantitative values remain in doubt.

This situation can be improved in two ways: by carrying out a more elaborate two-dimensional analysis; and by performing further experiments. Theoretical issues are not our concern here; it is certainly not difficult to conceive of analyses are likely to improve upon the one-dimensional approximation, although there are no obvious simple formulations.

More pressing is the need for better experimental work. It appears that the only way to gain significant improvement is to use larger apparatus. The ultimate source of almost all of our difficulties has been the need to infer a relatively small quantity as the difference

between relatively large quantities. The flow turning loss per unit area is proportional to the Mach number of the average flow and to the square of the amplitude of the acoustic field. Larger flow rates and more intense acoustic fields would clearly be helpful. And if the apparatus is larger, the total loss will increase, proportional to the square of the linear dimension. With judicious design, it may be possible to achieve very substantial increases in the flow turning losses relative to other contributions (such as viscous losses) thereby easing the problems of measurement.

4.2 Measurements of the Admittance Function for a Choked Nozzle

The unfortunate problems with data processing, discussed in Section 3.4, eventually prevented us from gathering satisfactory data for the admittance function. The main achievements have been to verify that the method developed at Georgia Tech is a thoroughly satisfactory method for reducing data taken in an impedance tube with flow; and the technique based on using a continuously operating supersonic wind tunnel will work, but important improvements must be made. There is no need to discuss data processing further.

Owing to the limited data eventually taken in this program, no unusual or new general conclusions can be drawn. The experimental errors are not excessively large for the cases run with no secondary flow: roughly 20% or less for the real part of the admittance function of a small conical nozzle in a plate. With secondary flow, the errors were unacceptably large, in some cases larger than the average values. The errors increase both with flow rate and with frequency, for reasons which we do not comprehend at this time. Because of the large errors, it is not possible to offer any general conclusions concerning the

influences of secondary flow and submergence. The data show only that the effects are not accountable as factors of ten.

By far the major experimental problem is signal/noise at pressure minima. Clearly the sensible solution is to use a larger source for the acoustic field. Electromechanical speakers are probably not satisfactory, but there are at least three other possibilities: pneumatic drivers or rotary valves; crystal drivers (which seem to be difficult to find for the audio range); and oscillating obstructions in the flow. The last is really a form of rotary valve in the broadest sense. Increasingl the signal is a soluble problem, although because the noise increases rapidly with increasing Mach number, only exploratory tests will verify the limits to which one may go.

Use of a continuously movable microphone to take data is essential, but in future work, an arrangement should be designed to make the measurements in the lateral boundary. Although we minimized the interference caused by a microphone concentrically placed in the tube, there is clearly some influence. Much worse, the necessity to take data through a long tube greatly reduces the total signal and aggravates the signal/noise problem.

With a continuously operating system, it is relatively straight-forward to study the effects of secondary flow. It is possible not only to determine the influences on the acoustical properties, but the possibility exists for making detailed observations of the flow field. That is an important subject which we did not pursue in the present program beyond a small number of exploratory tests. The basic problem of the structure of the acoustic field in an average flow field approaching fully developed

pipe flow remains untouched. We have obtained no measurements of the flow field in the vicinity of a nozzle with secondary flow, a subject which merits considerable attention. It appears that this problem would benefit greatly from application of laser-Doppler velocimetry. In principle one should be able to obtain measurements of both the fluctuating pressure and velocity as functions of position in regions upstream of the nozzle. The data would provide a means of determining the admittance function directly, both as a function of position, and averaged over a plane. This would be a helpful independent check of the results obtained using the apparatus as an impedance tube. The device merits development as a means of making, eventually, routine measurements of the behavior of choked nozzles.

V. REFERENCES

1. Culick, F. E. C. "Remarks on Entropy Production in the One-Dimensional Approximation to Unsteady Flow in Combustion Chambers", Comb. Sci. and Tech., V. 15 (1977) pp. 93-97.
2. Culick, F. E. C. "The Stability of One-Dimensional Motions in a Rocket Motor", Comb. and Sci. and Tech., V. 7 (1973) pp. 165-175.
3. Magiawala, K. "Measurements of Energy Exchange Between Acoustic Fields and Non-Uniform Flow Fields", Ph.D. Thesis, California Institute of Technology (May 1978).
4. Culick, F. E. C. and Magiawala, K., "Measurements of Energy Losses Associated with Interactions Between Acoustic Waves and a Steady Flow Field", Air Force Rocket Propulsion Laboratory, Report AFRPL-TR-78-6 (March 1978).
5. Magiawala, K. and Culick, F. E. C. "Measurements of Energy Exchange Between Acoustic Fields and Non-Uniform Steady Flow Fields", J. Sound and Vib. (to be published).
6. Tsien, H. S. "The Transfer Function of Rocket Nozzles", ARSJ, V. 22, No. 31 (May-June 1952), p. 139.
7. Crocco, L. and Cheng, S.-T. Theory of Combustion Instability in Liquid Propellant Rocket Motors, AGARDograph No. 8, Butterworths Publications, Ltd., London (1958) Appendix C.
8. Crocco, L., Monti, R. and Grey, J. "Verification of Nozzle Admittance Theory by Direct Measurement of the Admittance Parameter", ARSJ, V. 31, No. 6 (June 1961) pp. 771-775.
9. Zinn, B. T. et al "Experimental Determination of Three-Dimensional Liquid Rocket Nozzle Admittances", AIAA J., V. 11, No. 31 (Mar. 1973), pp. 267-272.
10. Bell, W. A., Daniel, B. R. and Zinn, B. T. "Experimental and Theoretical Determination of the Admittances of a Family of Nozzles Subjected to Axial Instabilities", J. Sound and Vib., V. 30, No. 2 (1973), pp. 179-190.
11. Zinn, B. T. et al "Damping of Axial Instabilities by the Minuteman II, Stage III and Minuteman III, Stage III, Exhaust Nozzles", Georgia Institute of Technology, Report AFRPL-TR-72-71 (August 1972).
12. "Nozzle Design Considerations for Attenuation of Axial Instabilities in the Minuteman II and III, Stage III Rocket Motors", Georgia Institute of Technology, Report AFRPL-TR-73-69 (September 1973).

13. Culick, F. E. C. (Ed.), "T-Burner Testing of Metallized Propellants", AFRPL Report TR-74-28 (Oct. 1974).
14. Shapiro, A. H. The Dynamics and Thermodynamics of Compressible Fluid Flow. The Ronald Press Company, New York (1953).
15. Rauscher, M. Introduction to Aeronautical Dynamics, John Wiley and Sons, Inc., New York (1953) p. 50.
16. Van Moorhem, W.K. "An Investigation of the Origin of the Flow-Turning Effect in Combustion Instability", 17th JANNAF Combustion Meeting (September 1980).
17. Culick, F. E. C. "Linear Analysis of One-Dimensional Oscillations in a Variable Area T-Burner", 9th JANNAF Combustion Meeting (1972).
18. Baum, J. D., Daniel, B. R. and Zinn, B. T. "Determination of Solid Propellant Admittances by the Impedance Tube Method", AIAA 18th Aerospace Sciences Meeting (Jan. 1980) AIAA Paper 80-0281.
19. Morse, P. Vibration and Sound, McGraw-Hill Book Co., New York (1948), pp. 239-244.
20. Muller, D. A. "A Method for Solving Algebraic Equations Using an Automatic Computer", Mathematical Tables and Other Aids to Computation (1956) pp. 208-215.

DAT
ILM